#3

THE SPECTRAL EMISSIVITY AND OPTICAL PROPERTIES OF TUNGSTEN

ROBERT DEAN LARRABEE

TECHNICAL REPORT 328

MAY 21, 1957

Loan Copy

RESEARCH LABORATORY OF ELECTRONICS
MASSACHUSETTS INSTITUTE OF TECHNOLOGY
CAMBRIDGE, MASSACHUSETTS

The Research Laboratory of Electronics is an interdepartmental laboratory of the Department of Electrical Engineering and the Department of Physics.

The research reported in this document was made possible in part by support extended the Massachusetts Institute of Technology, Research Laboratory of Electronics, jointly by the U. S. Army (Signal Corps), the U. S. Navy (Office of Naval Research), and the U. S. Air Force (Office of Scientific Research, Air Research and Development Command), under Signal Corps Contract DA36-039-sc-64637, Department of the Army Task 3-99-06-108 and Project 3-99-00-100.

MASSACHUSETTS INSTITUTE OF TECHNOLOGY

RESEARCH LABORATORY OF ELECTRONICS

Technical Report 328 May 21, 1957

THE SPECTRAL EMISSIVITY AND OPTICAL PROPERTIES OF TUNGSTEN

Robert Dean Larrabee

This report is based on a thesis submitted to the Department of Physics, M.I.T., May 13, 1957, in partial fulfillment of the requirements for the degree of Doctor of Science.

Abstract

An experiment designed to measure the spectral emissivity of tungsten at incandescent temperatures has been initiated. A direct comparison method is utilized in which the radiant intensity from a tungsten source is compared with the radiant intensity from an approximative black body, and the spectral emissivity is computed from the basic relation $E_{\lambda T} = S/B$, where $E_{\lambda T}$ is the spectral emissivity at temperature T and wavelength λ, S is the radiant intensity of the tungsten source, and B is the radiant intensity of the approximative black body.

We show that the spectral emissivity of tungsten is caused by the classical electromagnetic reflection and refraction of black-body light incident upon the metal-vacuum interface from inside the metal. Equations for the spectral emissivity of tungsten as a function of the direction of polarization and the angle of viewing the tungsten surface are developed in terms of the optical constants of tungsten. The optical constants of tungsten are computed by comparing these equations with the experimental data.

An attempt is made to explain the main features of these data in terms of a combination of the Lorentz elastically bound electron theory of insulators and the Drude-Zener-Kronig free-electron theory of metals.

Table of Contents

I.	Introduction	1
II.	Brief History of the Problem	2
III.	Experimental Technique	4
	3.1 Basic Experimental Procedure	4
	3.2 Constructional Details of the Tungsten Source	5
	3.3 The Emissivity Tube	6
	3.4 Purification of Tungsten by Heat Treatment	12
	3.5 Annealing Schedule for the Finished Tungsten Specimen	14
	3.6 Optical System	17
	3.7 Mechanical Considerations	20
	3.8 Source-Current Circuit	22
	3.9 Source-Current Regulator	23
IV.	Preliminary Measurements	26
	4.1 Measurement of Source Temperature	26
	4.2 Effects of Crystalline Structure	28
	4.3 Temperature Gradients	30
	4.4 The Through Hole	31
	4.5 The Black-Body Hole	33
V.	The Spectral Emissivity of Tungsten	36
VI.	Deviations from Lambert's Radiation Law in Tungsten Radiation	44
	6.1 First Approximation	44
	6.2 Second Approximation	48
VII.	Theoretical Interpretation of the Results	50
	7.1 Basic Mechanism of Metallic Thermal Radiation	50
	7.2 Calculation of the Emitted Light	51
	7.3 Alternative Derivation	54
	7.4 Normal Spectral Emissivity of a Metal	55
	7.5 Simplification of the E_n and E_p Equations	55
	7.6 Equations for the Parameters Z_1 and Z_2	56
	7.7 The Optical Constants N and K	57
	7.8 Comparison of Theory with Experiment	59
	7.9 Optical Constants of Tungsten	64

Table of Contents

VIII. Further Interpretation of Results 68
8.1 The Drude-Zener-Kronig Free-Electron Model 68
8.2 Modification of the Free-Electron Model 70
8.3 Development of the Modified Free-Electron Model 70
8.4 First Approximation to the Evaluation of the Parameters 71
8.5 Comments on the Evaluation of the Parameters 74
8.6 Conclusions 75

Appendix I Vacuum Considerations 76

Appendix II Description of Special Ionization Gauge 78

Acknowledgment 79

References 80

I. INTRODUCTION

Knowledge concerning the nature of electromagnetic radiation from incandescent bodies is important for several reasons. It is necessary for the construction of standard sources of radiation that use incandescent filaments as sources of light. It is also necessary for the practical application of optical-pyrometer methods. Furthermore, the characteristic thermal radiation from incandescent bodies yields further information about the basic structure of matter.

Thermodynamic considerations show that within a completely closed hollow body, with walls that are at a uniform temperature and opaque to electromagnetic radiation, the character of the radiant energy is determined entirely by the temperature of the body and is independent of the material from which the body is constructed and of its structural geometry. If a small hole (small compared with the inside dimensions of the hollow body) is made in one of the walls, the character of the radiation inside the body will not be seriously affected. Thus the radiation emerging from this small hole can be observed and studied. It can be shown that the radiation from this hole is identical (subject to certain limitations) with the radiation from a perfectly black body (a body that absorbs all incident light and reflects none) at the same temperature as the walls of the hollow body. Therefore, this radiation is called "black-body radiation," and the hollow enclosure with the small hole is called a "black body."

Planck was able to deduce the analytic formula for the density and spectral distribution of the radiant energy from a black-body radiator at a uniform temperature. This relation, called Planck's Radiation Law, is

$$I_{\lambda, T}\, d\lambda = \frac{8\pi ch}{\lambda^5} \frac{1}{e^{hc/KT\lambda} - 1}\, d\lambda \qquad (1)$$

where

$I_{\lambda, T}$ = radiant intensity per unit wavelength interval at wavelength λ and temperature T,

h = Planck's constant = 6.624×10^{-34} joule-second,

c = velocity of light = $2.9978 \times 10^{+8}$ meters/second,

k = Boltzmann's constant = 1.3805×10^{-23} joule/°K, and

e = base of natural logarithms = 2.71828.

In testing Planck's radiation law, and in subsequent studies of radiation, black bodies have been approximated in many forms, all of which are basically hollow enclosures provided with openings. Some of the more popular experimental black bodies are:

(a) Hollow cylinders, spheres, and so forth, with small holes in their walls (1, 2, 3).

(b) Closely wound spirals of metallic ribbon for the hollow enclosure, the gap between turns serving as the "hole" (4, 5).

(c) Long, open-ended, hollow cylinders (6, 7).

(d) Long hollow cylinders provided with small longitudinal slits in their

lateral areas (8, 9).

(e) Ribbons of metal bent into the shape of open V-wedges, the radiation from which approximates black-body radiation (10, 11, 12).

Different experimenters favored their own ways of approximating a black body for reasons of ease of construction and ability to heat to a uniform temperature. De Vos (1) and others have estimated that all of these radiators approximate black-body conditions rather well. De Vos estimated that the hollow cylinder with a small hole in its lateral area is probably the best of those listed above.

Although Planck's radiation law gives the characteristics of black-body radiation within experimental error, it fails to yield correct results when it is applied to the case of an incandescent metallic radiator. Since a metallic radiator is somewhat similar to a black-body radiator over certain ranges of temperature and wavelength, it has become common practice to introduce the following modification:

$$I_{\lambda, T}\, d\lambda = E_{\lambda T} \frac{8\pi ch}{\lambda^5} \frac{1}{e^{hc/KT\lambda} - 1} d\lambda \qquad (2)$$

where $E_{\lambda, T}$ is a dimensionless quantity called the "spectral emissivity" of the metal, which is, in general, a function of both wavelength and temperature, as well as of the metal that is used. The Laws of Thermodynamics reveal that the spectral emissivity of any body is between zero and unity (unity corresponding to a black body, and zero corresponding to a perfectly reflecting body).

It is our purpose to measure the spectral emissivity of tungsten over the visible region of the spectrum and to attempt to explain these measurements by theoretical means.

II. BRIEF HISTORY OF THE PROBLEM

Basically, the methods used for the experimental determination of the spectral emissivity of metals can be divided into two groups.

1. Indirect Methods

According to Kirchhoff's laws of radiation, the absorptivity and the emissivity of any surface are equal at all wavelengths. Also, since the sum of the absorptivity and the reflectivity equals unity for an opaque body, the emissivity can be computed from the equation

$$\text{Emissivity} = \text{Absorptivity} = 1 - \text{Reflectivity} \qquad (3)$$

if either the absorptivity or the reflectivity is known.

2. Direct, or Comparison, Methods

Emissivity can be computed, by definition, by measuring the ratio of the radiant intensity from a given surface to that from a black body at the same temperature.

Most of the early measurements of spectral emissivity were made by the indirect

method, since the techniques of reflectivity measurement had been developed in the field of optics. One such method (13, 14) consisted of comparing the light from a heated filament reflected in a tungsten mirror with the light from an identical filament without the mirror in the optical path. Another method (13, 14) consisted of comparing the radiation reflected from a tungsten strip with the same radiation reflected from a silver mirror of known reflectivity.

Two of the main experimental drawbacks of the indirect method of measuring emissivity are:

(a) In order to determine emissivity as a function of temperature, reflectivity measurements must be made in regions where the reflector itself emits an appreciable amount of thermal radiation. Since the emitted radiation must be separated from the reflected radiation, an upper bound is imposed on the temperature at which this method of measurement is practical.

(b) The assumptions in Eq. 3 require that the total radiation reflected into the hemisphere surrounding a plane reflector be measured and not just the specularly reflected component. This necessity arises because the reflectivity defined by Eq. 3 is the ratio of the total radiation reflected in all directions by the given surface to the incident radiation.

As a consequence of these drawbacks, and of the advantages afforded by the direct, or comparison, method, the indirect method has not had extensive use recently, except at low temperatures where the comparison method cannot be used.

In the direct method a black-body radiator and a metallic radiator have to be constructed. As we have said, several observers have approximated black bodies in different ways. Also, since the black-body radiator must be at the same temperature as the metallic radiator, most observers have constructed their black bodies from the metal to be measured so that the source of thermal radiation which is measured (i.e., compared with black-body radiation) forms an integral unit with the black body. Consequently, with the source and the black body in intimate physical and thermal contact, equality of temperature can be obtained with more certainty. However, a few observers have constructed black bodies that were entirely divorced from the source and have relied on other devices to ensure equality of temperature.

In spite of many measurements of the spectral emissivity of tungsten, doubt still remains about the correct values of emissivity, since there has been a considerable amount of disagreement among the observers (1). In fact, at the present time, standards laboratories in several countries use different values for the spectral emissivity of tungsten, under the same conditions of temperature and wavelength (1). In view of this lack of standard, Professor Wayne B. Nottingham suggested, in 1948, that an electronic photomultiplier photometer, which he developed during World War II might be well suited for making accurate comparison measurements of spectral emissivity. Following his suggestion, in 1948, Mutter (2) made measurements on tungsten, and, in 1950, McGlauchlin (15), followed by Stevenson and Philip (16), made measurements on tantalum.

Although Stevenson and Philip did not agree with McGlauchlin on the value of the emissivity of tantalum (even though they used the same piece of tantalum for their measurements), it is now felt that serious, accurate, and reliable measurements can be made on tungsten, and there is a possibility that measurements of the emissivity of tantalum, nickel, and molybdenum will be made in the future. Consequently, the author studied the problem and built the equipment for measurements with tungsten as a Master's thesis at the Massachusetts Institute of Technology in 1955 (17). The present report presents the results of continuing this work to the point at which definite data and theoretical interpretation are available, but not to the point of terminating the project.

III. EXPERIMENTAL TECHNIQUE

3.1 BASIC EXPERIMENTAL PROCEDURE

Since this study is concerned with the experimental determination of the spectral emissivity of tungsten in the range of incandescent temperatures, a direct comparison method is employed in which the radiant intensity from a tungsten source is compared with the radiant intensity from an approximative black-body source, and the spectral emissivity is computed from the basic relation

$$E_{\lambda T} = \frac{S}{B} \tag{4}$$

where

$E_{\lambda T}$ = spectral emissivity at temperature T and wavelength λ,

S = radiant intensity of the tungsten source, and

B = radiant intensity of the approximative black-body source.

The approximative black-body source consists of a hollow tungsten clyinder 1/8 inch in diameter, 4 inches long, with a 1-mil wall thickness. This tungsten cylinder has a hole of 13-mil diameter in its lateral surface to serve as the source of black-body radiation. When the cylinder is heated to incandescence by the passage of a well-regulated direct current, the small wall thickness ensures that temperature differences that develop between the inside and outside wall surfaces (18) will be negligible. Therefore, a spot selected on the outside surface of this tungsten cylinder can be utilized as the tungsten source.

The light whose radiant intensity is to be measured is separated from the undesired light by an optical system, which consists of a single quartz lens (equipped with shutter and diaphragm) and a 5-mil aperture that forms the "entrance slit" of a Bausch and Lomb monochromator (19, 20). The light passing through the monochromator falls upon a photomultiplier, and its intensity is measured within three-figure accuracy by the photometer developed by Professor Nottingham.

However, a correction must be made for scattered light. Another hole of 13-mil diameter, similar to the black-body hole, but passing completely through the hollow cylinder (i.e., through front and back walls), may be aligned with the optical axis of the lens system for the purpose of measuring this scattered component of radiation. This

"through hole" is backed by an (approximately) exponentially shaped appendage to the glass envelope (see Fig. 1) so that a minimum amount of light will be reflected and scattered into the monochromator from the region behind the through hole. If this through-hole reading of the photometer is represented by a, the emissivity is given by

$$E_{\lambda T} = \frac{S}{B} = \frac{S' - a}{B' - a} \tag{5}$$

where S' and B' are the uncorrected photometer readings for the tungsten source and the black-body hole, respectively.

3.2 CONSTRUCTIONAL DETAILS OF THE TUNGSTEN SOURCE

After a great deal of effort was spent in an unsuccessful attempt to purchase a seamless tungsten tube of the required dimensions, we decided that we would have to fabricate a hollow cylinder from 1-mil tungsten ribbon. Four basic types of construction were considered in which:

1. The ribbon can be spiraled into a shape which encloses a cylindrical volume with such a pitch that there are no gaps or overlaps between the turns.
2. The ribbon can be folded lengthwise into a cylindrical shape in such a manner that the folded edges:
    a. just touch (or leave a slight gap) but do not overlap.
    b. overlap enough to be welded together.
    c. are bent outward to form a protruding longitudinal welding tab.

With the first system it is difficult to ensure that there are no overlappings or large gaps between the turns, which, if present, could introduce undesirable temperature gradients along the cylinder. Such a system would be weak mechanically, and a great deal of trouble might develop in attempting to make it retain its shape over a wide temperature range.

The second system, 2a, has the same constructional and mechanical difficulties as the first system, but to a lesser degree. De Vos (1) has estimated that, for similar dimensions, the third system, 2b, would be more desirable than the second system. However, the lap-weld of the third system could introduce temperature gradients around the cylinder, since the inside lap would receive radiant energy from both sides, while the outside lap would receive an appreciable amount of radiant energy from only one side (it would radiate to "vacuum" on the other side). Consequently, the inside lap would tend to be at a higher temperature than the outside lap. However, with the protruding welding tab of the fourth system, 2c, all of the metal is receiving an appreciable amount of radiant energy on one side while radiating to "vacuum" on the other side. Therefore, since it appeared that the fourth system would introduce a minimum of temperature gradients and still be mechanically strong, it was used in this experiment.

A strip of 1-mil tungsten ribbon, 1/2 inch wide and 4 inches long, was mounted in a "jig" that cold-worked it to the desired shape. This jig could not be removed

immediately after the tungsten ribbon was cold-worked, since the high resilience of unannealed tungsten would cause the tungsten to return almost to ribbon shape again. However, after heating (both the tungsten and the jig) in a hydrogen furnace (900° C for 15 minutes), the "jig" could be removed and the tungsten would retain nearly the desired shape without becoming brittle.

The next step in the fabrication of the tungsten source was to weld the folded edges together along the protruding welding tab. This was necessary not only for reasons of mechanical strength, but also to ensure that this seam was so tight that it would not allow radiation to escape from the interior of the hollow cylinder. After much experimentation, it was discovered that the tungsten ribbon could be successfully welded to itself (but not welded simultaneously to the electrodes of the spot welder) if the electrodes were made of 1/16-inch diameter solid tungsten rod and the welding was done under a water-alcohol mixture (25 per cent alcohol to 75 per cent water, by volume). Since the purpose of the water was to cool the electrodes so that the ribbon would not weld to them, it was necessary to use a comparatively small heating current for a comparatively long time (one second) to allow for heat transfer. Since the water does not come in contact with the area between the two pieces of ribbon that are being welded together, this area is welded, while the ribbon itself is not welded to the electrodes. Although some recrystallization takes place at the weld and makes it mechanically weak, after a great many such welds were made along the 4-inch length of the tab, the resulting structure was extremely strong.

After many futile attempts to drill the necessary 13-mil black-body hole and through hole, it was found that they could be successfully produced by a punching operation. A solid drill rod of 1/8-inch diameter, with two properly positioned holes of 13-mil diameter passing perpendicularly through it, was inserted in the hollow tungsten cylinder. With these 13-mil holes as dies, the black-body hole and through hole were punched out by a 13-mil punch. In order to align the "two through holes" perfectly (one on each side of the hollow tungsten cylinder), a 13-mil rod (i.e., punch) was inserted in the already punched 13-mil hole (front half of through hole) through the hole in the solid 1/8-inch drill rod to punch out the necessary hole in the far side of the cylinder to complete the through hole.

Thus, the hollow tungsten cylinder, with a protruding welding tab and a black-body hole and a through hole, was fabricated from 1-mil tungsten ribbon.

3.3 THE EMISSIVITY TUBE

In order to accommodate the mounting for the hollow tungsten cylinder in a vacuum tube and to allow for passing current through it, we had to attach each end of the hollow cylinder to a rod of solid tungsten of 1/8-inch diameter. Experimentally, it was virtually impossible to weld the tungsten cylinder to this solid tungsten rod without also welding it to the spot-welder electrodes. Therefore, it was decided to "press-fit" these two pieces together mechanically. A groove, 1/8 inch long and 1 mil deep, was etched

into a solid tungsten rod 1/8 inch from one end. Thus, when the solid rod was inserted into the hollow tungsten cylinder for a 1/4-inch distance, it was possible to "press-fit" the end 1/8 inch of the hollow cylinder into this groove by wrapping 5-mil tungsten wire around the cylinder at this point. Of course, we had to cut back the protruding welding tab for a distance of 1/8 inch on each end of the hollow cylinder so that it would not interfere with the wrapping process. This arrangement provided a sufficiently strong connection for the purpose and was more than adequate to carry the required heating current (up to 70 amperes). In fact, when the hollow cylinder was subsequently heated to incandescence, this "press fit" became sufficiently hot to partially weld the components together.

The rest of the internal structure was held together mainly by "set-screw methods," and hence presented few welding problems. Four large kovar-cup, glass-to-metal seals were provided at the top of the emissivity tube to carry the comparatively large heating current, as well as to provide for adequate mechanical support for the internal structure of the tube (see Figs. 1, 2, 3, 4, and 5). Two of these seals (the ones in the front and back) were connected together inside the glass envelope by a nickel crossbar to which a vertical tungsten rod that extended down to the hollow tungsten cylinder was connected. The other two seals (the ones to the right and left) were connected to solid tungsten rods 1/8 inch in diameter that extended to the bottom assembly of the tube. These two tungsten rods not only carry current to the bottom of the tube, but also support the bottom assembly of the tube. Another 1/8-inch tungsten rod, originating from the bottom end of the hollow tungsten cylinder, also extended to the bottom of the tube. These three tungsten rods were electrically connected together by a large tantalum spring designed to be as flexible as possible so as to offer as little opposition to the thermal expansion of the hollow tungsten cylinder as possible. A spiral tungsten spring constructed from a rod of 40-mil diameter was included at the bottom of the tube assembly to provide a slight tension in the cylinder when the cylinder was at room temperature. This tended to damp out vibrations and to provide some support for the bottom of the central tungsten rod (the one connected to the hollow cylinder) while the tube was being processed. However, when the tube was in operation, this tension was no longer needed, and it was conveniently removed by the thermal expansion of the hollow tungsten cylinder.

A 0.75-inch diameter, 4-inch long quartz shield was mounted coaxially with the hollow tungsten cylinder in such a way that it could slide up and down on the vertical tungsten rods that carry current to the bottom of the tube. Initially this quartz shield was held in a position (against gravity) by four molybdenum springs so as to completely cover the hollow tungsten cylinder. The basic purpose of this shield was to protect the pyrex window of the emissivity tube from evaporated material during the outgassing and annealing operations (which will be discussed later). In normal operation of the tube this quartz shield would be in the way and would no longer serve a useful purpose. Consequently, by heating the molybdenum springs to a sufficiently high temperature (by passing a current through them), the strength of the springs was so reduced that the

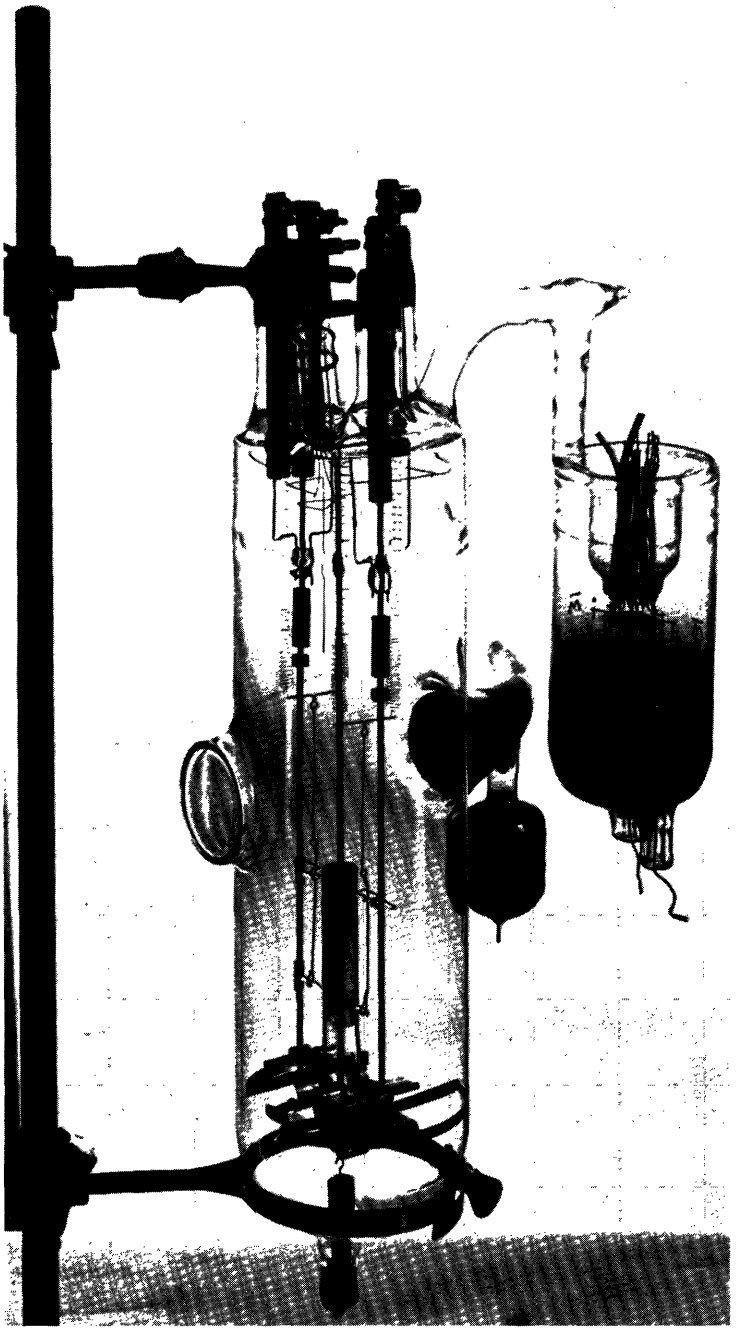

Fig. 1. Pictorial view of the emissivity tube.

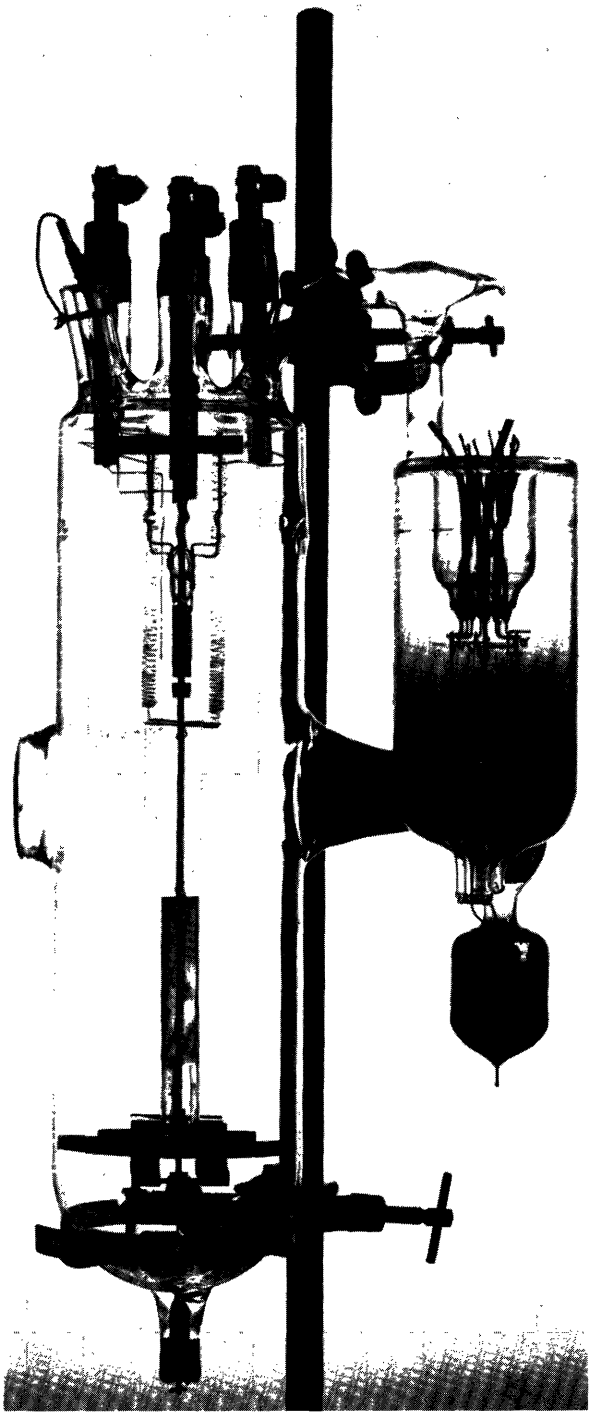

Fig. 2. Side view of the emissivity tube.

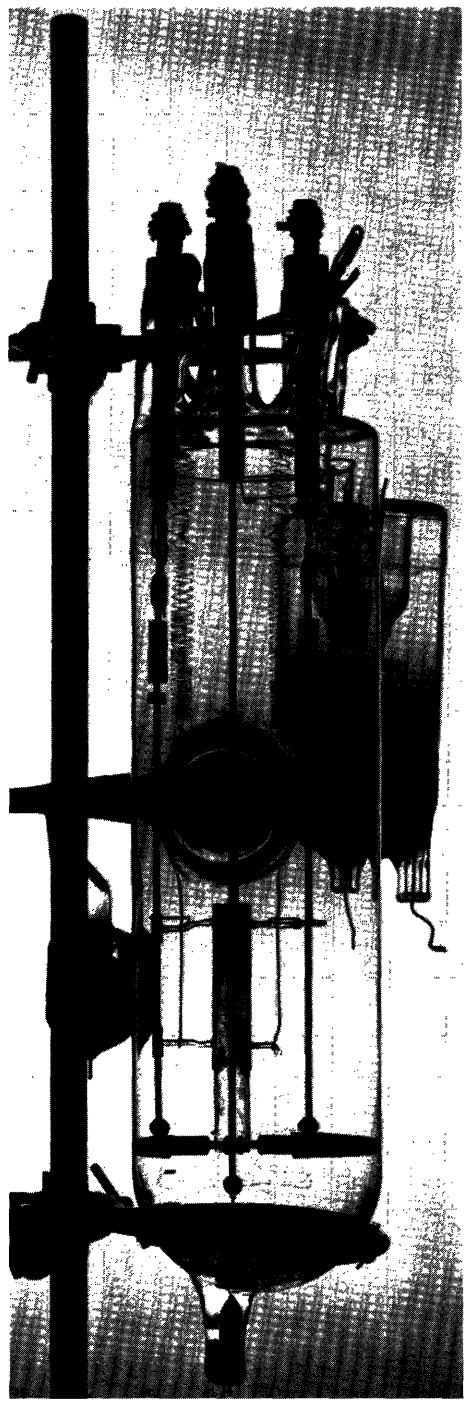

Fig. 3. Front view of the emissivity tube.

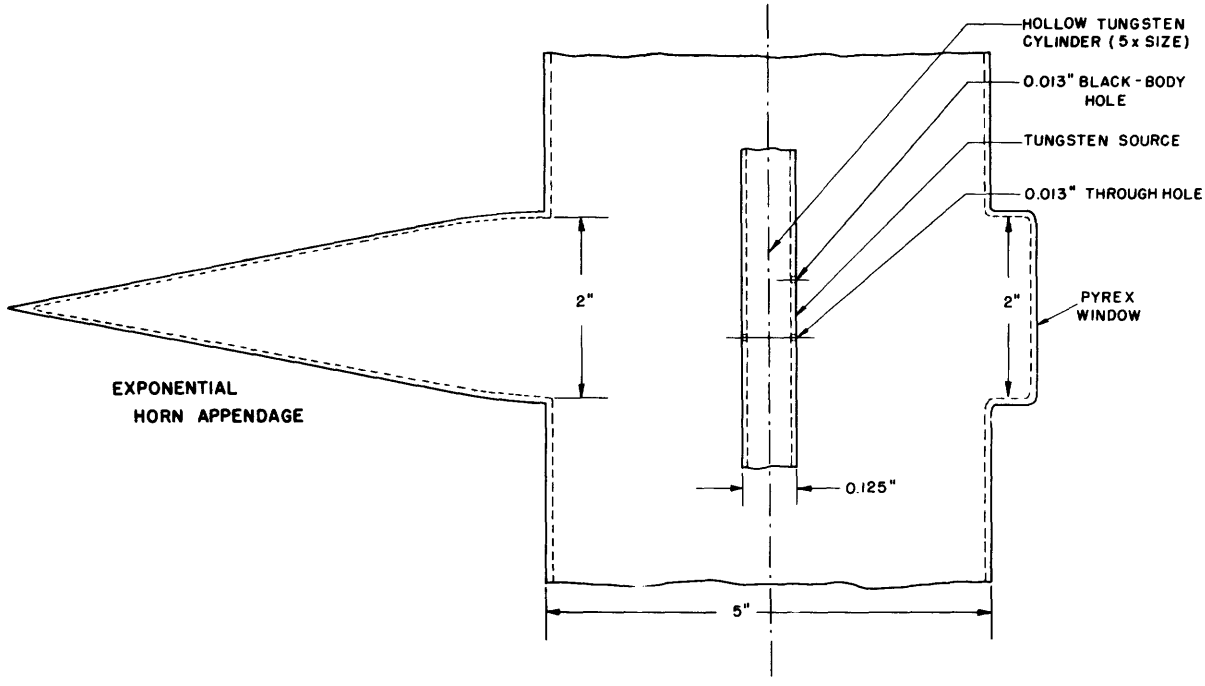

Fig. 4. Side-view diagram of the central part of the emissivity tube.

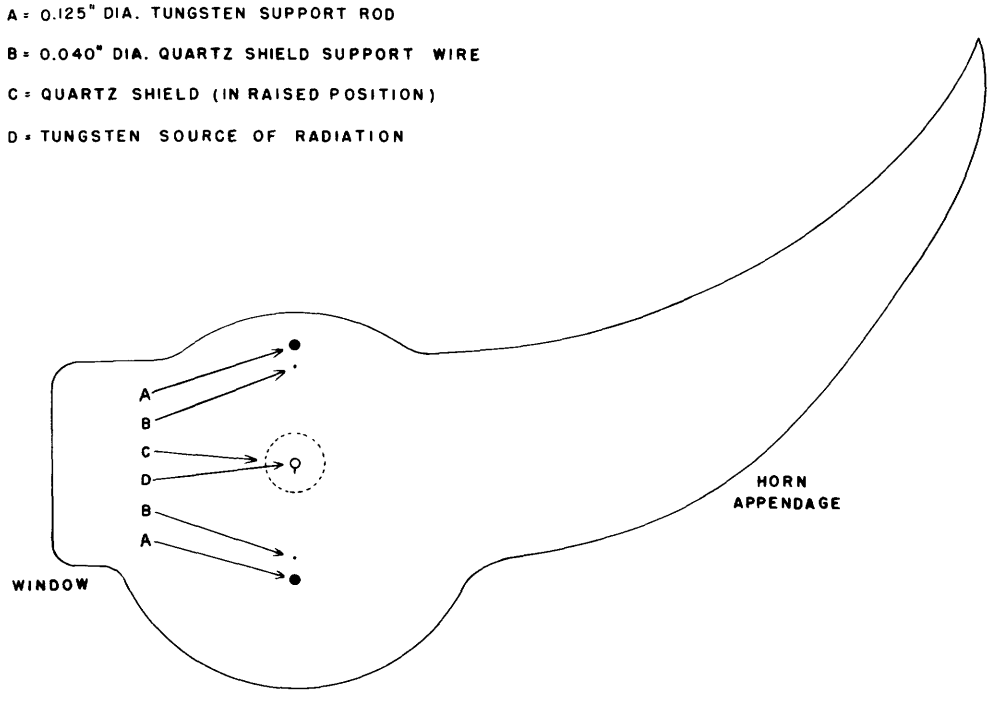

Fig. 5. Central cross section of the emissivity tube.

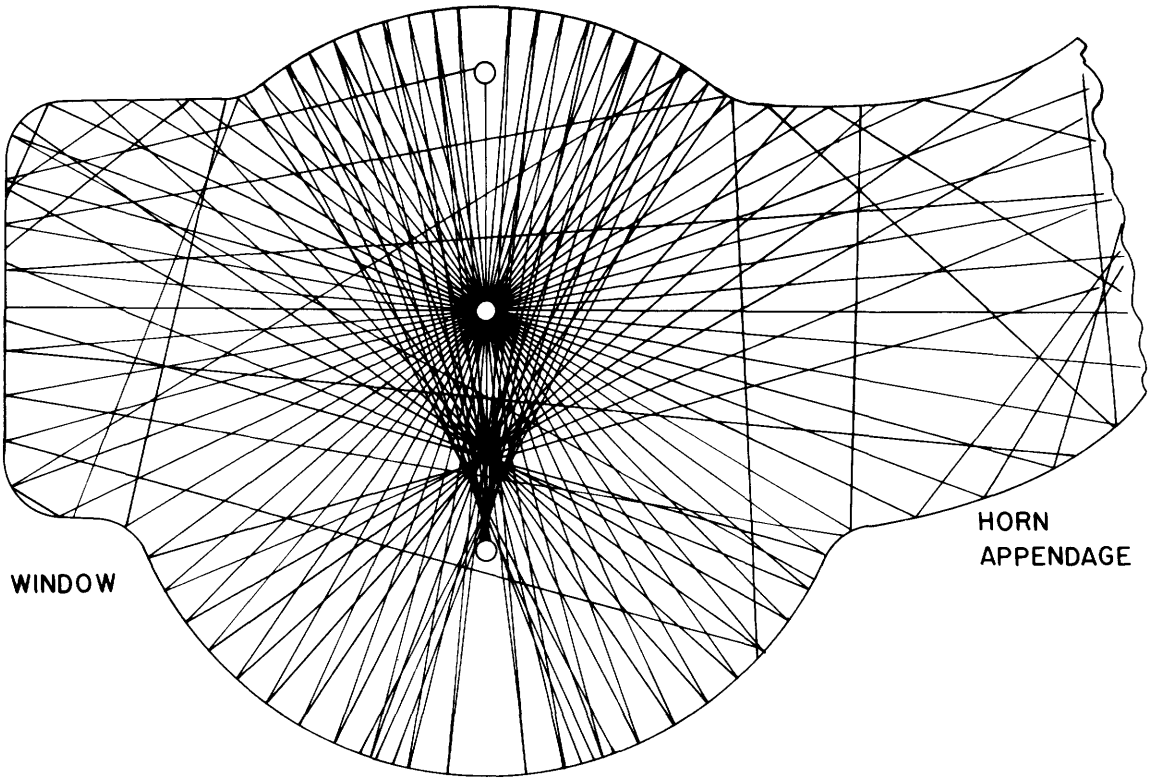

Fig. 6. Reflections from the glass envelope.

quartz shield would descend the vertical tungsten rods by the force of gravity and leave the hollow tungsten cylinder completely exposed. The quartz shield is shown in its lowered position in Figs. 1, 2, and 3.

The emissivity tube was equipped with an exponentially shaped horn appendage to ensure proper operation of the through hole. It can be shown that light falling on this horn from the inside of the emissivity tube is reflected along its walls and eventually out of its end. In order to ensure that any light external to the tube could not interfere with the action of the through hole, the outside surface of the exponential horn was painted with aquadag.

The hollow tungsten cylinder was mounted in a 5-inch O.D. cylindrically shaped glass envelope 1/2 inch to the left of center so that reflections from the glass walls would not form an image of the cylinder superposed on itself. Figure 6 illustrates the effect of offsetting the source and shows clearly how a distorted image of the cylinder is formed approximately 1/2 inch to the right of center or approximately one inch from the cylinder. We have demonstrated (17) that if the glass walls become contaminated with evaporated material, the amount of reflected light is sufficient to seriously disrupt the emissivity measurements if the source is not offset in this manner.

The emissivity tube was equipped with an ionization gauge so that the internal pressure could be monitored continuously. A small side tube attached to the exponential horn

appendage was provided which contained five barium getters for maintaining good vacuum conditions. De Vos (1) estimated that at pressures lower than 10^{-5} mm Hg the chemical effects of the remaining gas need not be feared. However, it appears to the author that the presence of any water vapor would tend to remove tungsten from the cylinder and deposit it on the walls of the glass envelope (21). It was with this "water cycle" in mind that a barium getter was selected.

3.4 PURIFICATION OF TUNGSTEN BY HEAT TREATMENT

In measuring the spectral emissivity of any metal, it is quite important to have an estimate of the purity of the metallic specimen. In the case of the refractory metals the finished specimen can be purified, to some extent, by proper heat treatment. The tungsten ribbon used in this experiment was supplied by Kulite Tungsten Company, 723 Sip Street, Union City, New Jersey. In a letter to the author, dated April 6, 1956, Mr. J. Kurtz, President of the Kulite Tungsten Company, made the following comments about the purity of his product:

> "The tungsten ribbon supplied you, is usually made from so-called non-sag silicated wire, which is a substantially pure tungsten – 99.9% tungsten. The impurities in the form of either sodium or potassium silicate, are introduced to the yellow tungsten oxide to control the grain growth and crystal structure of the finished tungsten wire. However, most of these impurities are driven off during the high temperature sintering operation which metallizes a bar of hydraulically pressed tungsten powder. Usually the impurities left in the finished rod or wire, are in the order of 0.1% and consist largely of SiO_2 and much smaller amounts of K or Na. It may well be that there are spectroscopic amounts of other elements, but these have never been of any consequence in regular commercial application."

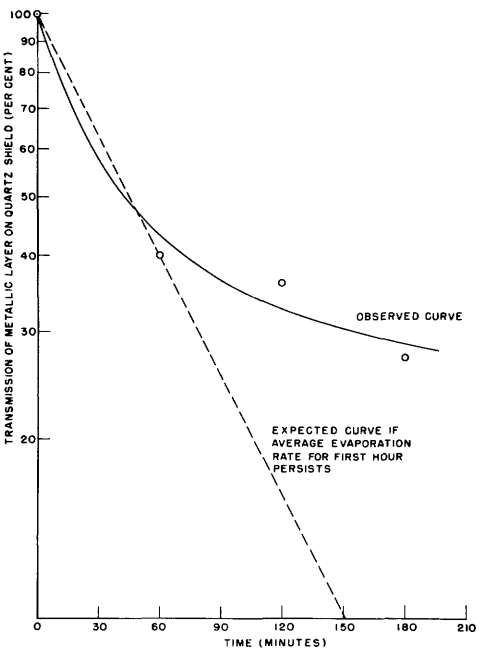

Fig. 7. Estimation of the source evaporation rate at 2750° K.

In order to determine to what extent this Kulite ribbon could be further purified by proper heat treatment, two identical 4-inch tungsten cylinders were fabricated from a single 8-inch length of this tungsten ribbon. One of the cylinders was used in the final emissivity measurements and the other was used in the following preliminary experiment. The second cylinder was mounted in the emissivity-tube envelope with the 0.75-inch (diameter) quartz shield placed coaxially over half of its axial length. The cylinder was maintained at 2750° K for four hours by the passage of unregulated alternating current (60 cps) obtained from a heavy-duty welding transformer. The optical transmission of the metallic film deposited (by evaporation) on the quartz shield was measured by comparing the apparent color temperature of the cylinder alone and the cylinder as viewed through the quartz shield. If the evaporation rate were a constant, we would expect an exponential decrease in the transmission as a function of time.

The wide departure of the observed data from this exponential law (see Fig. 7) indicates that the initial rate of evaporation is quite large in comparison with the subsequent rates. In order to ensure that this rapid initial rate is caused by the evaporation of relatively volatile impurities in the specimen (which would purify the tungsten sample), the metallic specimen and a sample of unheat-treated tungsten were spectrographically analyzed by Dr. Rockwell Kent of Raytheon Manufacturing Company, Newton, Massachusetts, with the following results:

Impurity Element	Mole Percentage Impurity	
	Untreated sample (per cent)	Heat-treated sample (per cent)
Ag	0.001 to 0.0001	0.0003 to 0.00003
Ca	0.001 to 0.0001	0.001 to 0.0001
Cu	0.01 to 0.001	0.001 to 0.0001
Fe	0.01 to 0.001	0.001 to 0.0001
Mg	0.001 to 0.0001	0.001 to 0.0001
Mo	0.01 to 0.001	0.01 to 0.001
Ni	0.001 to 0.0001	Not Detected
Pb	0.003 to 0.0003	0.001 to 0.0001
Sn	0.003 to 0.0003	0.003 to 0.0003
Total	0.040 to 0.0040	0.0183 to 0.00183

The following elements were not detected in either sample: Al, As, Au, B, Ba, Cd, Co, Cr, Ga, Ge, Hg, In, K, Mn, Na, Sb, Si, Sr, Ti, Zn.

Dr. Kent made these comments about this semiquantitative analysis:

> "Because of the complexity of the tungsten spectrum, there is some difficulty in its analysis for trace elements. We have a method which is quite sensitive for trace elements that are more volatile than W, but it is necessary to have the W in

a powder or powdered compound. Attempts at dissolving and converting to oxide were successful, but we found that we added more impurities than were already present. We were finally successful in obtaining the oxide by heating the foil for several hours at about 700° C in air. It is possible that some loss of the most easily volatilized elements could occur, but we are sure that there has been no pickup."

The sodium and/or potassium, and possibly the silicon impurities, mentioned by Mr. Kurtz were probably lost in the oxidizing process described by Dr. Kent. In any event, we would not expect to find these impurities in the heat-treated sample, for they would be evaporated during the early stages of the 2750° K heat-treatment.

It is thus apparent that even the relatively pure sample of tungsten received from Kulite Tungsten Company was noticeably purified by this heat-treatment. Consequently, an annealing schedule for the finished tungsten specimen that was to be used in the subsequent emissivity measurements had to be selected with these data in mind.

3.5 ANNEALING SCHEDULE FOR THE FINISHED TUNGSTEN SPECIMEN

It was necessary to anneal the finished tungsten specimen to allow for recrystallization and reorientation of the material from which the specimen is formed so that the optical and electrical properties of the specimen would not vary with time. De Vos (22) recommended the following annealing schedules:

100 hours at 2400° K or
20 hours at 2600° K or
2 hours at 2800° K.

But there are two other matters which must be taken into account in the present experiment. If the specimen is maintained too long at too high a temperature, the pyrex window of the emissivity tube will become very opaque by virtue of the metal deposited upon it. Also, by considering the data presented in the previous section, it should be possible to select an annealing schedule that would appreciably purify the tungsten specimen. The annealing schedule was selected with all these things in mind.

The quartz shield discussed above can be used to completely cover the source during the anneal and thus protect the window from the evaporated metal. However, as the quartz shield becomes contaminated with evaporated metal its transmission decreases, its absorption (and thus its emissivity) increases, and its temperature rises appreciably. Consequently, as the shield becomes contaminated not only will it reflect more of the incident energy back to the tungsten cylinder (by virtue of its reflecting metallic film) but also its thermal radiation will increase because of its higher temperature and higher emissivity. Thus, if the input electric power to the source is held constant, the source temperature will increase with time. This will result in increased evaporation, decreased quartz-shield transmission, and so forth. This vicious circle has a marked effect on the life of the specimen. Indeed, the life of the specimen discussed in the previous section was only four hours. It is therefore undesirable to allow the quartz shield to become too opaque.

Inspection of the curve presented in Fig. 7 reveals that the evaporation rate is

comparatively constant after the first hour of operation at 2750° K. This suggests that one hour of operation at this temperature will purify the specimen appreciably.

However, following the suggestion of De Vos, one hour of operation at 2750° K is not sufficient to anneal the specimen. We decided arbitrarily that the evaporation rate of tungsten is low enough at 2500° K that prolonged operation at this temperature would not lower the transmission of the window by an objectionable amount. Interpolation of De Vos' recommended annealing schedules reveals that 50 hours of operation at 2500° K should suffice for a satisfactory anneal.

With all these factors in mind, the tungsten cylinder was given the following annealing treatment:

1. The tungsten cylinder was maintained at 2750° K for one-half hour by passing an unregulated alternating current (60 cps) through it. During this phase of the anneal the quartz shield completely covered the specimen, and the emissivity tube was connected to the vacuum pumps.

2. The quartz shield was lowered by heating the molybdenum springs, the emissivity tube was sealed off the vacuum pumps, and the tungsten cylinder was heated by the passage of well-regulated direct current (which was periodically reversed in direction) through it as follows:

   a. 2500° K for 30 hours,
   b. 2800° K for one-half hour,
   c. 2500° K for 20 hours.

During the first stage of this annealing schedule the transmission of the quartz shield was measured by an optical pyrometer. The results of these measurements confirm the data obtained from the previous study.

During the later stages of the annealing schedule the optical transmission of the window was monitored by the same optical pyrometer that was used above (effective pyrometer wavelength = 645 mμ). Measurements of the apparent source temperature as viewed through the window were made with the electric input power to the source held constant. The voltage across the source was also monitored by a Leeds and Northrup Type K potentiometer (for a constant 60-amp current). These data are summarized in Fig. 8. The erratic fluctuations of the source voltage during the middle part of the annealing process are probably caused by a combination of specimen purification (tending to lower the voltage) and metallic evaporation (tending to raise the voltage). However, during the last phase of the heat-treatment, the source voltage was observed to increase approximately linearly at a rate of 0.003 volt per hour, and the transmission of the pyrex window was observed to decrease exponentially with a time constant of 300 hours. A tungsten evaporation rate of 21.8 monolayers per hour explains the linear increase in source voltage if the effects of source purification are negligible. (A monolayer of tungsten is defined here as a film of tungsten with a density of 4.84×10^{-7} gram/cm^2.) The number of monolayers falling on the window can be computed from the geometry of the emissivity tube, since the mean free path of the evaporated material is greater than the

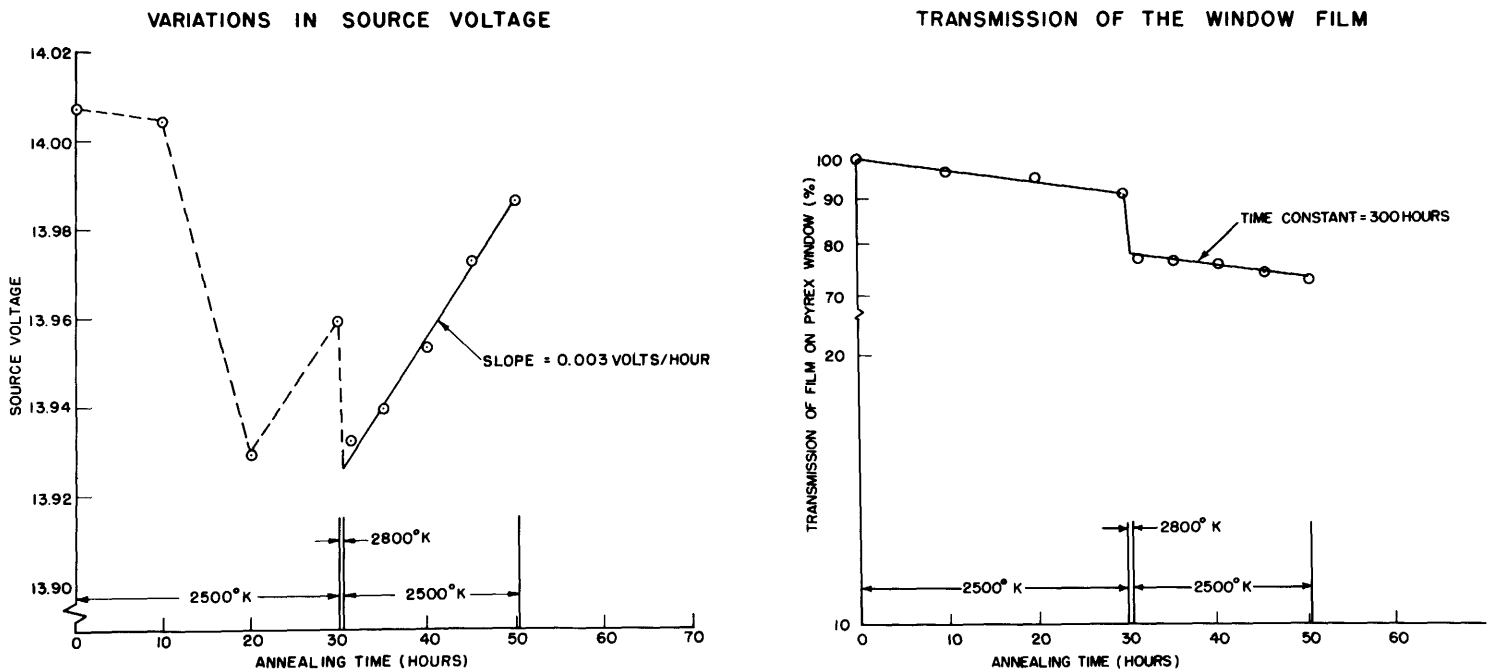

Fig. 8. Changes that occurred during the annealing process.

tube dimensions at the pressures encountered within the emissivity tube (approximately 5×10^{-8} mm Hg, N_2 equivalent). In this way, the transmission of the metallic film on the pyrex window can be computed as a function of the number of monolayers on it, with the following result:

$$\text{Transmission of film on window} = e^{-N/128} \tag{6}$$

where N is the number of monolayers in the film.

If we use this relationship and the measured window transmission, it is estimated that approximately 2100 monolayers of metal (approximately 2 per cent of the source material) were evaporated during the last three stages of this annealing schedule.

No unexplained systematic changes of the optical or electrical properties of the tungsten specimen were observed after this annealing schedule. It is estimated that the heat-treatment given the specimen in this annealing schedule and the heat-treatment it received while its temperature scale was being determined (which will be discussed in Section IV) was nearly twice as much as De Vos recommended. Also, when all factors are considered, it is estimated that the tungsten source is better than 99.99 per cent pure tungsten by virtue of the purification it received during the annealing process.

3.6 OPTICAL SYSTEM

A single f/3.5, 2.5-inch quartz lens equipped with shutter and diaphragm was mounted in front of the pyrex window of the emissivity tube. This lens was adjusted so that an image of the incandescent cylinder magnified 1 1/2 times was formed on a circular aperture of 5-mil diameter that formed the "entrance slit" of a Bausch and Lomb monochromator (19, 20). The light passing through the monochromator was viewed by an RCA Type 931-A nine-stage photomultiplier phototube. This phototube was selected on the basis of high sensitivity and low leakage from a stockpile of thirty new unused tubes.

Since the Type 931-A photomultiplier is so very much more sensitive to the short wavelengths (in the range 400 to 800 mμ), we had to insert a high- (wavelength) pass Kodak Wratten filter between the monochromator exit slit and the phototube to aid the action of the monochromator. We were given a wide selection of these filters so that we could select a filter with a wavelength cut off just below the wavelength that was to be measured. Similarly, a Kodak Wratten filter No. 18-A was used in this same capacity for wavelengths shorter than 400 millimicrons.

The output current of the Type 931-A phototube gives a direct measure of the relative intensity of the light falling on its cathode. Two different electrometers were used (one at a time) to measure this current so that each would serve as a check on the performance of the other. It is noteworthy that no significant difference was found in the readings of these two instruments in any stage of the experiment.

The first instrument was developed by Professor Wayne B. Nottingham, of the Massachusetts Institute of Technology, during World War II. In his system the photocell current develops a small voltage across a precision resistor which is amplified, in turn,

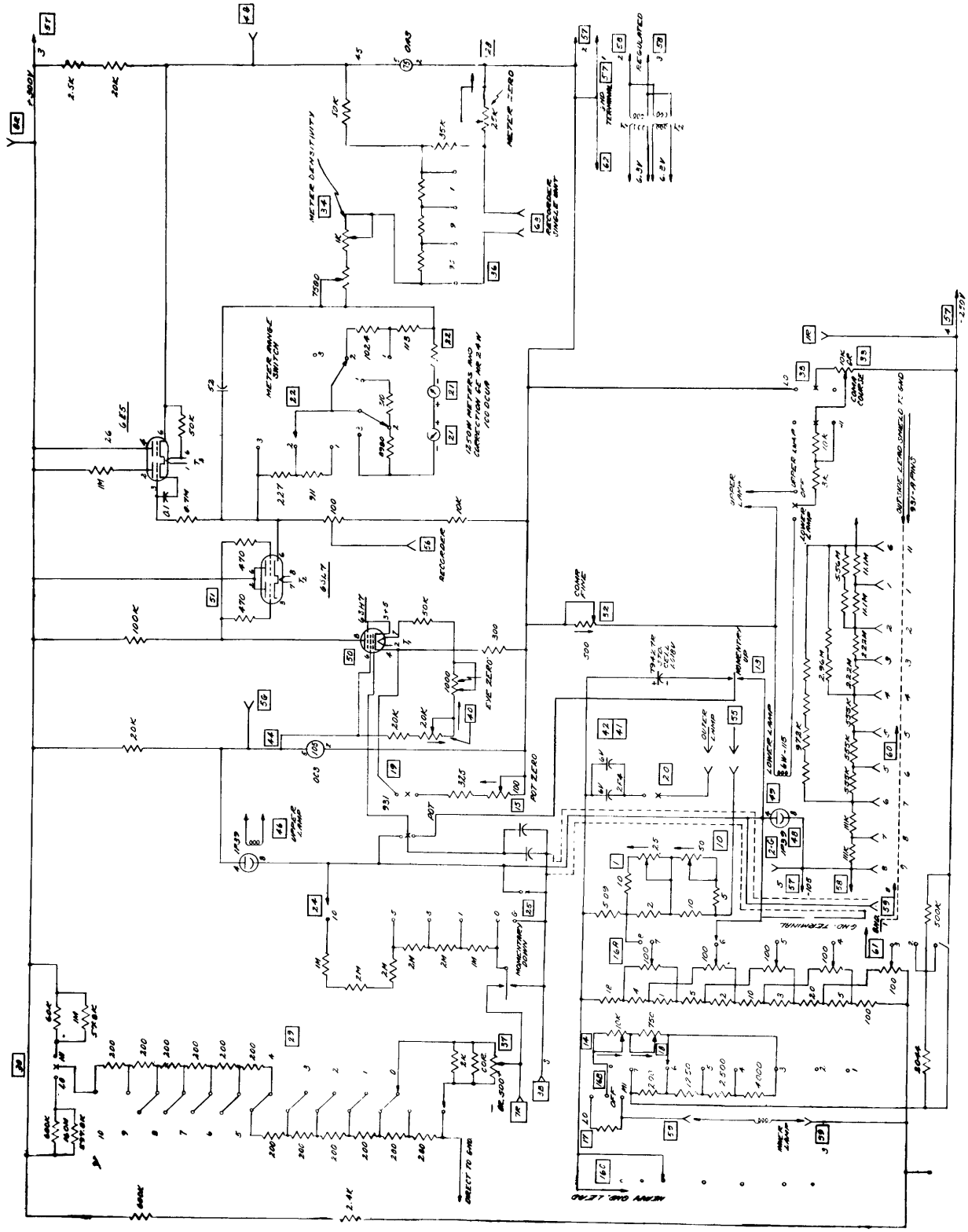

Fig. 9. Schematic diagram of the Nottingham 931 photometer.

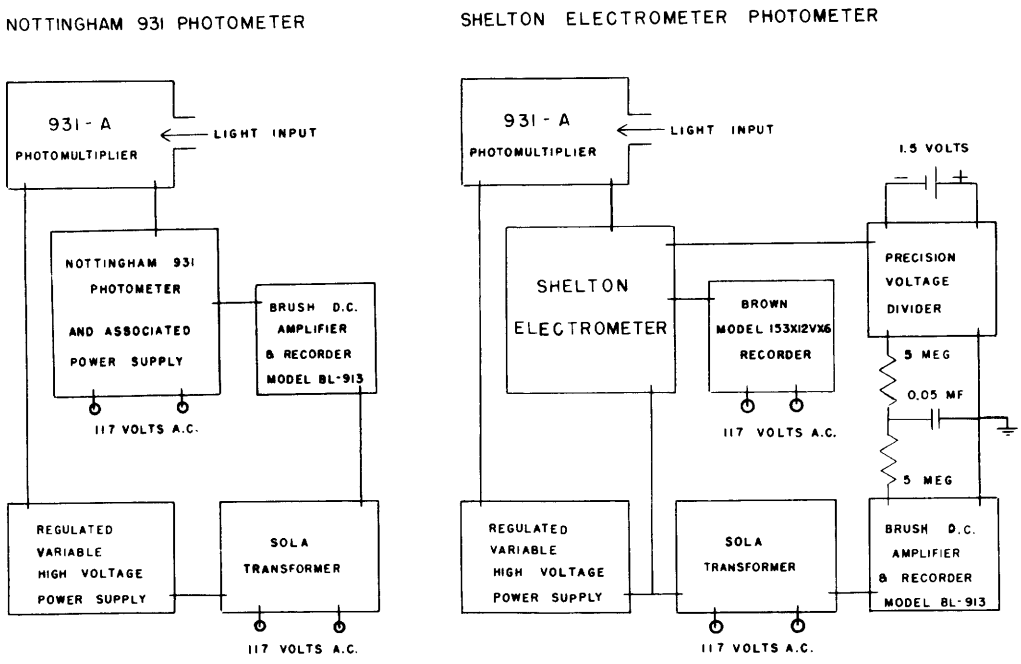

Fig. 10. Block diagrams of the dc photometers.

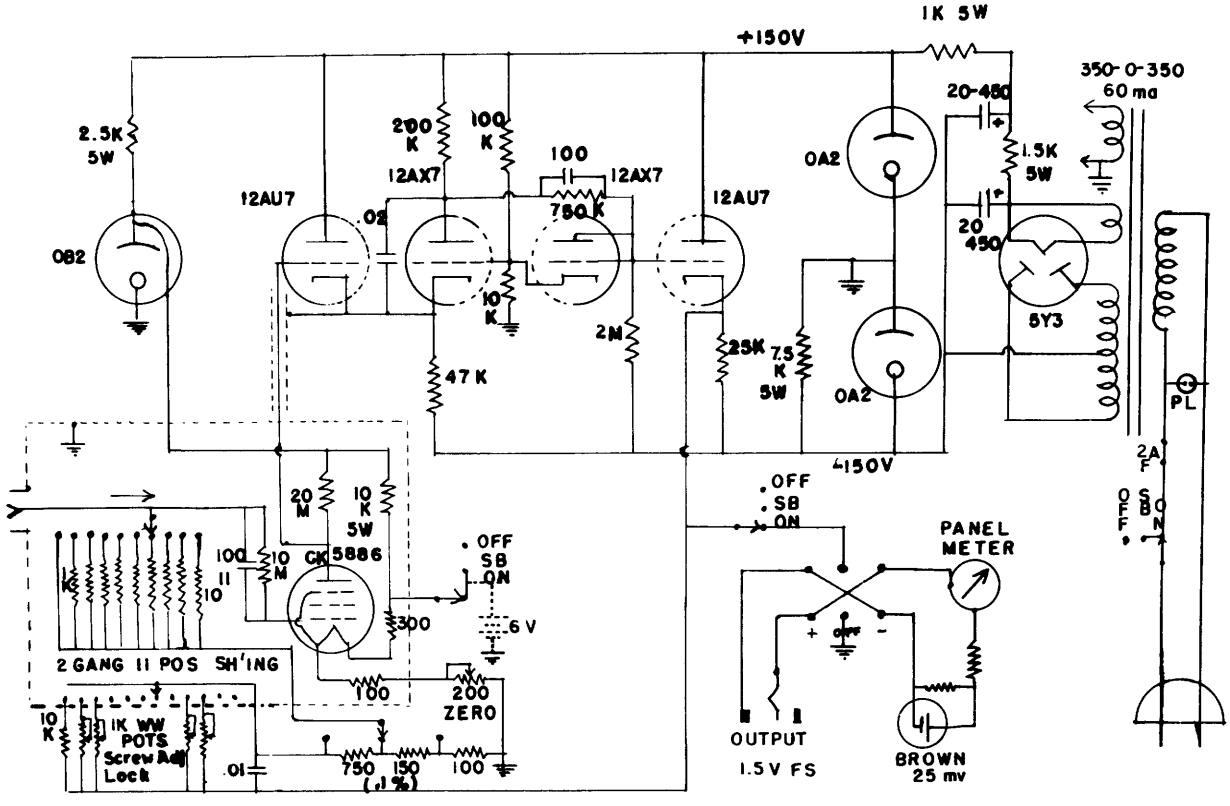

Fig. 11. Schematic diagram of the Shelton electrometer.

by a two-stage dc amplifier (see Fig. 9). Provision is made for reducing the amplifier-input voltage to zero by the application of a known bucking voltage derived from a precision voltage divider. Consequently, this amplifier serves only as a null indicator, so that the accuracy of the instrument is not limited by the stability and linearity of the amplifier. The amplifier output can be observed on meters, on a magic-eye tuning indicator, or, as in this experiment, on a small Brush recorder which enabled visual averaging over the ever-present small fluctuations in light intensity.

The second photometer is built on the same basic principle as the Nottingham instrument (see Fig. 10). The heart of this photometer is a vacuum-tube electrometer developed by Mr. Haywood Shelton (23) in connection with his doctoral thesis. As shown in Fig. 11, this electrometer incorporates a 100 per cent feedback arrangement to ensure that the output gives a faithful measure of the input. The electrometer-output voltage can be observed directly on a Minneapolis-Honeywell Brown recording potentiometer or, by way of another precision bucking-voltage source, on the Brush recorder.

After sufficient practice, we were able to obtain an accurate (three-figure accuracy) reading of the relative light intensity falling on the Type 931-A photocathode in a relatively short time (approximately 5 seconds).

3.7 MECHANICAL CONSIDERATIONS

In order to ensure that mechanical vibrations from the building or accidental shock did not destroy the relative positions of the tungsten cylinder and the optical axis of the lens system, a single mechanical system was constructed which gave firm support to the optical system (lens, monochromator, and photocell) and also provided the mounting for the emissivity tube. We hoped that the system would vibrate as a whole, leaving the relative positions of the tungsten cylinder and the optical system unchanged.

Since it was necessary during the experiment to translate and/or rotate the tungsten cylinder relative to the optical axis of the lens system, this mechanical assembly provided for accurate adjustment (within 0.001 inch) of all three degrees of translation and semi-accurate adjustment (within 0.1 degree) of two of the three degrees of rotation. To facilitate discussion of these motions, consider the following rectangular coordinate system:

1. Assume that the X-axis coincides with the optical axis of the lens system.

2. Assume that the Z-axis is vertical and parallel to the axis of the hollow tungsten cylinder and that it lies on the lateral surface of the cylinder so that the optical system views the light radiated from the origin of this coordinate system.

3. Assume that the Y-axis is perpendicular to the other two axes so as to form a right-handed coordinate system.

Translational motion in the X-(focusing) and in the Y-(scanning) directions was obtained by mounting the entire optical system on a cross-feed lathe vise which is shown schematically in Fig. 12. Since accurate adjustments had to be made in the Z-(vertical) direction as quickly as possible (in order to align the optical axis with the positions of the

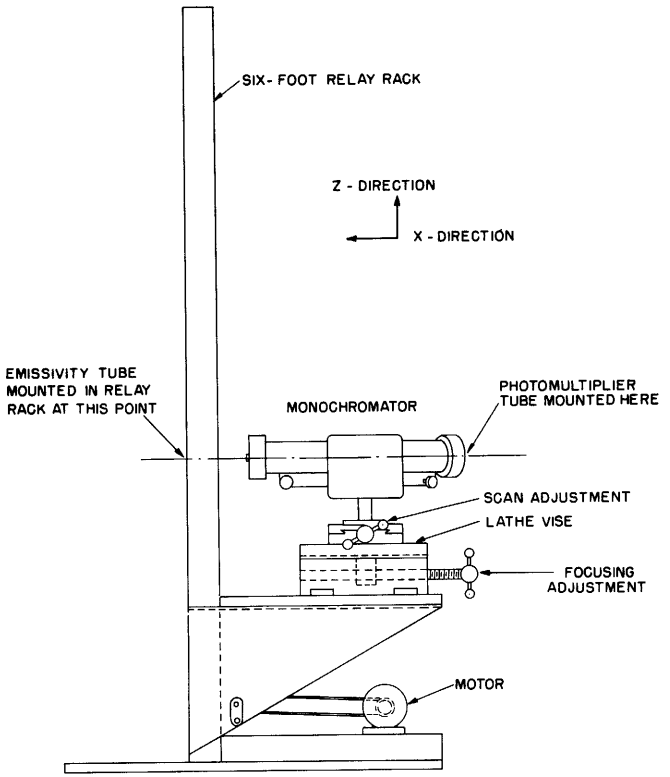

Fig. 12. Optical system mounting assembly.

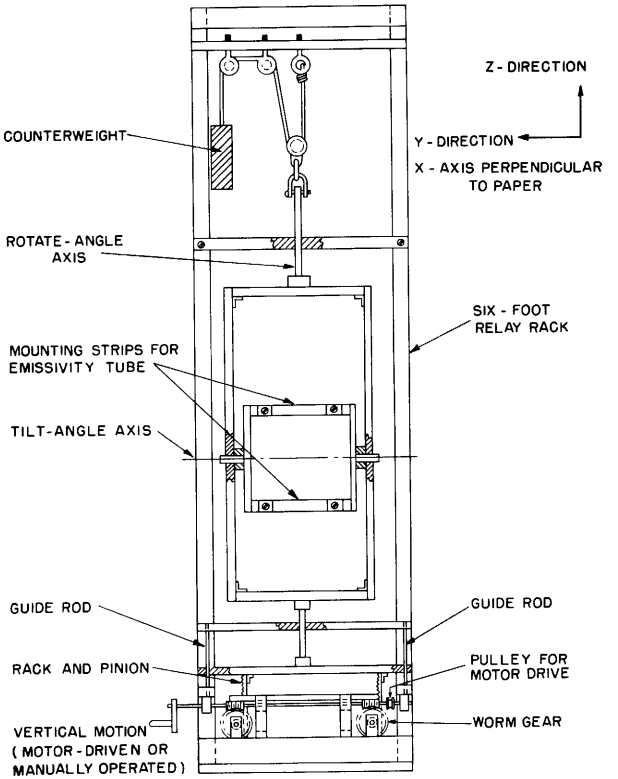

Fig. 13. Emissivity-tube mounting assembly.

black body, source, and through hole), a counterbalanced, motor-driven system of worm, rack, and pinion gears with automatic stops was constructed which was capable of positioning the emissivity tube in the Z-direction within 0.001 inch of the desired position in a maximum time of 15 seconds (see Fig. 13). The azimuthal angle (i.e., the angle between a "diameter line" of the tungsten cylinder and the X-axis in the XY-plane) and the polar angle (i.e., the angle between the cylinder axis and the Z-axis) will be called the "rotate" and "tilt" angles, respectively. Since these angles are not very critical, they were adjusted by moving a lever (by hand) over a calibrated scale.

3.8 SOURCE-CURRENT CIRCUIT

The method by which the hollow tungsten cylinder was heated to incandescence by the passage of direct current is illustrated in Fig. 14. A 15-volt, 3000-ampere electroplating generator was used as a primary power source. In an attempt to stabilize the output of this generator, a 500-amp current (approximately) was continuously "bled off" through a water-cooled bleeder resistor, R_1. Since we had to apply more than 15 volts

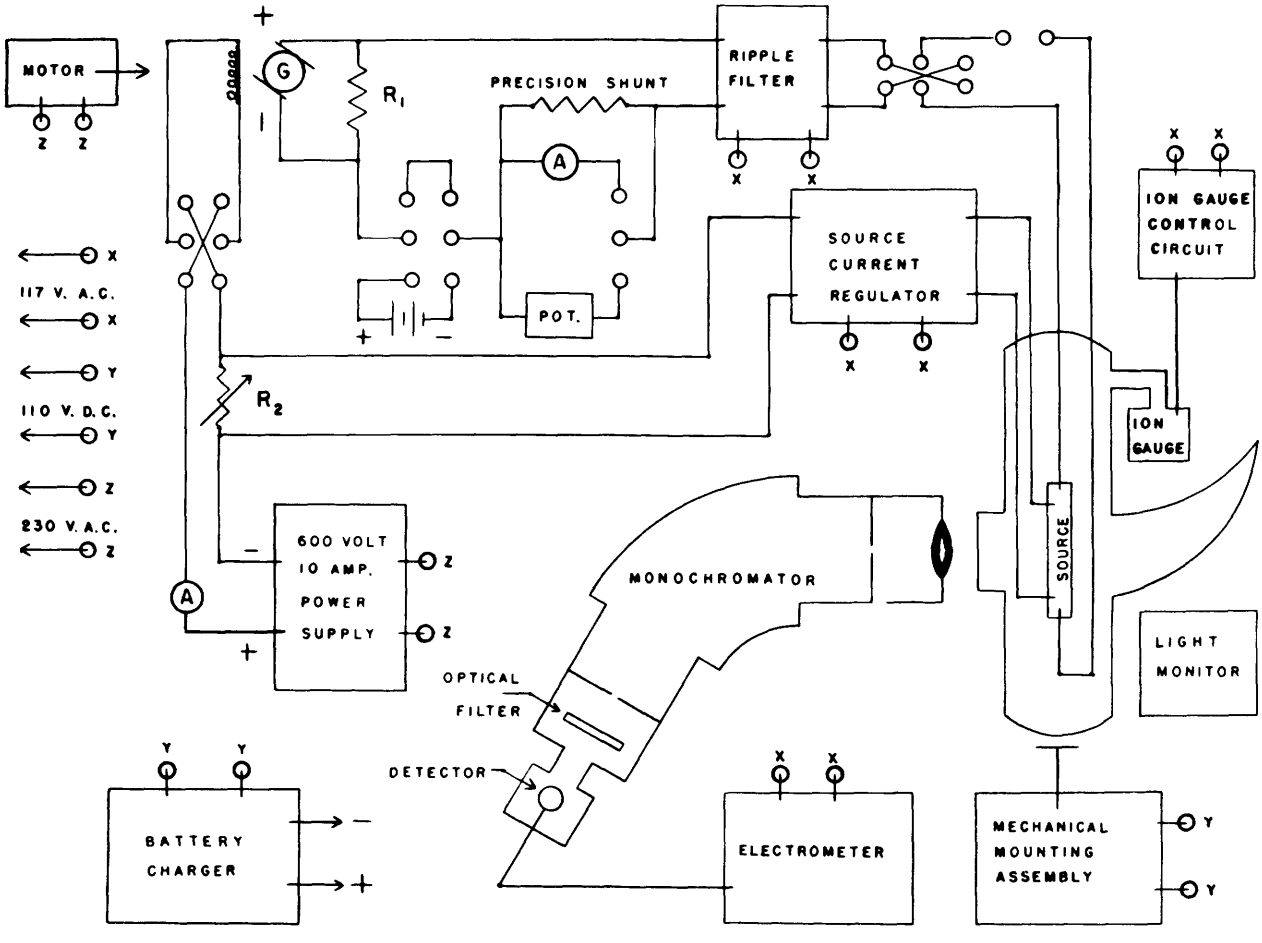

Fig. 14. Schematic diagram of the experimental apparatus.

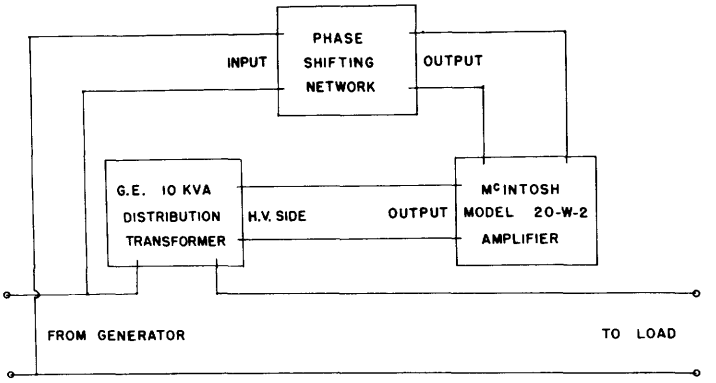

Fig. 15. Block diagram of the ripple filter.

to the circuit in order to heat the tungsten cylinder to the higher temperatures, a 6-12 volt storage battery (composed of six automotive storage batteries connected in series-parallel) was inserted into the source-current circuit. Since the output of the electroplating generator contained a large 10-cps ripple component (approximately ±1 per cent), a ripple filter composed of an amplifier and a coupling transformer (General Electric Company Type 115 single-phase distribution transformer 13,500 volts to 115/230 volts) was included in the circuit (see Fig. 15). A 600-volt, 10-amp, variable dc power supply was used to supply the generator shunt-field power so that we could obtain full rated voltage from the generator and still have some resistance left in the shunt-field rheostat, R_2, to allow for proper operation of the source-current regulator (which will be discussed in Sec. 3.9). Since De Vos (1) recommended that the direction of current flow through the tungsten specimen be periodically reversed in the interest of maintaining a smooth surface in spite of recrystallization, a reversing switch was included in the circuit.

3.9 SOURCE-CURRENT REGULATOR

The regulator used to control the heating current of the tungsten cylinder was really a voltage regulator that tended to maintain a constant voltage across the tungsten cylinder. However, if we assume that the electrical and mechanical characteristics of the tungsten cylinder are independent of time (after annealing), this regulator is equivalent to a current regulator. As we can see from Fig. 16, this regulator is equivalent to a variable resistance in parallel with the shunt-field rheostat of the generator. The plate-to-cathode resistance of the 6L6 control tube(s) was varied by changing the grid bias which in turn was derived from the output voltage of a Type 929 photocell in the 6L6 grid circuit. A Leeds and Northrup moving-coil spotlight galvanometer was connected so that it deflected if the source voltage differed from a comparison (i.e., bucking) voltage supplied by a battery-driven voltage-divider network. The physical arrangement of the circuit was such that when the source voltage was at the desired value, the galvanometer was undeflected, and its "spotlight" illuminated one-half of the Type 929

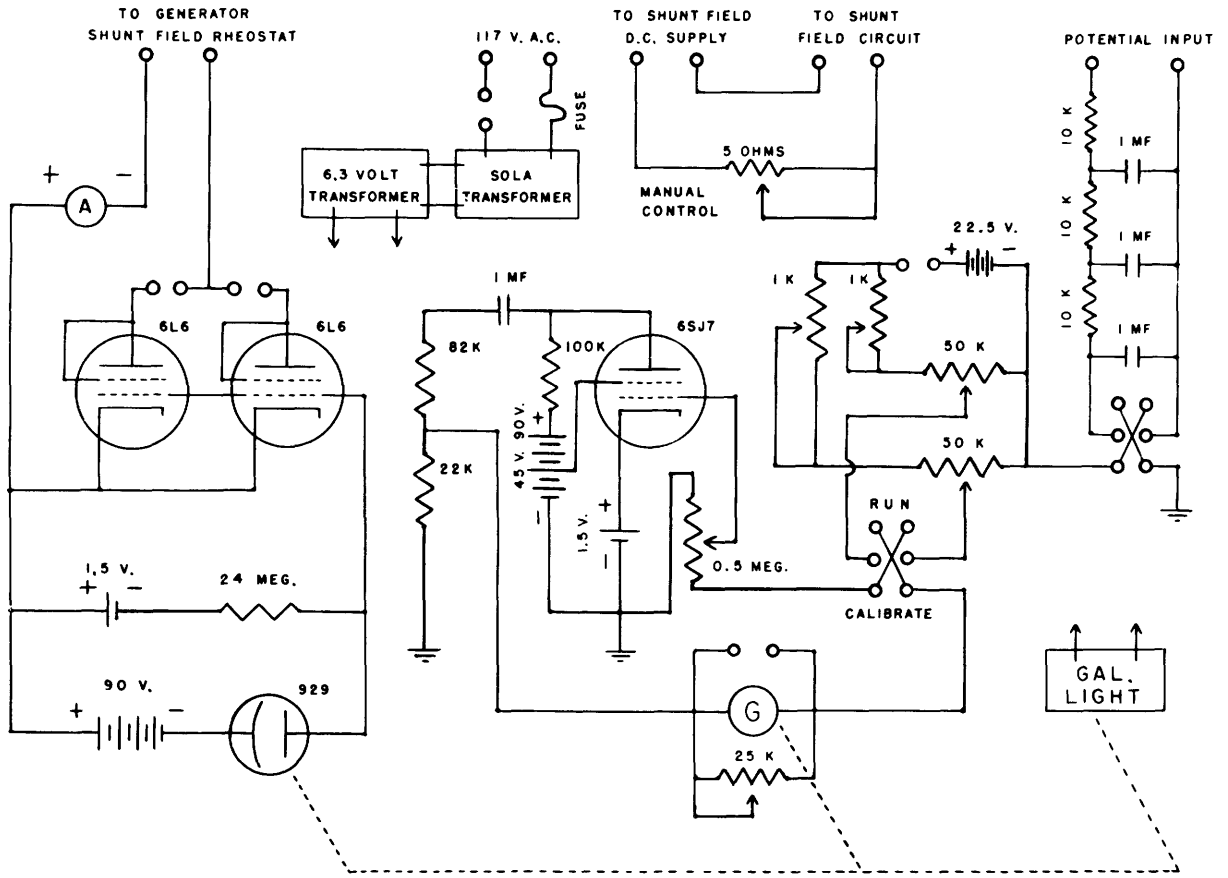

Fig. 16. Schematic diagram of the source-current regulator.

phototube cathode. Consequently, any small change in the generator-output voltage resulted in a galvanometer deflection which, in turn, resulted in a change in the shunt-field current so that the initial output-voltage change was corrected.

In order to reduce the initial overshoot of the galvanometer, and hence reduce its tendency to oscillate, a transient amplifier (i.e., an ac amplifier) with a time constant approximately equal to the generator time constant was so connected that it temporarily fed back an inverse voltage into the galvanometer circuit. This amplifier, however, will not reduce the average sensitivity of the regulator to a steady-error voltage because the coupling condenser in the amplifier plate circuit will eventually reach its new equilibrium charge and the feedback voltage will disappear, allowing the regulator to display full sensitivity to the assumed steady-error signal. Since the rise and decay characteristics of the amplifier and the generator were not identical, we did not expect that the incorporation of this amplifier into the circuit would completely solve all stability problems. However, it seemed to stabilize the regulator a great deal.

A little experimentation with the regulator showed that for a control current of 40 ma per tube (a value suitable for the present purpose) the average fluctuation was approximately 10 ma and appeared to be quite random (i.e., not oscillatory). Continued

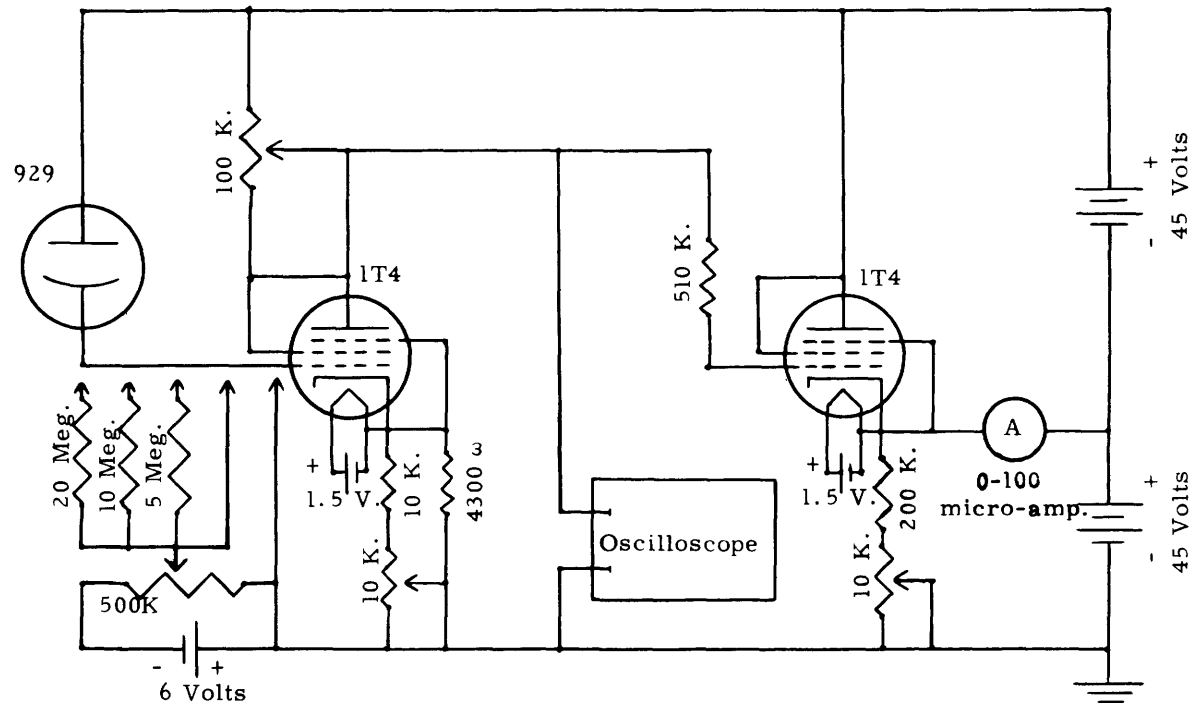

Fig. 17. Schematic diagram of the light monitor.

monitoring with a Leeds and Northrup Type K potentiometer connected to a precision ammeter shunt resistor revealed that the maximum variation of average source current was one part in a thousand, while the average variations were considerably less than this value. With some help from the operator (when the error became so large as to deflect the spotlight completely off the photocell) this regulator was capable of holding the source current within one part in two thousand over a time interval of several hours.

In order to ensure that the average temperature of the hollow tungsten cylinder had not drifted from its initial setting, and to measure any oscillatory variations of temperature about its mean value, a light monitor was used in this experiment. Light from the hollow tungsten cylinder was allowed to fall on a Type 929 phototube located at the rear of the emissivity tube next to the exponential horn appendage. As shown in Fig. 17, the phototube-output voltage was coupled to the input of a dc amplifier along with a variable bucking voltage. This bucking voltage was adjusted so that a suitable reading was obtained on a 0-100 microammeter in the output stage of the amplifier. Any drift in the average temperature (such as would be caused by the regulator spotlight leaving the photocell cathode) would immediately be recognized as a change in this meter reading. An oscilloscope was coupled to the first stage of the dc amplifier to yield a picture of the fluctuations in temperature about the mean value. The gain and phase of the amplified ripple signal fed to the coupling transformer of the ripple filter (Fig. 15) was adjusted in accordance with observations of this oscilloscope display. Thus, this light monitor in conjunction with the source-current regulator and ripple filter ensured that

the temperature of the tungsten cylinder did not differ widely from the desired value.

IV. PRELIMINARY MEASUREMENTS

4.1 MEASUREMENT OF SOURCE TEMPERATURE

Since the temperature coefficient of spectral emissivity is comparatively low, the absolute temperature of the source need not be known exactly. It was therefore felt that the accuracy obtainable with an ordinary disappearing filament optical pyrometer was sufficient for the purpose. A Leeds and Northrup optical pyrometer was calibrated against a similar reference pyrometer that had just been sent for calibration to the National Bureau of Standards. Readings of the apparent temperature of the tungsten surface and of the black-body hole were taken over the range 1100° K to 2700° K as follows:

1. Readings were taken at intervals of 0.5 amp in the range 13.0 to 50.0 amps of heating current (approximately 1100° K to 2200° K).

2. Readings were taken at intervals of 1.0 amp in the range 50.0 to 62.0 amps of heating current (approximately 2200° K to 2500° K).

3. Readings of only the apparent surface temperature were taken at intervals of 2.0 amps in the range 62.0 to 70.0 amps of heating current (approximately 2500° K to 2700° K).

The lower limit (1100° K) was imposed by the visibility of the source in the pyrometer telescope. The upper limit was arbitrarily set by the permissible contamination of the pyrex window by the evaporation of tungsten. If the measurements had been extended to higher temperatures, the transmission of the window would have been lowered by an undesirable amount.

At each heating-current value, the apparent temperatures of the source and of the black-body hole were measured four times in succession, the precaution being taken to thoroughly destroy the old optical balance of the pyrometer before each new measurement. Since it was found that the author's judgment of the optical balance differed from day to day, the procedure described above was repeated on four nonconsecutive days. Thus, the temperature was measured 16 times at each heating-current value quoted above. Since the optical pyrometer was calibrated by the author, we decided that other people (with different optical characteristics) should not be allowed to make measurements, as was previously planned (17).

A correction to both the surface and the black-body temperatures had to be made because of the presence of the pyrex window (and its metallic film). The optical transmission of the pyrex window alone was measured by the Color Measurements Laboratory of M.I.T. at the effective pyrometer wavelength (645 mμ) before the final assembly of the emissivity tube and it was found to have a value of 0.916. The transmission of the film on the window was determined from the data taken during the annealing operation discussed above. With these transmission values known, the corrected temperature could be computed from the following approximate relation derived from

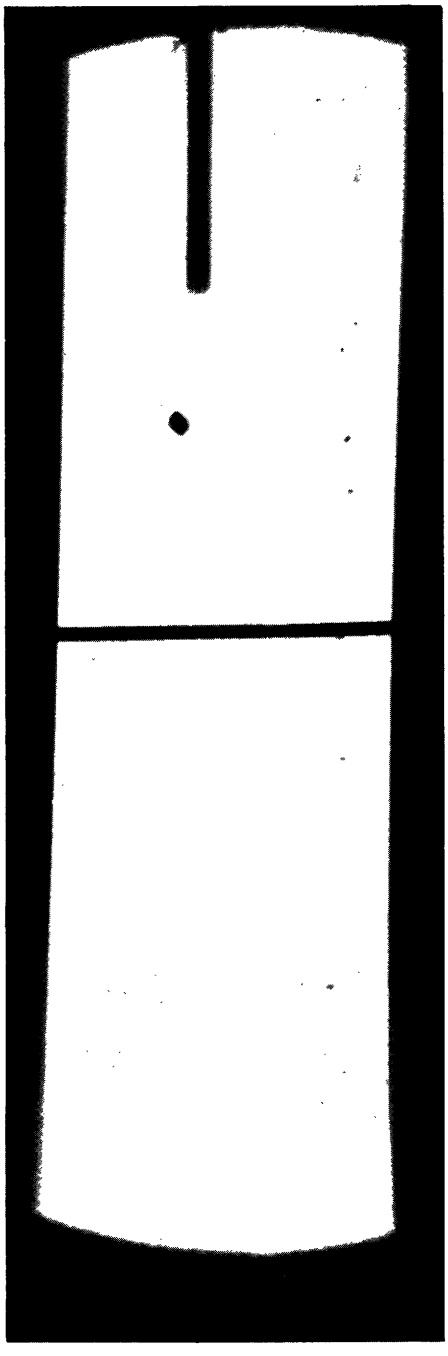

Fig. 18. Photograph of the tungsten specimen as viewed through the optical pyrometer.

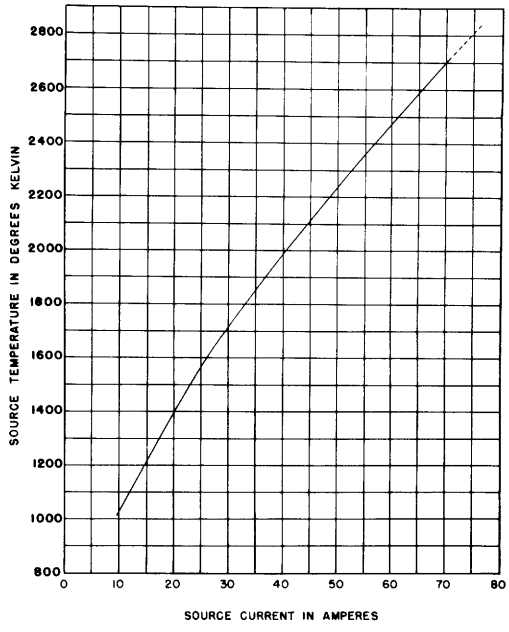

Fig. 19. Temperature scale of the tungsten source.

the Planck radiation law (Eq. 1):

$$\frac{1}{T_1} - \frac{1}{T_2} = \frac{K\lambda}{hc} \ln \frac{1}{\text{TRANSMISSION}} \tag{7}$$

where T_1 is the measured apparent temperature, T_2 is the corrected temperature, and λ is the pyrometer effective wavelength = 6.45×10^{-7} meter.

The relative accuracy of the surface temperatures was greater than the accuracy of the black-body temperatures because of the smallness of the black-body hole in comparison with the optical-pyrometer reference filament (see Fig. 18). The emissivity data of De Vos (1) was used to convert the surface temperatures into true (black-body) temperatures. The temperatures computed in this way agreed with the measured black-body temperatures within a mean square error of 2.6° K. This justifies the use of De Vos' emissivity data for the present problem.

A smooth curve, which fitted these computed true temperatures best, fitted within a mean square error of approximately 3° K. When all known sources of error are analyzed, with the exception of the error in the calibration of the reference pyrometer, we feel that the points on this final curve are accurate within a maximum mean square error of 10° K. (The error in the calibration of the reference pyrometer is approximately ±5° K at 1400° K, and ±15° K at 3100° K.)

The results of these measurements are illustrated in Fig. 19 and summarized as follows:

True Temperature (°K)	Heating Current (amp)	Slope of the curve (°K/amp)
1200	14.50	41.7
1400	19.87	35.2
1600	26.07	30.9
1800	32.96	28.1
2000	40.45	26.0
2200	48.50	24.4
2400	56.95	23.3
2600	65.75	22.4

4.2 EFFECTS OF CRYSTALLINE STRUCTURE

The question arises whether or not the emissivity ratio depends upon the crystallographic orientation of the surface under investigation. Certainly, if this effect exists, it must be small, since evidence of crystalline structure has never been observed in a tungsten specimen viewed through an optical pyrometer.

Since the present apparatus is capable of measuring relative light intensity with a greater precision than an optical pyrometer, an attempt was made to detect the presence

of crystalline structure in the present specimen for different angles of viewing the surface and for different degrees of polarization. The tungsten specimen that had been maintained at 2750° K for four hours (see section 3.4) had a well-developed crystalline structure that was plainly visible under the microscope. The average crystal size was 13.9 ± 8.0 mils along the cylindrical axis and 5.6 ± 4.0 mils perpendicular to the cylindrical axis. It is not unreasonable to estimate that the present specimen has crystals of approximately the same size. Since the optical system views an area 3.3 mils in diameter (aperture size/magnification), crystals of this size should be discernible if they emit different amounts of light.

The emissivity tube was raised mechanically in front of the stationary optical system by means of a synchronous motor attached to the elevator mechanism at a rate of about 1 mil per second. The output of the Shelton electrometer was observed on the Brush recorder. A disk Polaroid between the pyrex window of the emissivity tube and the quartz lens served as a polarizer. We could adjust the cross-feed lathe vise, on which the optical system was mounted, so as to offset the axis of the lens from the axis of the hollow tungsten cylinder in the scan direction. Thus, as the emissivity tube was raised, the optical system scanned along a vertical line drawn on the lateral surface of the cylinder viewing the tungsten surface at some predetermined angle. Readings were taken of relative light intensity against axial position (elevation) of the cylinder for normal viewing angle (0°), 30° viewing angle, and 60° viewing angle, for each direction of polarization (i.e., perpendicular and parallel to the plane of incidence). Crystalline structure should show up on these curves as reproducible fluctuations in the general trend of the curve that are caused by the axial temperature gradient (see section 4.3).

Fluctuations caused by small variations in the heating current were quite evident in the data, and they limited the accuracy to which intensity measurements could be made. When all factors were considered, we felt that fluctuations of ±0.4 per cent in intensity would be quite noticeable above the random fluctuations and could be easily checked for reproducibility. In the data taken at normal viewing angle and at 30° viewing angle no reproducible fluctuations were found. However, at 60° viewing angle reproducible fluctuations with a magnitude of 0.6 ± 0.15 per cent were evident in the data.

There are several effects besides crystalline structure which, if present, could give rise to such reproducible fluctuations. Nonuniformity in the thickness of the cylindrical wall of the specimen could cause local temperature variations which could correspond to the observed light-intensity variations. However, we felt that this kind of nonuniformity should effect all of the data equally (on the average) and not favor the large viewing angles; therefore we did not consider it an important factor. Similarly, variations in the transmission of the emissivity-tube window can be considered negligible. Distortions in the shape of the cylinder as small as one degree could give rise to light-intensity fluctuations, as observed in the 60° viewing-angle curve. Inspection of the data presented in Section VI, sections 6.1 and 6.2, reveals that this effect

definitely favors the large viewing angles. However, contrary to the experimental evidence, it also reveals that the fluctuations observed for the two degrees of polarization should be 180° out of phase. For this reason, it was decided that the effects of local distortions in the shape of the cylinder would not account for the observed fluctuations.

In view of all these considerations, it can be said with a fair degree of confidence that, for the tungsten specimen used in this experiment, the apparent emissivity variations caused by crystallographic structure, local distortions in shape, and nonuniform wall thickness were equal to or less than ±0.6 per cent in the temperature interval 2000° K to 2400° K and the wavelength interval 400 to 700 mμ (the ranges of temperature and wavelength represented by the data), for viewing angles ≤ 60°.

4.3 TEMPERATURE GRADIENTS

Since the output light intensity is a rapidly varying function of temperature (in accordance with the modified Planck radiation law, Eq. 2), it is important to have knowledge of any temperature gradients that might exist in the neighborhood of the black-body hole.

Since the solid tungsten rods that support the ends of the hollow tungsten cylinder conduct some heat away from the cylinder, we would expect a temperature variation along the axial length of the cylinder. However, from symmetry arguments, this effect will be a minimum at the center of the hollow tungsten cylinder equidistant from the solid supporting rods. This was the reason for placing the black-body hole in this favorable position.

The Planck radiation law (Eq. 1) can be used to show that the temperature difference between two points with different output light intensities is approximately:

$$\Delta T = T_1 - T_2 = \frac{T_o^2 K \lambda}{hc} L_N \frac{I_1}{I_2} \tag{8}$$

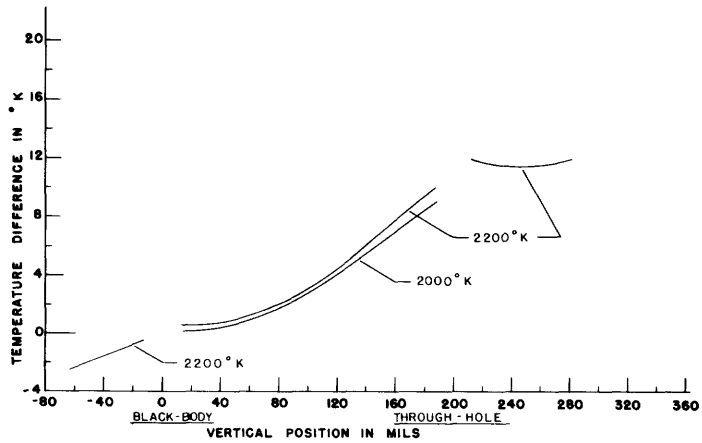

Fig. 20. Axial temperature gradient in the source for the indicated black-body temperatures.

where T_1, I_1 and T_2, I_2 are the temperature and radiant intensity at one position called "1" and another position called "2," respectively, where $T_o^2 = T_1 T_2$. By using this relation we can compute the difference in temperatures corresponding to the variation in light intensity as the cylinder is scanned in the axial direction between the black-body and through-hole positions (as we did in the study of the effects of crystalline structure). In this way, we obtain a plot of the temperature difference against the axial position. Figure 20 represents the results of such measurements, with the assumption that the black-body temperature is known from the pyrometer measurements. It is important to note that if the spot selected for the emissivity measurements is chosen close enough to the black-body hole position, there will be a negligible difference in temperature between them (the spot actually used was 30 mils below the black-body hole). The temperature difference of approximately 12° K between the black-body and through-hole positions was attributed, at least in part, to the increased current density at the through-hole position because of the presence of the "two through holes." Since the through-hole reading was a comparatively small correction to the emissivity, this temperature difference is a second-order effect and will be neglected in the interpretation of the results.

Angell (18) studied the possibility of the existence of a temperature difference between the inside and outside of a cylinder that is similar to the one used in this experiment. His results lead to the conclusion that this effect is negligible for a cylinder of the present dimensions. The method of fabrication of the cylinder from the flat ribbon was selected in order to minimize temperature gradients around the cylindrical cross section. Consequently, it would appear that the only sizeable temperature gradient present is the gradient in the Z-direction, and, by taking the necessary precautions, the effects of this temperature gradient can be made negligible.

4.4 THE THROUGH HOLE

The manner in which the radiant light intensity varies as the through hole is scanned in the Y-(scan) and the Z-(vertical) directions is shown in Fig. 21. Notice the comparatively constant light intensity of the cylindrical surface on either side of the through-hole minimum. Since the front and rear sections of the through hole were not exactly circular or of the same size (the front hole is probably a little larger), an irregular "black-body effect" was observed at the edges of the through hole. This effect is quite noticeable in the photograph of Fig. 18 as an annular ring of bright light around the edge of the through hole. In Fig. 22 the emissivity tube has been rotated about the Z-axis to purposely misalign the through hole in order to show the back wall of the cylinder. Notice how well the "black-body effect" shows up in this picture. If this black-body effect were not present, the variation in light intensity as we proceed from the center of the through hole would be almost independent of the chosen direction (for a limited distance), as we would expect if the radiation at this point was composed only of scattered light. The relative flatness of the through-hole minimum would also tend to justify this conclusion.

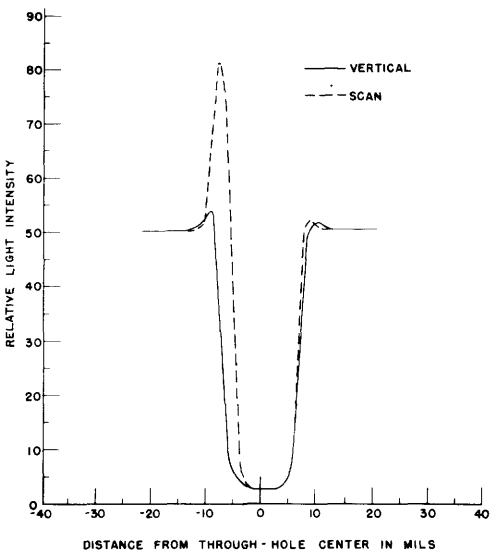

Fig. 21. Vertical and scan through-hole cross sections.

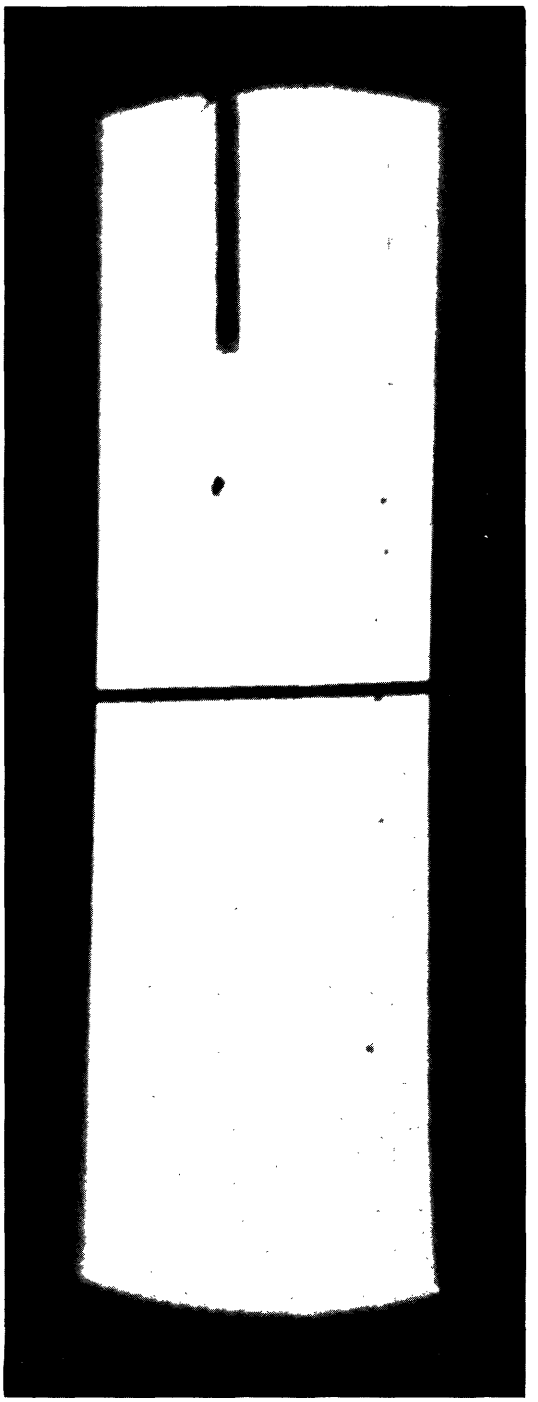

Fig. 22. Photograph of the tungsten specimen as viewed through the optical pyrometer.

4.5 THE BLACK-BODY HOLE

It is apparent that light entering the black-body hole at normal incidence can be reflected out again by the action of the rear wall of the hollow cylinder. Consequently, the system will not appear as a black body when viewed in this position. However, with sufficient rotation in the azimuthal direction or sufficient tilting in the polar direction, it becomes impossible for an incident ray of light to be reflected out of the black-body cavity by a single reflection from the rear wall of the cylinder (assuming specular reflection at the rear wall). Therefore, we would expect the rotate- and tilt-angle light-intensity profiles of the center of the black-body hole to show a broad minimum at normal incidence, leveling off to black-body radiation at sufficiently large viewing angles (3° to 4°) in either direction.

It was necessary to correct the observed light-intensity profiles of the black-body cavity for the transmission characteristics of the pyrex window (and its metallic film). It will be shown in Section VI that the tungsten surface radiates in accordance with Lambert's cosine law (to a good approximation) for unpolarized light at small viewing angles. Therefore, it was possible to measure the relative transmission of the window as a function of the viewing angle by observing the apparent rotate- and tilt-angle light-intensity profiles of the surface of the hollow tungsten cylinder. The relative correction factor (reciprocal relative window transmission) obtained in this way is shown in Fig. 23. The observed light-intensity profiles of the black-body hole were multiplied by this correction factor to obtain the values of light intensity that would have been obtained in the absence of the window. Notice that the window is properly aligned in the rotate direction, but is approximately two degrees misaligned in the tilt direction.

The observed rotate- and tilt-angle light-intensity profiles of the center of the black-body hole (corrected for the varying window transmission) are shown in Fig. 24. The central minimum at normal viewing angle is quite apparent in these curves. The zero positions of the rotate and tilt angles were defined as those positions in which the "two

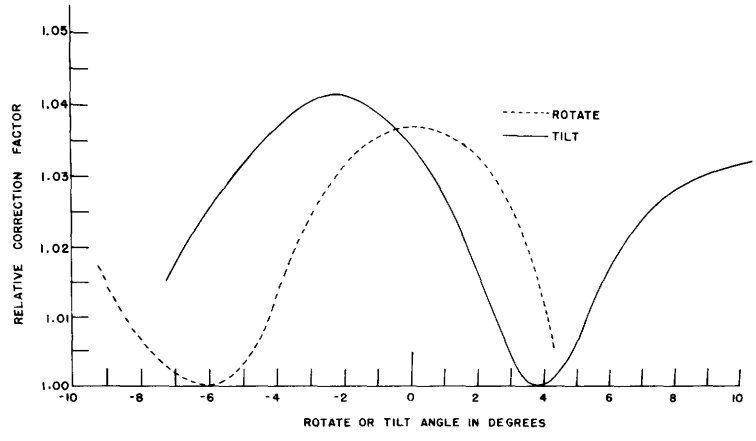

Fig. 23. Window-transmission correction factor.

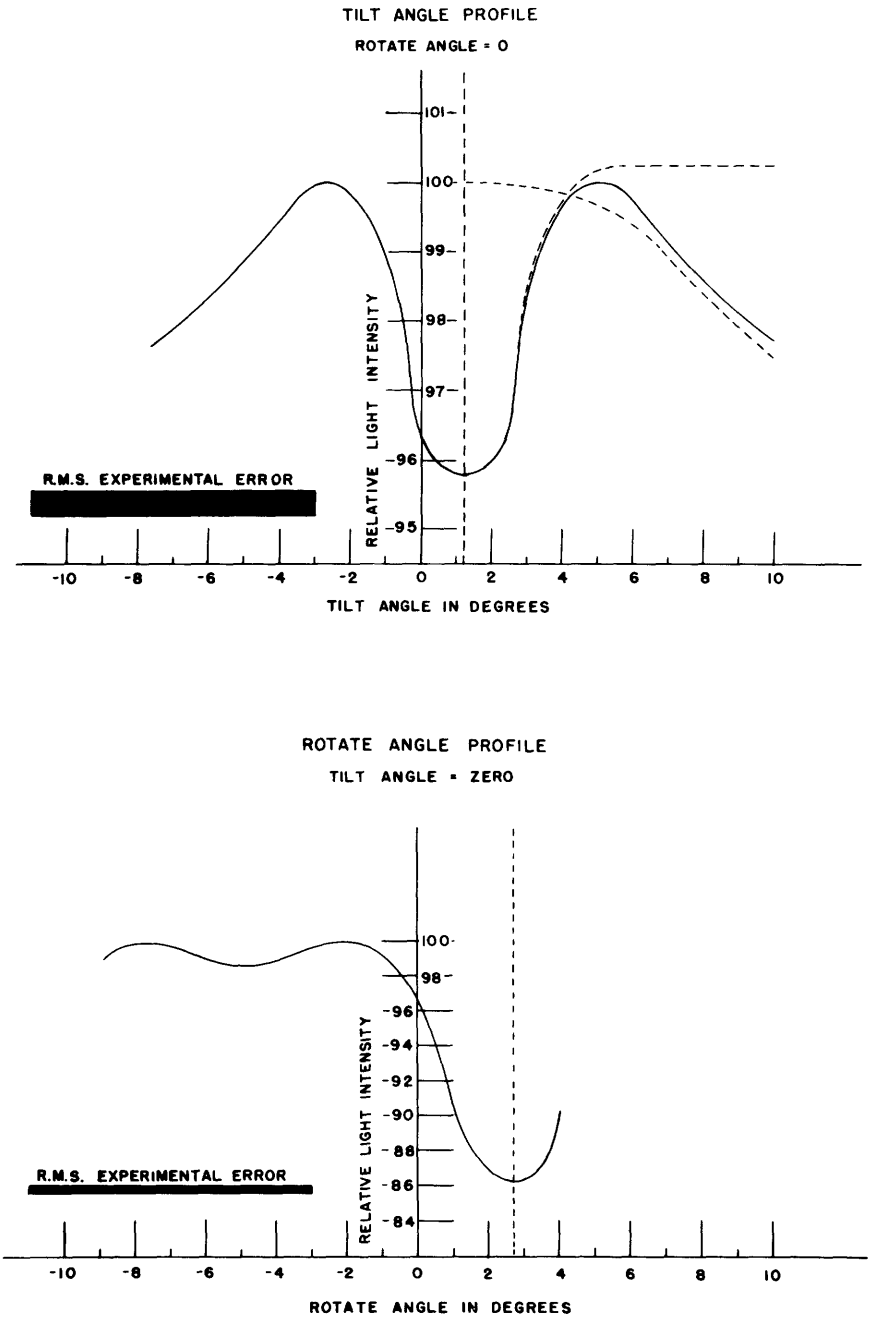

Fig. 24. Angular cross sections at the center of the black-body hole.

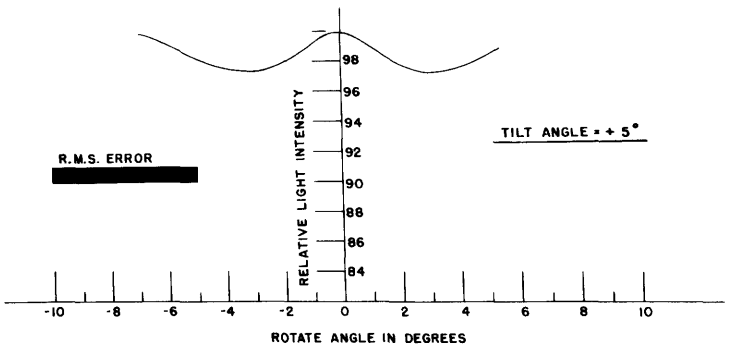

Fig. 25. Rotate-angle profile at the tilt-angle maximum.

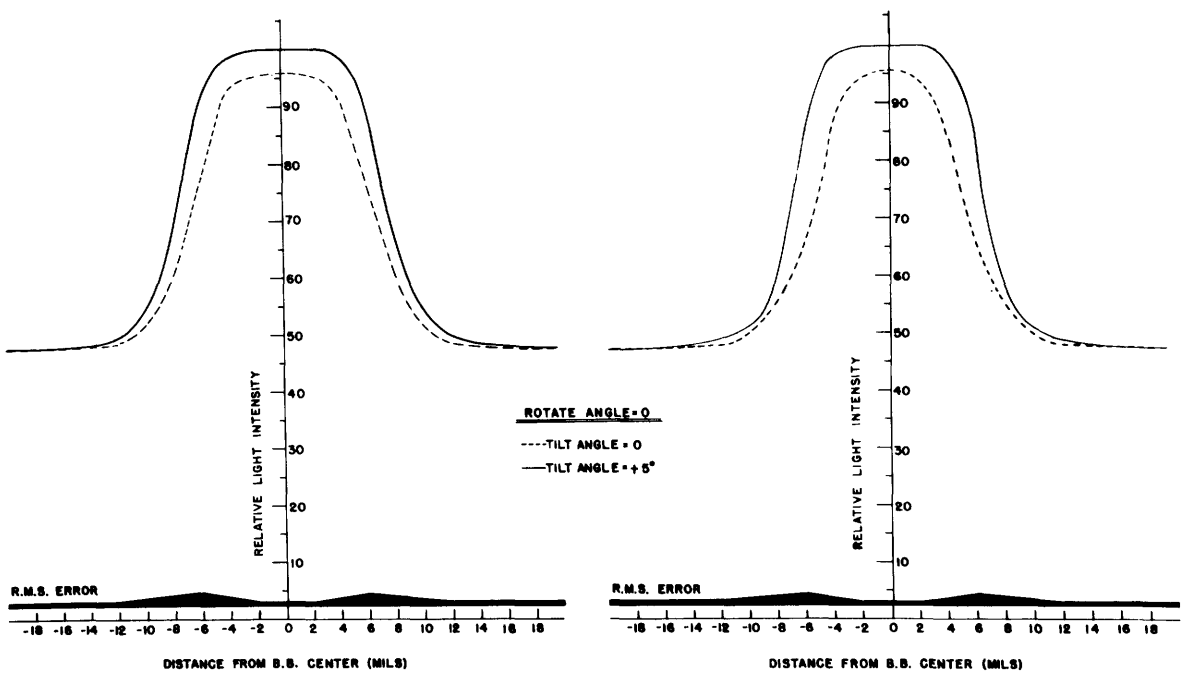

Fig. 26. Vertical and scan cross sections of the black-body hole.

through holes" were aligned along the axis of the optical system. Consequently, normal viewing angle for the black-body hole should be defined in terms of these minimum points (as shown by the vertical dashed lines of Fig. 24) instead of the zero of the rotate and the tilt angles.

Notice that the two curves of Fig. 24 rise to the same height (arbitrarily assigned the value of unity) and then decline with larger viewing angles instead of remaining constant as we expected. The dashed curve on the right-hand side of the tilt-angle profile illustrates what might be happening. A combination of the expected curve and some mechanism tending to reduce the light intensity with increasing viewing angle can give rise to the observed curve. If this is true, we estimate that the peak of the observed tilt-angle (or rotate-angle) profile would not quite reach the black-body value (of approximately 1.002). The mechanism responsible for this postulated "fall-off characteristic" remains a mystery to the author. A thorough investigation of the experimental technique failed to reveal any experimental parameter that could account for this effect (lens aberration, improper adjustment or alignment, temperature gradients, and so on). As far as the author knows, there is no reason to expect this behavior from the black-body cavity.

As shown in Fig. 25, the tilt-angle maximum (and presumably the rotate-angle maximum) represents the maximum amount of light obtainable from the black-body hole and is, therefore, the best approximation to black-body conditions obtainable with the present arrangement. The scan and vertical cross sections (Fig. 26) for zero tilt angle and for +5° tilt angle (the tilt-angle maximum point) seem to confirm this assumption.

Consequently, the tilt-angle maximum at +5° was assumed to represent black-body radiation in the emissivity measurements. However, in estimating the rms error of the emissivity measurements, the uncertainty about the correctness of this assumption (assumed to be 0.2 per cent) was taken into account.

V. THE SPECTRAL EMISSIVITY OF TUNGSTEN

The basic method used to measure the spectral emissivity of tungsten was summarized in section 3.1. Figure 27 illustrates the basic principle of this method. Since we had to view the black-body hole at a tilt angle of +5° in order to obtain black-body radiation, the peak of the black-body hole maximum in Fig. 27 (which was obtained at normal viewing angle) is approximately 4 per cent below the black-body level. Since the through-hole reading was approximately 2 per cent of the black-body reading at all temperatures and wavelengths, the value of 2.3 indicated in Fig. 27 is typical of the values obtained throughout the experiment.

In the experimental measurement of spectral emissivity, the complete curve of Fig. 27 did not have to be taken, since only the three indicated points are of interest. In the interest of maintaining constant source temperature, we decided to measure the black-body and tungsten-surface light intensities as rapidly as possible. Therefore, the tungsten surface was viewed at a tilt angle of +5°, instead of taking the time to

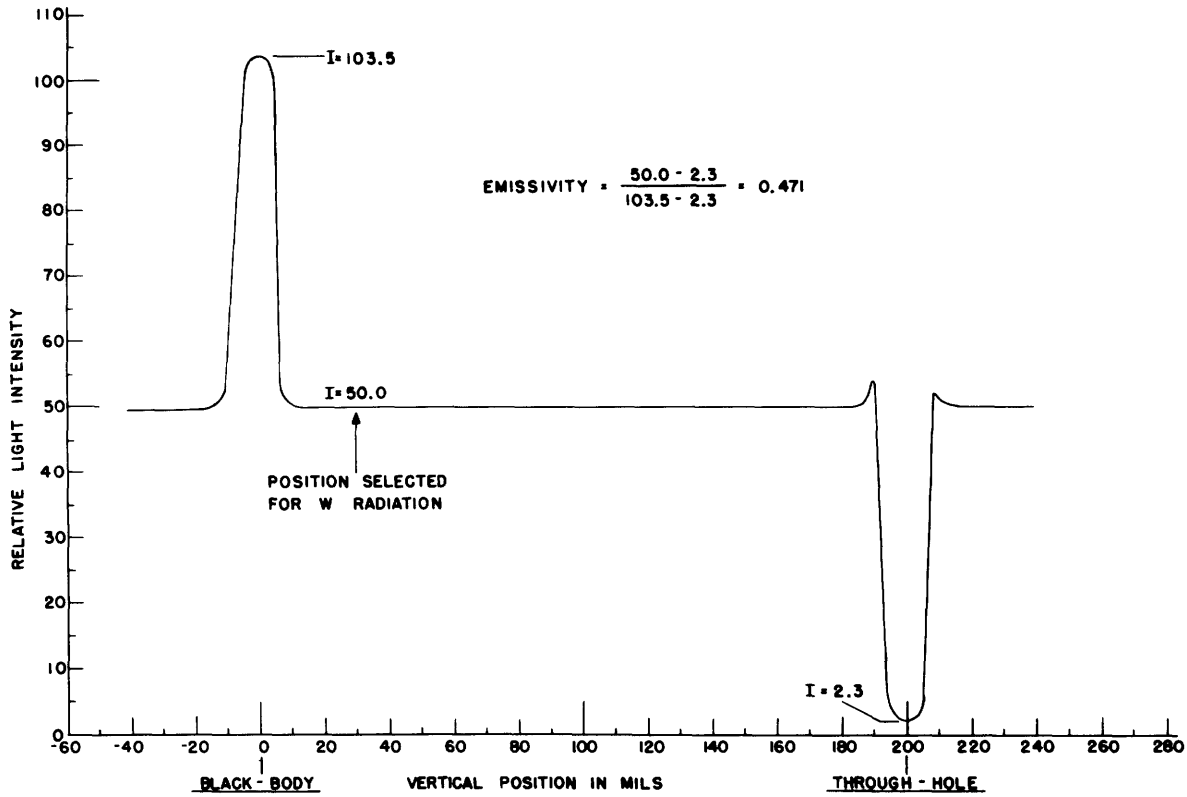

Fig. 27. Graphical illustration of the method of emissivity computation.

adjust this angle to zero after each black-body reading. However, as will be shown in Section VI, this leads to a negligible error (for unpolarized light), and hence it will be assumed that the emissivity values so measured represent the emissivity when the tungsten surface is viewed normally.

The spectral emissivity of the tungsten specimen was measured over the temperature interval 1600° K to 2400° K and over the wavelength interval 310 to 800 mμ as follows:

Source Temperature	Range of wavelengths
1600° K	400 to 700 mμ
1800° K	360 to 700 mμ
2000° K	340 to 800 mμ
2200° K	320 to 800 mμ
2400° K	310 to 800 mμ

In the range 310 to 400 mμ the emissivity was measured at intervals of 10 mμ, while in the range 400 to 800 mμ the emissivity was measured at intervals of 20 millimicrons.

In the analysis of the emissivity data the emissivity was assumed to follow a smooth curve of the form

$$E_{\lambda, T} = f_o(\lambda) + f_1(\lambda)\, T + f_2(\lambda)\, T^2 \qquad (9)$$

where $f_o(\lambda)$, $f_1(\lambda)$, and $f_2(\lambda)$ are functions of the wavelength to be determined by comparison with the experimental data, and T is the absolute temperature. Since the value of $f_2(\lambda)$ computed in this manner was numerically smaller than the rms error of the calculation, we assumed that the accuracy of the emissivity data was insufficient to justify the retention of this term in Eq. 9. Consequently, the resulting emissivity will vary linearly with the temperature as determined by the value of $f_1(\lambda)$. Since $f_1(\lambda)$ is determined from data obtained as the difference of two nearly equal numbers (emissivity values at different temperatures), the rms deviation of the computed points was quite large. Hence the data did not justify more than the linear least-square approximations shown in Fig. 28. By using these values of $f_1(\lambda)$, $f_o(\lambda)$ was determined as the average of all the emissivity data reduced to a common temperature. Consequently, having determined the numerical values of $f_o(\lambda)$, $f_1(\lambda)$, and $f_2(\lambda)$, we could use Eq. 9 to determine the actual values of the spectral emissivity of tungsten as a function of wavelength and temperature. These data are shown in Fig. 29 and tabulated in Table I. Notice that, by using Eq. 9, we can extrapolate the low-temperature data to the extremes of wavelength of the high-temperature data (i.e., from 310 to 800 mμ). The dark band along the bottom of Fig. 29 represents the estimated rms error of the emissivity measurement. This value was determined as the sum of the rms deviation of the experimental data from the curves of Fig. 29 and the estimated 0.2 per cent rms error in the validity of the black body (see section 4.5).

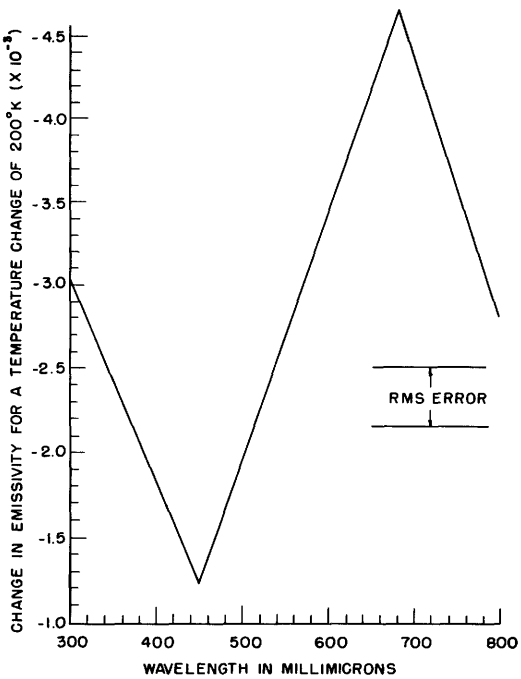

Fig. 28. Effect of temperature on the emissivity ratio.

We might ask if it is possible to find a simple analytic representation of these emissivity data. A glance at the values of $f_1(\lambda)$ (Fig. 28) reveals that there are three regions of wavelength characterized by three different linear approximations to $f_1(\lambda)$. With these data in mind, least-square straight lines were fitted to the emissivity data in these three regions of wavelength with the following results:

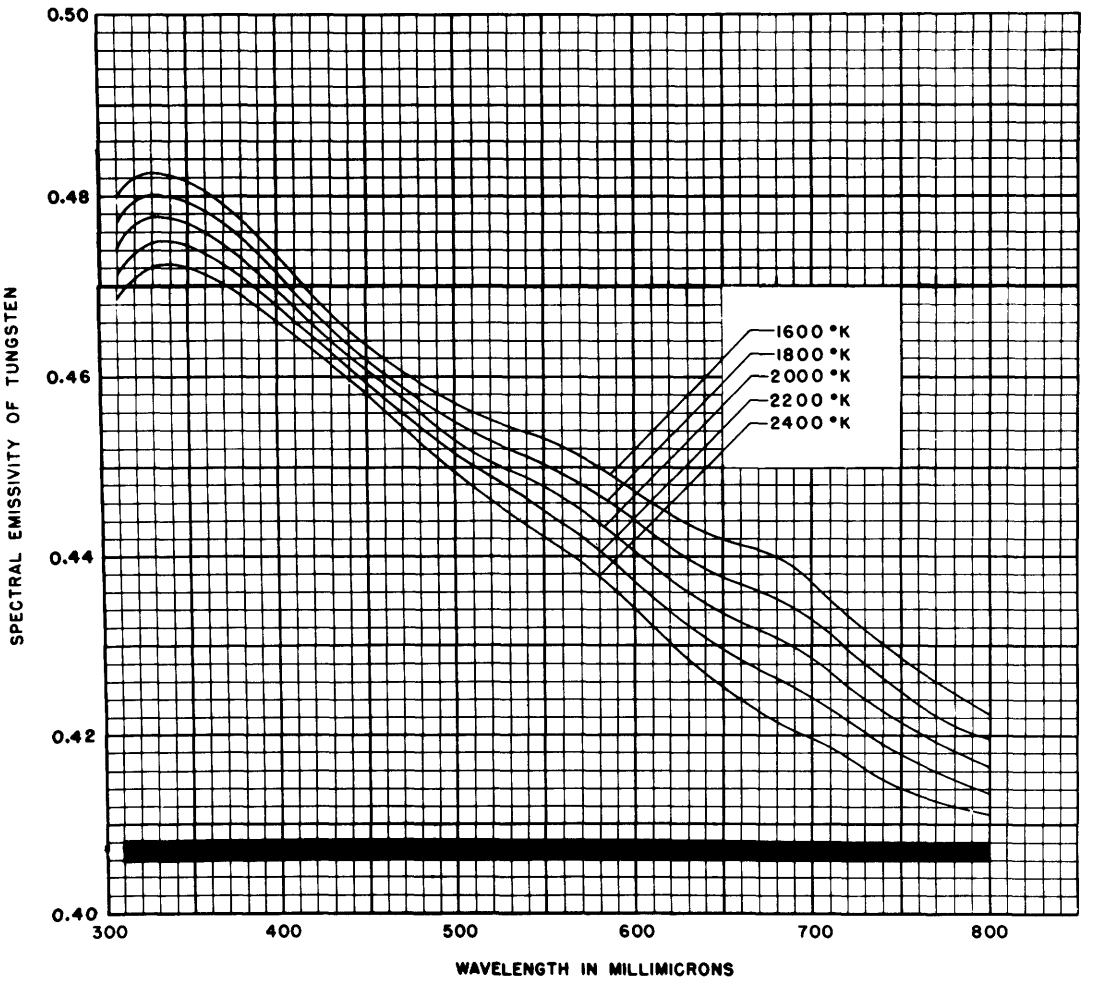

Fig. 29. The spectral emissivity of tungsten (data).

Wavelength Interval	Emissivity Equation
350 to 450 mμ,	$E_{\lambda T} = 0.6075 - 0.3000\lambda - 0.3265 \times 10^{-4}T + 0.5900 \times 10^{-4}\lambda T$
450 to 680 mμ,	$E_{\lambda T} = 0.4655 + 0.01558\lambda + 0.2675 \times 10^{-4}T - 0.7305 \times 10^{-4}\lambda T$
680 to 800 mμ,	$E_{\lambda T} = 0.6552 - 0.2633\lambda - 0.7333 \times 10^{-4}T + 0.7417 \times 10^{-4}\lambda T$

(10)

where T is the temperature in °K, and λ is the wavelength in millimicrons.

It is apparent from Fig. 30 that these analytic expressions fit the emissivity data very well. In fact, it can be said that the deviations (or undulations) in the original data are well below the rms error of the experiment and, therefore, are not considered very significant. Indeed, it is felt that these analytical expressions represent the measured

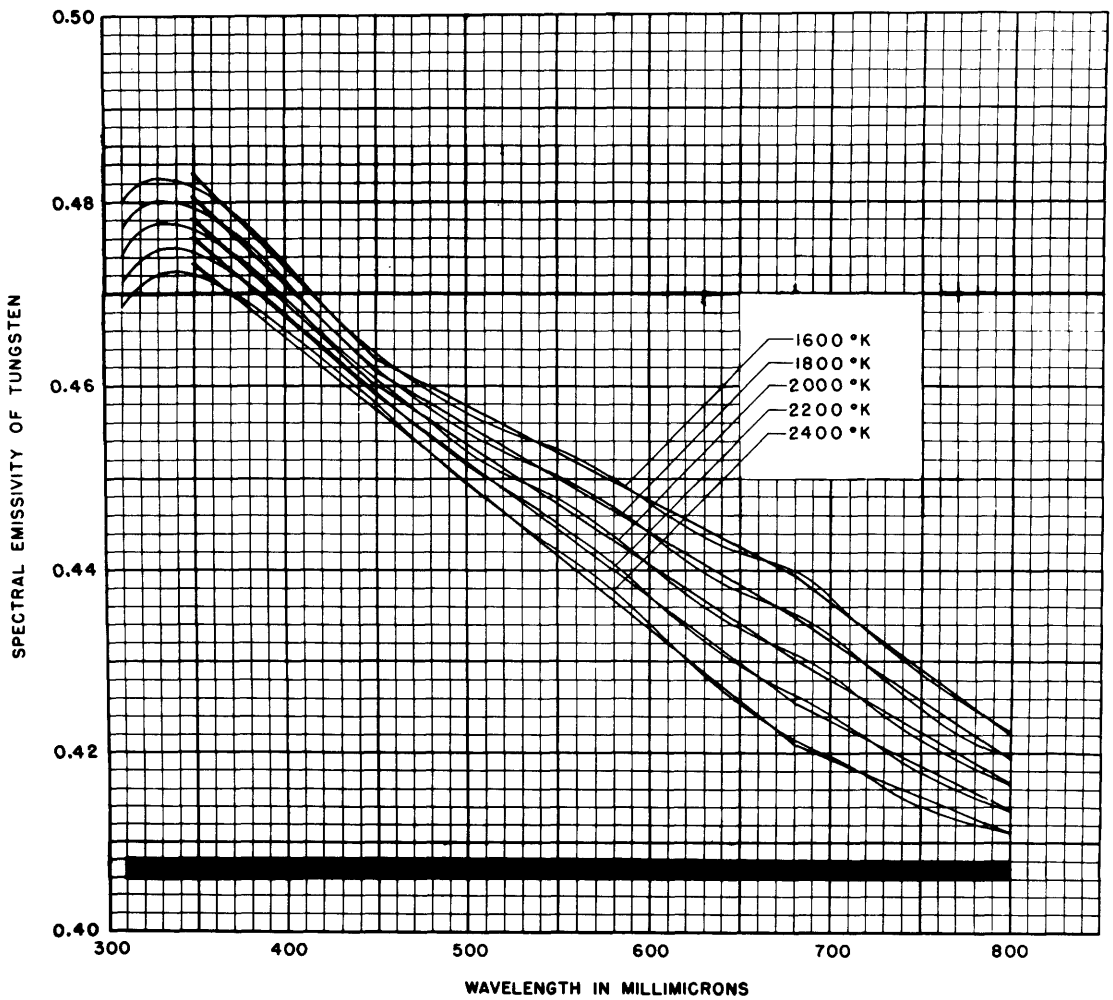

Fig. 30. The spectral emissivity of tungsten (experimental results and analytic approximation).

Table I. Spectral Emissivity of Tungsten.

Wavelength	Temperature				
(mμ)	1600° K	1800° K	2000° K	2200° K	2400° K
300	—	—	—	—	—
310	0.4798	0.4769	0.4740	0.4711	0.4682
320	0.4823	0.4795	0.4767	0.4739	0.4711
330	0.4828	0.4801	0.4774	0.4747	0.4720
340	0.4823	0.4798	0.4773	0.4748	0.4723
350	0.4816	0.4792	0.4768	0.4744	0.4720
360	0.4804	0.4781	0.4758	0.4735	0.4712
370	0.4791	0.4769	0.4747	0.4725	0.4703
380	0.4775	0.4754	0.4733	0.4712	0.4691
390	0.4754	0.4735	0.4716	0.4697	0.4678
400	0.4735	0.4717	0.4699	0.4681	0.4663
420	0.4694	0.4678	0.4662	0.4646	0.4630
440	0.4651	0.4638	0.4625	0.4612	0.4599
460	0.4620	0.4606	0.4592	0.4578	0.4564
480	0.4595	0.4578	0.4561	0.4544	0.4527
500	0.4571	0.4552	0.4533	0.4514	0.4495
520	0.4553	0.4531	0.4509	0.4487	0.4465
540	0.4539	0.4514	0.4489	0.4464	0.4439
560	0.4522	0.4494	0.4466	0.4438	0.4410
580	0.4501	0.4470	0.4439	0.4408	0.4377
600	0.4477	0.4443	0.4409	0.4375	0.4341
620	0.4450	0.4413	0.4376	0.4339	0.4302
640	0.4428	0.4388	0.4348	0.4308	0.4268
660	0.4412	0.4369	0.4326	0.4283	0.4240
680	0.4400	0.4354	0.4308	0.4262	0.4216
700	0.4375	0.4331	0.4287	0.4243	0.4199
720	0.4340	0.4299	0.4258	0.4217	0.4176
740	0.4304	0.4266	0.4228	0.4190	0.4152
760	0.4274	0.4239	0.4204	0.4169	0.4134
780	0.4246	0.4215	0.4184	0.4153	0.4122
800	0.4222	0.4194	0.4166	0.4138	0.4110

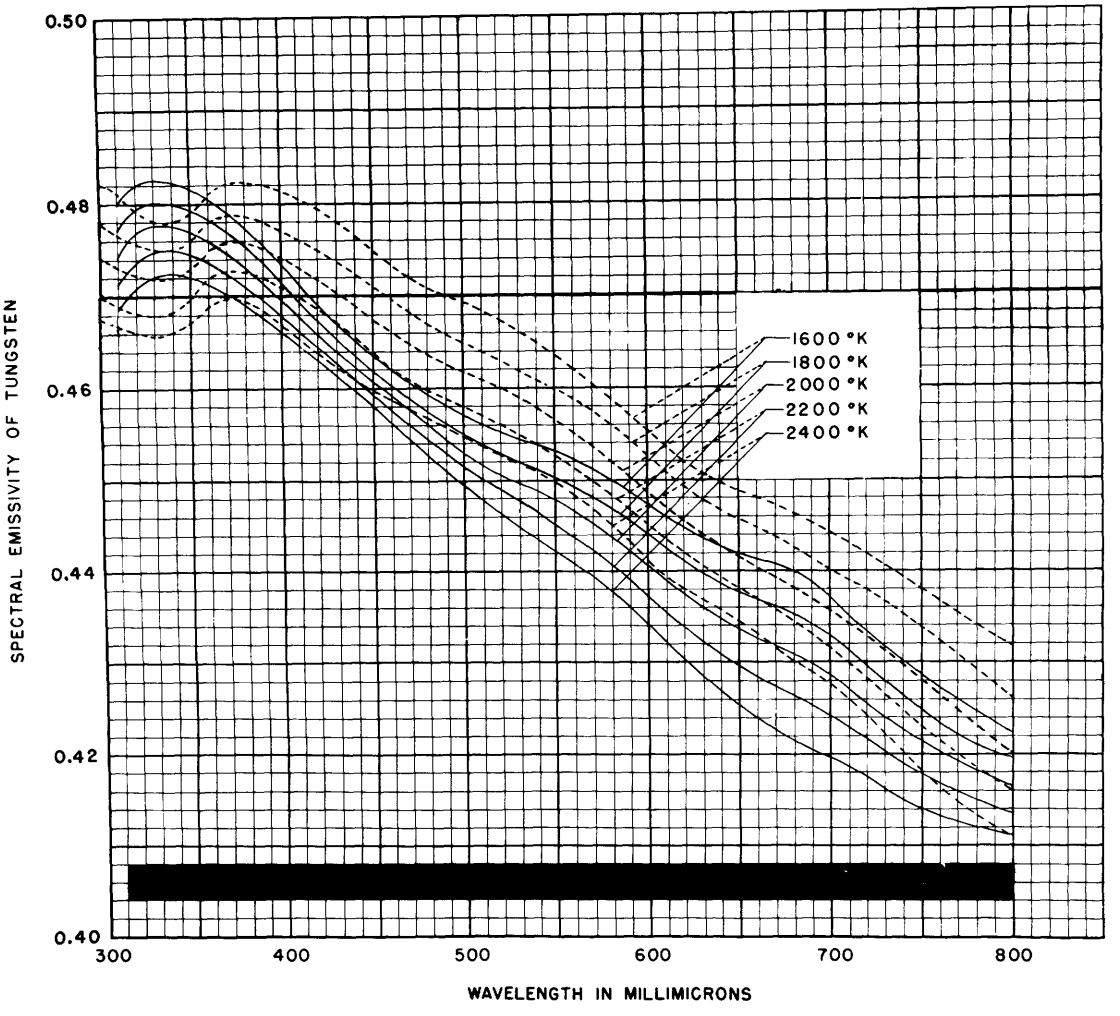

Fig. 31. The spectral emissivity of tungsten
— present experiment
-- J. C. De Vos, Physica 20, 690 (1954)

emissivity values (within their region of validity) as well as the curves of Fig. 29 do.

De Vos (1) measured the spectral emissivity of tungsten in a manner similar to the present method except that no correction for scattered light was made. It is evident that if the scattered light correction is omitted for the data presented in Fig. 27, an emissivity value of 50.0/103.5 = 0.483 is obtained, instead of the more correct value of 0.471. Consequently, it is apparent that the effect of the scattered-light correction is to lower the measured emissivity values approximately 2.5 per cent. Inspection of Fig. 31 reveals that the present data are significantly lower than De Vos' data over the greater part of the optical spectrum. It is reasonable, therefore, to assume that this difference is attributable to scattered light in De Vos' experiment which is of about the

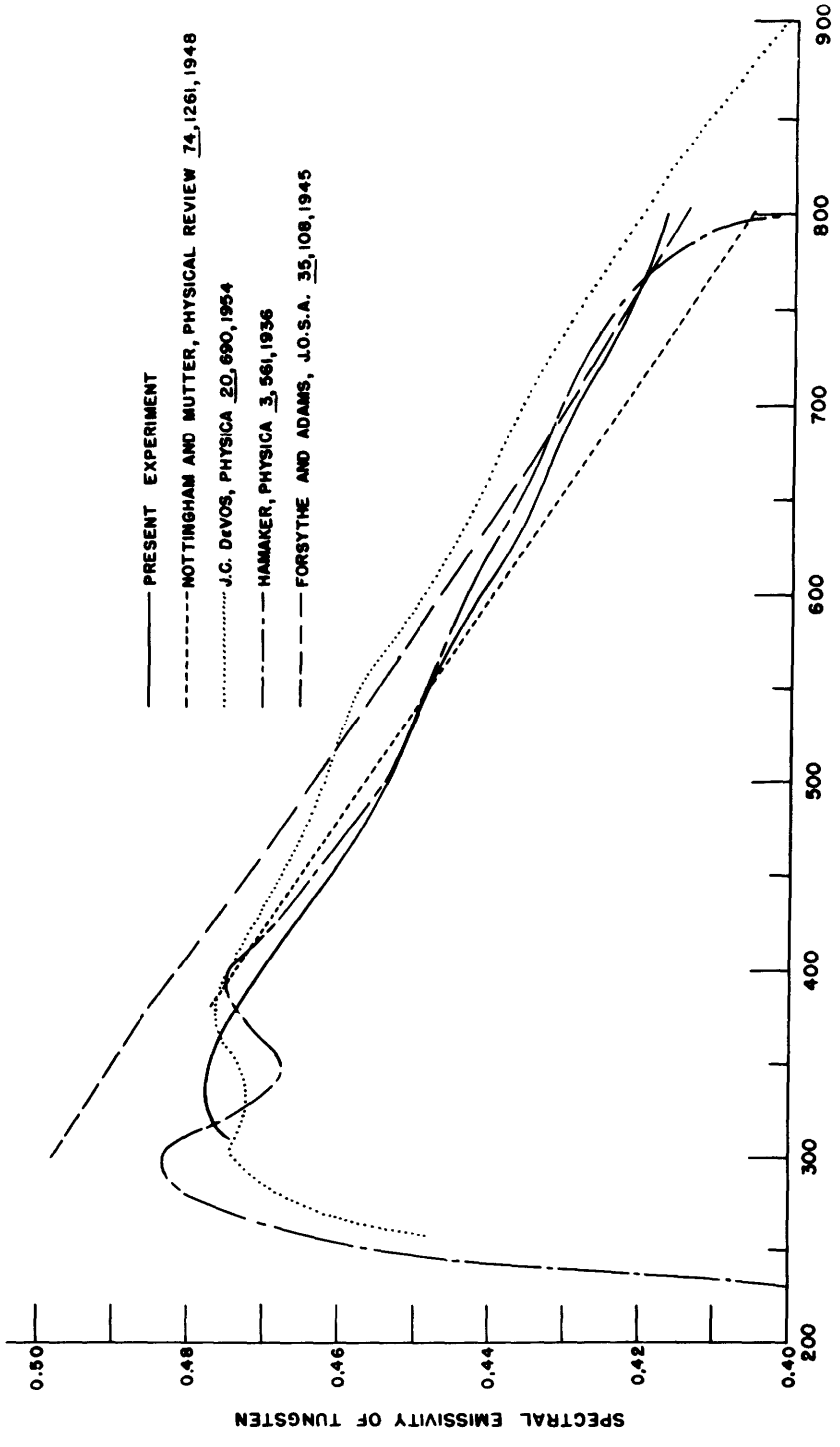

Fig. 32. The emissivity of tungsten at 2000° K as obtained by several observers.

same magnitude as in the present experiment.

Figure 32 presents a comparison of the present emissivity data with data obtained by some recent observers (1, 2, 24, 25). Notice that the present emissivity values tend to be slightly lower than the values obtained by other observers. This is considered significant, since the majority of experimental errors (neglect of scattered light, non-ideal black bodies, and so forth) tend to increase the measured emissivity ratio. We feel, therefore, that the present data are a closer approximation to the spectral emissivity of tungsten than are the results of previous experiments.

De Vos (1) discussed the applicability of the results of emissivity experiments to tungsten strip lamps and to standard sources of radiation, and he concluded that, if certain precautions are taken, such results can be applied directly to tungsten strip lamps. In Sections VII and VIII we shall utilize these emissivity values in connection with theories on the optical properties of tungsten.

VI. DEVIATIONS FROM LAMBERT'S RADIATION LAW IN TUNGSTEN RADIATION

6.1 FIRST APPROXIMATION

Lambert's radiation law states that the radiant intensity from a black-body radiator varies with the cosine of the angle of viewing. However, since the area viewed varies inversely with the cosine of the viewing angle, a black-body radiator appears uniformly bright at all viewing angles.

It is well known (26, 27) that tungsten radiation does not obey Lambert's cosine law. It is the purpose of this portion of the experiment to estimate the magnitude of this deviation.

Since we had to view the tungsten surface at all angles from normal to tangential, we could not tilt or rotate the emissivity tube in front of the optical system by a sufficient amount because of the finite size of the pyrex window. However, it was possible to offset the axis of the optical system from the axis of the hollow tungsten cylinder so as to view the lateral surface of the cylinder at any angle. Since the optical system viewed a small circular area 3.3 mils in diameter, a rather large range of angles was viewed instead of the single angle desired. Since this effect became very great at the larger viewing angles, the accuracy of the method was destroyed. Nevertheless, by measuring the relative light intensity (at each direction of polarization) as a function of the average angle viewed, a rough estimate of the magnitude of the deviations from Lambert's law can be obtained.

The cross-feed lathe vise upon which the optical system was mounted was attached to a synchronous motor that moved the optical system in the Y-(scan) direction at a rate of approximately 0.2 mil per second. The relative light intensity emitted from the cylinder was measured by the Shelton electrometer and was recorded by the Brown potentiometer. In this way, the Brown recorder traced the curve of light intensity against the average viewing angle.

These data were taken over the temperature interval 2000° K to 2400° K and over

the wavelength interval 400 mμ to 700 mμ at both directions of polarization (i.e., with the electric vector parallel and perpendicular to the plane of incidence). No significant variation either with wavelength or temperature was noted in the data. The relative light intensity at normal (0°) viewing angle (which, by symmetry, is independent of the direction of polarization) was arbitrarily assigned the value of 0.5000. The observed light intensities at other viewing angles are indicated in Fig. 33. Notice that the parallel component increases markedly with increasing viewing angle and the perpendicular component decreases with increasing viewing angle. This is a very marked deviation from Lambert's law (which implies that the observed light intensities should remain constant with viewing angle).

The curve labeled "total radiation" is the sum of the parallel and perpendicular components and therefore represents the variation in intensity of unpolarized light with viewing angle. Notice that Lambert's law is more closely approximated in this case (particularly at the small viewing angles). It is difficult on the scale of Fig. 33 to represent this curve correctly in the region between 0° and 30° of viewing angle. The following data should be read on this part of the curve:

Viewing Angle (degrees)	Value of the Total Radiation Curve (dimensionless units)
0	1.000
5	0.998
10	0.997
15	0.996
20	0.997
25	1.001
30	1.009

These data should also be used in reading the curves labeled "total radiation" in Fig. 34 and Fig. 39.

The curve labeled "polarization" represents the degree of polarization of the light emitted as a function of the viewing angle; it is computed according to the relation

$$\text{Polarization} = \frac{P - N}{P + N} \tag{11}$$

where P and N represent the intensities of the parallel component and the perpendicular (normal) component, respectively. It is quite evident that at the larger viewing angles the light is highly polarized. The dark band along the top of Fig. 33 represents the rms error of the measurement.

Worthing (26) measured this effect in 1926, using optical pyrometer methods. Figure 34 illustrates a superposition of his data on the present data. (Worthing found no significant variation with temperature over the range 1750° K to 2470° K.) In view

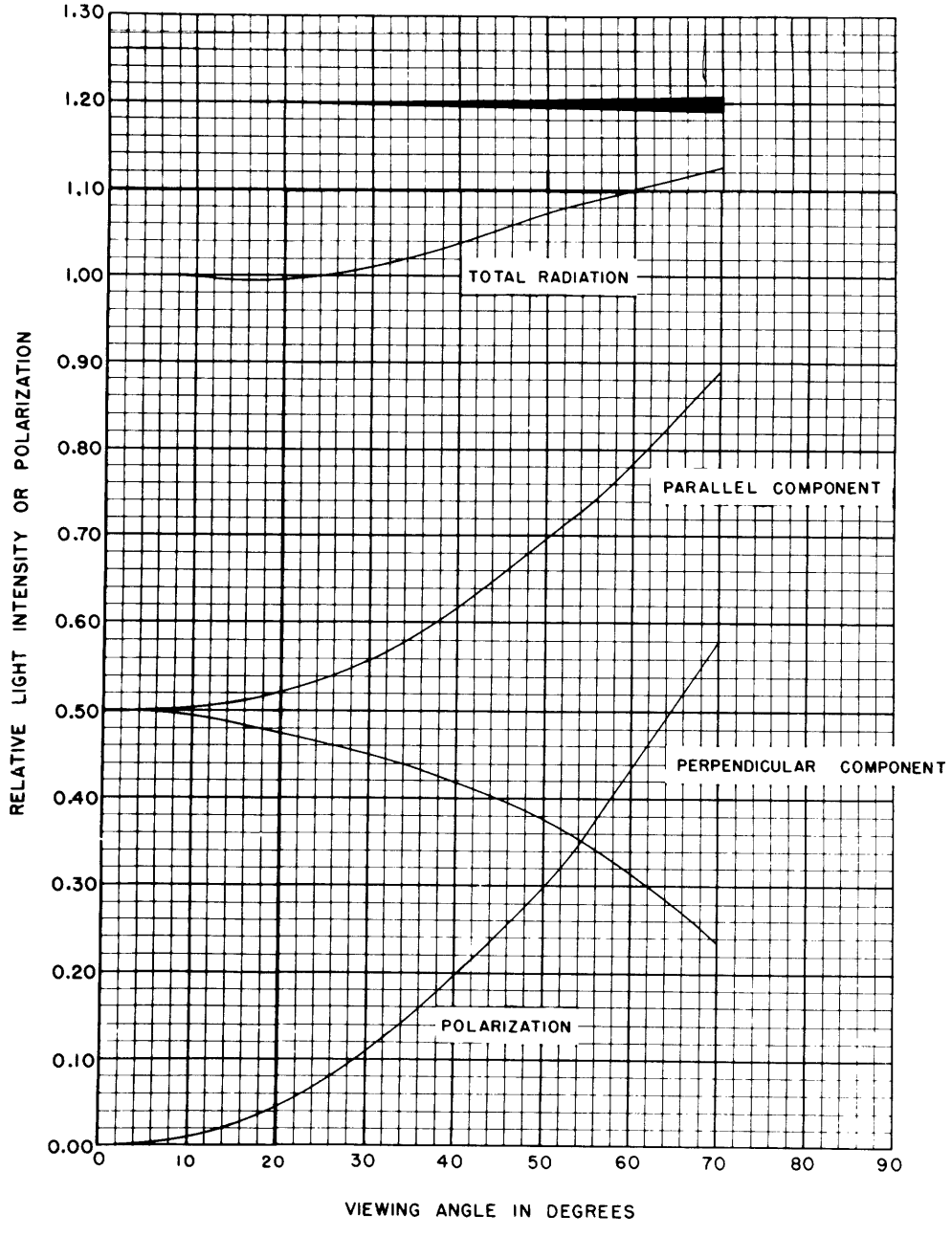

Fig. 33. Deviation from Lambert's cosine law in tungsten radiation (data).

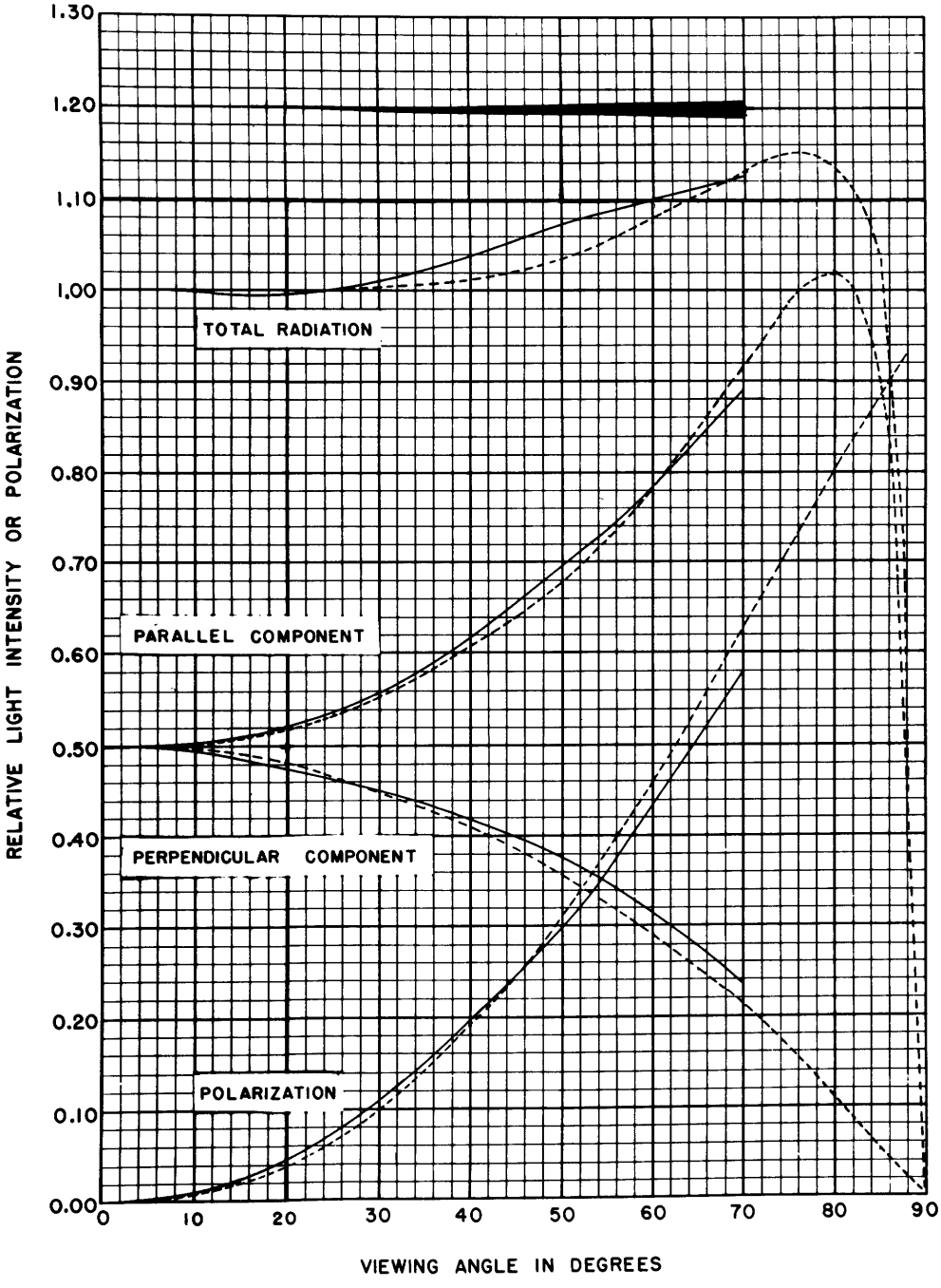

Fig. 34. Deviation from Lambert's cosine law in tungsten radiation
— present experiment
-- A. G. Worthing, J. Opt. Soc. Am. 13, 635 (1926)

of the comparatively large rms error of measurement (dark band) and the wide range of angles viewed in the present experiment, the deviations indicated in Fig. 34 are not considered significant. Consequently, we feel that Worthing's data are more reliable than ours and thus represent the characteristics of the present tungsten specimen at the one wavelength of 665 mμ (the effective wavelength of Worthing's optical pyrometer). Worthing (26) labeled the polarization components of Fig. 34 opposite to the way they are labeled in this report. We assume that Worthing used the convention of indicating the direction of polarization with reference to the magnetic vector instead of to the electric vector, as the custom now is. If this assumption is not made, the data of the present experiment and Worthing's data are in marked disagreement.

6.2 SECOND APPROXIMATION

Since Worthing was able to obtain data at only 665 mμ, the question naturally arises as to how these curves (Fig. 34) vary with wavelength. Since the crude experiment discussed above failed to reveal any measurable wavelength dependence, it can be inferred that this variation is not extremely large. It will be shown in Section VII that the peak of the parallel polarization-component curve of Fig. 34 is very sensitive to changes in the optical constants of tungsten. Notice that, in the present experiment, both the rms error of the measurement and the range of angles viewed become very large as this peak is approached. Consequently, it is possible to have an appreciable wavelength variation which would have remained undetected in the experiment discussed in section 6.1.

There are some theoretical considerations that will give an insight into this problem. Thermodynamic considerations show that it is impossible to have a thermal radiator radiate in excess of the black-body value under any conditions of equilibrium. This determines a definite upper bound on the numerical value of the peak of the parallel-component curve in terms of the normal spectral emissivity of tungsten. This upper bound can be expressed as follows:

$$\text{Upper bound} = \left\{\frac{0.5000}{E_n}\right\} 1 \qquad (12)$$

where E_n is the spectral emissivity of tungsten at normal viewing angle. The value $0.5000/E_n$ represents the necessary factor for normalizing the relative light intensity at normal viewing angle to the value 0.5000, while the second factor of unity represents the relative light intensity from a black-body radiator. If we use the present emissivity data at 665 mμ, this upper bound is 1.135 at 1600° K and 1.186 at 2400° K. Notice that the observed value of this peak (1.020) is well below this upper bound. However, as the wavelength decreases, the normal spectral emissivity increases, and so the upper bound decreases in accordance with Eq. 12. At 400 mμ and 2000° K the upper bound is 1.064. Consequently, we would expect the peak of the parallel-component curve to decrease with decreasing wavelength and hence to remain at a "safe" distance

below this upper bound.

In order to measure how this peak varies with wavelength, a General Electric #18AT10/1-6V (SR8 Fil.) gas-filled tungsten strip lamp was mounted in front of the optical system in place of the emissivity tube. This strip lamp was oriented so that it could be rotated by a synchronous motor at a rate of approximately 0.25 rpm in front of the stationary optical system. In this way, the optical system viewed the flat tungsten ribbon at all angles from normal to tangential as the strip lamp was rotated. The output of the Shelton electrometer was observed on the Brown recording potentiometer in order to provide a graphical picture of the relative light intensity as a function of viewing angle. By simply adjusting the monochromator, measurements could be made at any wavelength in the optical range.

There were, however, two factors which destroyed the accuracy of this crude experiment. The purity and condition of the surface of the tungsten strip were virtually unknown. Since the lamp was annealed at approximately 2600° K for 20 hours (as recommended by De Vos (1)), it is felt that recrystallization of the tungsten was practically complete and that the evaporated material (tungsten and impurities) might act as a physical getter to purify the gas within the envelope. Since the relative transmission of the glass envelope as a function of viewing angle was not known, it was necessary to compare the present measurements (at 665 mμ) with Worthing's data (26) (which was assumed to be correct) in order to measure this nonuniform window-transmission characteristic.

The numerical value of the peak of the parallel-component curve of Fig. 34 was measured over the wavelength interval 350 mμ to 750 mμ (in 50-mμ steps) and over the temperature interval 2000° K to 2400° K (in 200° K steps). No significant variation with temperature was noted. Within the error of the experiment (±1°), these peaks all occurred at a viewing angle of 79° (in agreement with Worthing's data). These data are shown in Fig. 35 and are summarized as follows:

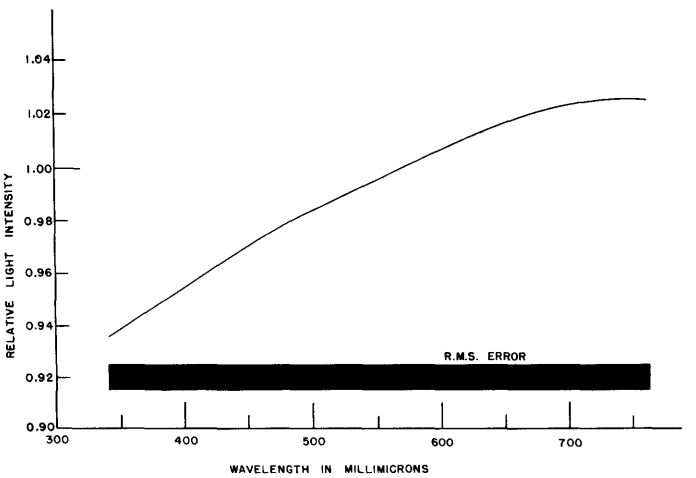

Fig. 35. Value of the peak of the parallel component.

Wavelength (mμ)	Numerical value of peak of parallel-component curve
350	0.939
400	0.955
450	0.971
500	0.984
550	0.995
600	1.006
665	1.020
700	1.023
750	1.026

Notice that this peak does decrease with decreasing wavelength, as predicted. To a first approximation, the numerical value of this peak is a constant per cent (approximately 90 per cent) of the upper bound determined by the normal spectral emissivity of tungsten.

In Section VII equations for the parallel- and perpendicular-component curves of Fig. 34 will be derived. By making use of the data listed above and the data on the normal spectral emissivity of tungsten, we can evaluate the parameters that appear in these equations. Thus we shall be able to compute the spectral emissivity of tungsten as a function of the four variables of wavelength, temperature, polarization, and angle of viewing the surface.

VII. THEORETICAL INTERPRETATION OF THE RESULTS

In Sections I-VI an experiment designed to measure the spectral emissivity of tungsten as a function of wavelength, temperature, polarization, and viewing angle has been discussed. The results of this experiment are summarized in Figs. 28-35. The rest of this report will be devoted to the theoretical interpretation of these results. However, before such an interpretation is possible, a theory on thermal radiation in metals must be developed.

7.1 BASIC MECHANISM OF METALLIC THERMAL RADIATION

The following "thought experiment" will illustrate the basic mechanism of thermal radiation in metals. Consider a beam of plane-polarized monochromatic light to be incident upon the surface of a semi-infinite metallic slab, as illustrated in Fig. 36. If the metal has an emissivity, E, its reflectivity will be given by (1 - E). Consequently, the fraction (1 - E) of the incident light will be reflected to the left at the metal-vacuum interface. The remaining light (i.e., the fraction E of the incident light) will be transmitted across the metal-vacuum interface into the metal and eventually will be completely absorbed.

Let there be a reference plane aligned parallel to the metal-vacuum interface and

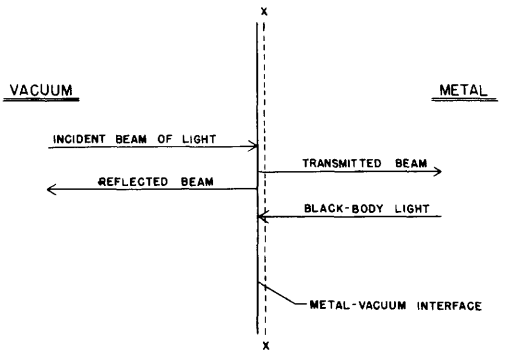

Fig. 36. Illustration of the thought experiment.

located a differential (i.e., small) distance behind it, as shown by the dashed line x-x in Fig. 36. Notice that all light traversing this reference plane to the right will be completely absorbed by the metal. In other words, the metal appears as a black body to all light traversing this plane to the right. Consequently, if the metal slab is at a uniform temperature, thermodynamic considerations show that there must be black-body light from inside the metal traversing this plane to the left. Therefore, the metal-vacuum interface is "bathed" in black-body light characterized by the assumed uniform temperature of the metallic slab.

Notice that this important result is independent of the material of which the metallic slab is made. The two basic assumptions that have been made are:

1. The metallic slab is at a uniform temperature.
2. The metallic slab is thick enough to absorb completely all light traversing its thickness.

Notice that the second assumption is not valid for such things as thin, semitransparent, metallic films, transparent objects such as glass or quartz, and for most materials in the range of X-ray frequencies and higher. However, if these two conditions are satisfied, we can conclude that black-body light is incident upon the metal-vacuum interface from inside the metal.

We might well ask why this black-body light is not observed as thermal radiation from the metal. The answer to this question lies in the fact that the metal has different optical constants from the vacuum, and classical electromagnetic theory requires reflection and refraction processes at the boundary. Consequently, it will be assumed that the spectral emissivity of a metal is a surface effect describable in terms of classical electromagnetic theory.

7.2 CALCULATION OF THE EMITTED LIGHT

In electromagnetic theory a material is completely characterized by its permeability and permittivity. In the case of tungsten it can be assumed that the magnetic effects are negligible compared with the electrical effects. In fact, this assumption is a good approximation even in the case of ferromagnetic substances, since the domain structures cannot follow optical frequencies. Therefore, the permeability of tungsten will be taken as μ_o (i.e., the permeability of vacuum).

The permittivity of tungsten, however, is not negligible. In fact, the situation is complicated because tungsten has a conductivity, as well as a polarizibility. Von Hippel

has shown (28) that this problem can be solved by the introduction of a complex permittivity defined by

$$\text{permittivity of tungsten} = \epsilon = \epsilon' - j\,\sigma/\omega \tag{13}$$

where ϵ' represents the polarization of the tungsten structure and the imaginary term ($j = \sqrt{-1}$) represents the contribution of the conductivity, σ, at the radian frequency ω. Thus, the characteristic impedance of the metal, Z_m, assumes the form

$$Z_m = \left(\frac{\mu_o}{\epsilon}\right)^{1/2} = \left(\frac{\mu_o}{\epsilon' - j\frac{\sigma}{\omega}}\right)^{1/2} \tag{14}$$

which, of course, is a complex quantity.

Consider a plane-polarized monochromatic beam of black-body light from inside the metal to be incident upon the metal-vacuum interface in such a way that it makes an angle ϕ with the inward surface normal. Part of this light will be transmitted to the vacuum after undergoing a refractive change in direction at the metal-vacuum interface. Let the angle which this transmitted beam makes with the outward normal to the surface be called ψ. The light that is not transmitted into the vacuum will be reflected back into the metal at the metal-vacuum interface and, consequently, will never be detectable from measurements made outside the metal. Let the components of the incident light with their electric vectors normal and parallel to the plane of incidence (i.e., the plane containing the normal to the metallic surface and the propagation vector of the incident light) be designated by the subscripts n and p, respectively. Fresnel's equations (28) for the relative intensity of the electric vector of the transmitted light (E_t) and the reflected light (E_r) in terms of the incident light (E_i) become

$$\left(\frac{E_t}{E_i}\right)_n = \frac{2\,Z_v \cos\phi}{Z_v \cos\phi + Z_m \cos\psi} \tag{15a}$$

$$\left(\frac{E_t}{E_i}\right)_p = \frac{2\,Z_v \cos\phi}{Z_v \cos\psi + Z_m \cos\phi} \tag{15b}$$

$$\left(\frac{E_r}{E_i}\right)_n = \frac{Z_v \cos\phi - Z_m \cos\psi}{Z_v \cos\phi + Z_m \cos\psi} \tag{15c}$$

$$\left(\frac{E_r}{E_i}\right)_p = \frac{Z_v \cos\psi - Z_m \cos\phi}{Z_v \cos\psi + Z_m \cos\phi} \tag{15d}$$

and Snell's law of refraction (28) becomes

$$\sin\phi = \left|\frac{\gamma_v}{\gamma_m}\right| \sin\psi \tag{16}$$

where

$$Z_v = \sqrt{\frac{\mu_o}{\epsilon_o}} = \text{characteristic impedance of the vacuum,}$$

$$Z_m = \sqrt{\frac{\mu_o}{\epsilon' - j\frac{\sigma}{\omega}}} = \text{characteristic impedance of tungsten,}$$

$$\gamma_v = j\omega\sqrt{\mu_o\epsilon_o} = \text{propagation factor in vacuum, and}$$

$$\gamma_m = j\omega\sqrt{\mu_o\epsilon} = j\omega\sqrt{\mu_o\left(\epsilon' - j\frac{\sigma}{\omega}\right)} = \text{propagation factor in tungsten.}$$

If we introduce the dimensionless complex quantity Z given by

$$Z = \frac{Z_m}{Z_v} = \left(\frac{\epsilon_o}{\epsilon' - j\frac{\sigma}{\omega}}\right)^{1/2} = \left(\frac{\epsilon'}{\epsilon_o} - j\frac{\sigma}{\omega\epsilon_o}\right)^{-1/2} = (\kappa' - j\kappa'')^{-1/2} \tag{17}$$

where

$$\kappa' = \frac{\epsilon'}{\epsilon_o} \qquad \text{and} \qquad \kappa'' = \frac{\sigma}{\omega\epsilon_o}$$

Eqs. 15 and 16 become

$$\left(\frac{E_t}{E_i}\right)_n = \frac{2\cos\phi}{\cos\phi + Z\cos\psi} \tag{18a}$$

$$\left(\frac{E_t}{E_i}\right)_p = \frac{2\cos\phi}{\cos\psi + Z\cos\phi} \tag{18b}$$

$$\left(\frac{E_r}{E_i}\right)_n = \frac{\cos\phi - Z\cos\psi}{\cos\phi + Z\cos\psi} \tag{18c}$$

$$\left(\frac{E_r}{E_i}\right)_p = \frac{\cos\psi - Z\cos\phi}{\cos\psi + Z\cos\phi} \tag{18d}$$

$$\sin\phi = |Z|\sin\psi \tag{18e}$$

However, since the purpose of this analysis is to compute the transmitted power per unit area (or intensity) and not the magnitude of the electric field, it is convenient to compute the reflected power from Eqs. 18 and then compute the transmitted power by using the law of conservation of energy. Since the reflected light never leaves the metal, the ratio of the reflected light intensity to the incident black-body intensity is given by

$$\text{Reflectivity} = \left(\frac{E_r}{E_i}\right)^2 \tag{19}$$

Hence, the transmitted light intensity becomes

$$\text{Transmitted Intensity} = \left\{1 - \left(\frac{E_r}{E_i}\right)^2\right\}\text{Incident Intensity} \tag{20}$$

Since the vacuum has different optical properties from the tungsten, the transmitted light intensity is NOT given by $(E_t/E_i)^2$ multiplied by the incident intensity. Since the incident intensity corresponds to black-body radiation, the emissivity of the metal can be expressed as

$$\text{Emissivity} = 1 - \left\{\frac{E_r}{E_i}\right\}^2 \tag{21}$$

If the emissivity of the normal polarization component is called E_n and the emissivity of the parallel component is called E_p, Fresnel's equations (i.e., Eqs. 18c and 18d) can be used to show that

$$E_n = 1 - \left\{\frac{E_r}{E_i}\right\}_n^2 = 1 - \left\{\frac{\cos\phi - Z\cos\psi}{\cos\phi + Z\cos\psi}\right\}^2 \tag{22a}$$

$$E_p = 1 - \left\{\frac{E_r}{E_i}\right\}_p^2 = 1 - \left\{\frac{\cos\psi - Z\cos\phi}{\cos\psi + Z\cos\phi}\right\}^2 \tag{22b}$$

Consequently, Eqs. 22a, 22b, and 18e are analytic equations for the spectral emissivity of a metal in terms of the optical constants of that metal. Notice that the change in emissivity with polarization and viewing angle (ψ) is determined by these equations, while the variation in emissivity with wavelength and temperature can be attributed to a change in the optical constants (i.e., Z) of the metal with wavelength and temperature.

7.3 ALTERNATIVE DERIVATION

Another approach to the derivation of Eqs. 22a, 22b, and 18e, which is not fundamentally different, is quite interesting. Consider a plane-polarized (either normal or parallel) beam of monochromatic light to be incident upon the metal-vacuum interface from the vacuum side. The intensity of the reflected beam can be computed from Fresnel's and Snell's equations in a manner similar to the calculation outlined above. The reflectivity of the metal is given by

$$\text{Reflectivity} = \frac{\text{Reflected Intensity}}{\text{Incident Intensity}} \tag{23}$$

However, since the emissivity is (1 - reflectivity), the emissivity is easily computed. The results of such a computation yield Eqs. 22a, 22b, and 18e with the same assumptions inherent in the calculation. Therefore, nothing new or more general is obtained. Although this alternative derivation is more direct, it is felt that the first derivation gives a greater insight into the mechanism responsible for the thermal radiation of a metal.

7.4 NORMAL SPECTRAL EMISSIVITY OF A METAL

If the metallic surface is viewed normally, the angle ψ is zero. Snell's law (Eq. 18e) reveals that ϕ is also zero. Consequently, in this special case Eqs. 22a and 22b both assume the simple form

$$E_n = E_p = 1 - \left\{\frac{1 - Z}{1 + Z}\right\}^2 \tag{24}$$

Notice that the emissivity of the parallel component must equal the emissivity of the normal component under this special condition, since, by symmetry, there is no real difference between these two quantities.

Since Z is a complex dimensionless quantity, it is convenient to define

$$Z = Z_1 + jZ_2 \tag{25}$$

where Z_1 and Z_2 are real numbers representing the real and imaginary parts of Z. In terms of Z_1 and Z_2, Eq. 24 becomes

$$E_p = E_n = 1 - \left\{\frac{1 - Z_1 - jZ_2}{1 + Z_1 + jZ_2}\right\}^2 = 1 - \frac{(1 - Z_1)^2 + Z_2^2}{(1 + Z_1)^2 + Z_2^2} \tag{26}$$

Since all the terms in Eq. 26 are real, it is a very convenient expression for correlating this theory with the experiment. However, this correlation cannot be made now, since it would involve evaluating the parameters Z_1 and Z_2 in terms of the one experimental observable, namely, the normal spectral emissivity of tungsten. But Eq. 26, which yields one connection between theory and experiment, will be used in the subsequent discussion.

7.5 SIMPLIFICATION OF THE E_n AND E_p EQUATIONS

From Snell's law (Eq. 18e) and by the application of trigonometric theorems, Eqs. 22a and 22b can be rewritten in the following form which does not include the angle ϕ:

$$\cos\phi = \left\{1 - \sin^2\phi\right\}^{1/2} = \left\{1 - |Z|^2 \sin^2\psi\right\}^{1/2}$$

But, since

$$|Z|^2 = Z_1^2 + Z_2^2$$

we have

$$\cos\phi = \left\{1 - \left(Z_1^2 + Z_2^2\right)\sin^2\psi\right\}^{1/2}$$

We shall now assume that $\left(Z_1^2 + Z_2^2\right)$ is small compared with unity, so that the approximation

$$\cos\phi \approx \left(1 - \frac{Z_1^2 + Z_2^2}{2}\sin^2\psi\right)$$

is valid. If this value of $\cos\phi$ is inserted in Eqs. 22a and 22b, the following equations are obtained for the E_p and E_n emissivities in terms of the observed viewing angle ψ and the dimensionless parameters Z_1 and Z_2

$$E_n = 1 - \frac{\left(2 - \left(Z_1^2 + Z_2^2\right)\sin^2\psi - 2Z_1\cos\psi\right)^2 + (2Z_2\cos\psi)^2}{\left(2 - \left(Z_1^2 + Z_2^2\right)\sin^2\psi + 2Z_1\cos\psi\right)^2 + (2Z_2\cos\psi)^2} \tag{27a}$$

$$E_p = 1 - \frac{\left(Z_1 - Z_1\left(Z_1^2 + Z_2^2\right)\frac{\sin^2\psi}{2} - \cos\psi\right)^2 + \left(Z_2 - Z_2\left(Z_1^2 + Z_2^2\right)\frac{\sin^2\psi}{2}\right)^2}{\left(Z_1 - Z_1\left(Z_1^2 + Z_2^2\right)\frac{\sin^2\psi}{2} + \cos\psi\right)^2 + \left(Z_2 - Z_2\left(Z_1^2 + Z_2^2\right)\frac{\sin^2\psi}{2}\right)^2} \tag{27b}$$

Notice that both of these equations reduce to Eq. 24 at zero viewing angle (i.e., when $\psi = 0$). It is also interesting to note that at $\psi = 90°$ (tangential viewing) both E_n and E_p reduce to zero (independent of the values of Z_1 and Z_2).

It is important to remember the assumption that $\left(Z_1^2 + Z_2^2\right)$ is small compared with unity which was made to ensure that the approximation used in deriving Eqs. 27a and 27b would be valid. But the numerical values of Z_1 and Z_2 that are obtained in the following sections are certainly small compared with unity. Consequently, this is a self-consistent assumption in the range of wavelength and temperature that is of interest in this experiment.

7.6 EQUATIONS FOR THE PARAMETERS Z_1 AND Z_2

Equations 27a and 27b express the spectral emissivity of a metal in terms of the dimensionless parameters Z_1 and Z_2. It is of interest to develop the relationship between these parameters and the fundamental optical constants of the metal (i.e., κ' and κ'' of Eq. 17). Inspection of Eqs. 17 and 25 reveals that

$$Z = Z_1 + jZ_2 = (\kappa' - j\kappa'')^{-1/2} = \left\{\left(\frac{\kappa'}{\kappa'^2 + \kappa''^2}\right) + j\left(\frac{\kappa''}{\kappa'^2 + \kappa''^2}\right)\right\}^{1/2} \tag{28}$$

Consequently, Z_1 is the real part and Z_2 is the imaginary part of this expression. A little manipulation will show that

$$Z_1 = + \left\{ \frac{+\sqrt{\kappa'^2 + \kappa''^2} + \kappa'}{2(\kappa'^2 + \kappa''^2)} \right\}^{1/2} \tag{29a}$$

$$Z_2 = + \left\{ \frac{+\sqrt{\kappa'^2 + \kappa''^2} - \kappa'}{2(\kappa'^2 + \kappa''^2)} \right\}^{1/2} \tag{29b}$$

If Eqs. 29a and 29b are solved simultaneously for κ' and κ'', we obtain

$$\kappa' = \frac{Z_1^2 - Z_2^2}{\left(Z_1^2 + Z_2^2\right)^2} \tag{30a}$$

$$\kappa'' = \frac{2Z_1Z_2}{\left(Z_1^2 + Z_2^2\right)^2} \tag{30b}$$

Thus, if Z_1 and Z_2 can be found by comparing theory with experiment, Eqs. 30a and 30b can be used to find κ' and κ''.

7.7 THE OPTICAL CONSTANTS N AND K

The propagation factor, γ_m, for light traveling in tungsten is defined by

$$\gamma_m = j\omega (\mu_o \epsilon)^{1/2} = j\omega \left[\mu_o \left(\epsilon' - j\frac{\sigma}{\omega} \right) \right]^{1/2}$$

$$\gamma_m = j\omega (\mu_o \epsilon_o)^{1/2} (\kappa' - j\kappa'')^{1/2} = j\frac{\omega}{c} (\kappa' - j\kappa'')^{1/2}$$

where $c = \dfrac{1}{\sqrt{\mu_o \epsilon_o}}$ = the velocity of light in vacuum. Therefore, the electric vector of a plane-polarized light wave propagating through tungsten in the X-direction can be represented by

$$\vec{E} = \vec{E}_o \, e^{j\omega t - \gamma_m x} \tag{31}$$

where $\vec{E}_o$ is a constant vector. Since γ_m is a complex quantity, it is convenient to define it as

$$\gamma_m = \alpha + j\beta$$

where α and β are the real and imaginary parts of γ_m, respectively. Equation 31 can be written in the form

$$\vec{E} = \vec{E}_o \, e^{j\omega t - (\alpha + j\beta)x} = \vec{E}_o \, e^{-\alpha x} \, e^{j(\omega t - \beta x)} \tag{32}$$

Therefore, it is apparent that the phase velocity of this light wave can be expressed as

$$\text{Phase Velocity} = V_p = \omega/\beta$$

Therefore, the index of refraction, N, of the metal can be expressed as

$$N = \frac{c}{V_p} = \frac{c\beta}{\omega}$$

but

$$\beta = \text{Imaginary part of } \gamma_m$$

$$\beta = \frac{\omega}{c}(\text{Real part of } \sqrt{\kappa' - j\kappa''})$$

$$\beta = +\frac{\omega}{c}\left\{\frac{+\sqrt{\kappa'^2 + \kappa''^2} + \kappa'}{2}\right\}^{1/2}$$

Therefore,

$$N = +\left\{\frac{+\sqrt{\kappa'^2 + \kappa''^2} + \kappa'}{2}\right\}^{1/2} \tag{33}$$

Notice that because of the presence of the conductivity of the metal (i.e., the term κ''), the index of refraction, N, is not given by $\sqrt{\kappa'}$ as it would be for a lossless nonmagnetic dielectric.

It is also apparent from Eq. 32 that the electric vector of the light wave will be attenuated by the factor $e^{-\alpha x}$ as it propagates along the X-direction in the metal. The factor α can be expressed in terms of κ' and κ'' as follows:

$$\alpha = \text{Real part of } \gamma_m$$

$$\alpha = j\frac{\omega}{c}(\text{Imaginary part of } \sqrt{\kappa' - j\kappa''})$$

$$\alpha = +\frac{\omega}{c}\left\{\frac{+\sqrt{\kappa'^2 + \kappa''^2} - \kappa'}{2}\right\}^{1/2}$$

For simplicity of representation, let

$$\left\{\frac{+\sqrt{\kappa'^2 + \kappa''^2} - \kappa'}{2}\right\}^{1/2} = K$$

Therefore, α can be expressed in terms of the dimensionless parameter K as

$$\alpha = \frac{\omega}{c}K = \frac{2\pi K}{\lambda_o}$$

where $\lambda_o = \frac{2\pi c}{\omega}$ = the wavelength of the light wave in vacuum. Consequently, it is apparent that the electric vector of the light wave is attenuated by the factor

$$e^{-\frac{2\pi K}{\lambda_o}x}$$

as it propagates through the metal. The dimensionless parameter K that characterizes the rate of attenuation is called the "extinction coefficient," and it is given by

$$K = +\left\{\frac{+\sqrt{\kappa'^2 + \kappa''^2} - \kappa'}{2}\right\}^{1/2} \tag{34}$$

Since N and K are the imaginary and real parts of the complex expression $(\kappa' + j\kappa'')^{1/2}$, it is often convenient to define a complex index of refraction, N^*, given by

$$N^* = N - jK = \sqrt{\kappa' - j\kappa''}$$

where N and K are the index of refraction and the extinction coefficient as defined. Notice that this definition is a generalization of the relationship $N = \sqrt{\kappa'}$ which is valid for lossless nonmagnetic materials.

It is of interest to note that some authors have used different definitions in place of the extinction coefficient, K. They define the complex index of refraction as $N^* = N(1 - jK_o)$, where N is as defined above and the quantity K_o (called the "index of absorption") is given by $K_o = K/N$.

7.8 COMPARISON OF THEORY WITH EXPERIMENT

It was mentioned in section 7.4 that the normal emissivity equation (Eq. 26) gives a very convenient connection between this theory and the experiment. However, since the two parameters Z_1 and Z_2 are to be evaluated, another connection with the experiment must be found. Equations 27a and 27b, which express the emissivity of tungsten as a function of viewing angle and polarization, will be used for this purpose.

Worthing (26) measured the relative light intensity of tungsten radiation as a function of viewing angle and polarization at the one wavelength of 665 millimicrons. His data are summarized in Fig. 34. Equations 27a and 27b will represent these curves if one correction is made. Equations 27a and 27b yield the actual normal spectral emissivity of tungsten when $\psi = 0$, while the curves of Fig. 34 have been arbitrarily normalized to 0.5000 at $\psi = 0$. Therefore, it is necessary to multiply the expressions of Eqs. 27a and 27b by the factor $0.5000/E_{normal}$ before they can represent the data of Fig. 34. Consequently, when these equations are normalized in this way, they can serve as the second connection between theory and experiment. Actually, any point on the curves of Fig. 34 could be so used, but, since it can be shown that the peak of the parallel-component curve is very sensitive to changes in the parameters Z_1 and Z_2, this point was selected.

Inspection of Worthing's data (26) reveals that the numerical value of this peak is 1.02, and it occurs at a viewing angle of 79° at all temperatures between 1750° K and 2470° K. Consequently, these data together with the normalized equation (Eq. 27b), and

the spectral emissivity data (Fig. 30) together with Eq. 26 provide two equations for the two unknowns Z_1 and Z_2. Since data are available in the temperature range 1600° K to 2400° K (with a slight extrapolation of Worthing's temperature range), Z_1 and Z_2 can be found as a function of temperature by a trial-and-error solution of these two equations. The results of this computation are summarized below and are illustrated in Fig. 37.

Values of Z_1 and Z_2 at the Wavelength 665 mμ

Temperature	Value of Z_1	Value of Z_2
1600° K	0.1459	0.1017
1800	0.1442	0.1058
2000	0.1423	0.1101
2200	0.1405	0.1142
2400	0.1387	0.1179

Once Z_1 and Z_2 have been found, Eqs. 30a and 30b can be used to find the numerical values of κ' and κ''. The value of the index of refraction, N, and the extinction coefficient, K, follow from Eqs. 33 and 34 when κ' and κ'' are known. The results of these computations are listed below and shown in Figs. 37 and 38.

Optical Constants of Tungsten at 665 mμ

Temperature	Value of κ'	Value of κ''	Value of N	Value of K
1600° K	10.939	29.66	4.613	3.215
1800	9.383	29.82	4.508	3.308
2000	7.756	29.90	4.396	3.401
2200	6.233	29.86	4.286	3.484
2400	4.860	29.78	4.186	3.558

Since $\kappa'' = \sigma/\omega\epsilon_o$, the conductivity of the tungsten metal at the optical frequency corresponding to 665 mμ can be found. Figure 38 illustrates how the optical conductivity compares with the dc conductivity.

Having found the numerical values of Z_1 and Z_2 at the one wavelength 665 mμ, we are in a position to see how well the theory and the experiment agree. The optical constants of tungsten at 2000° K (i.e., $Z_1 = 0.1423$ and $Z_2 = 0.1101$) were substituted in the normalized equations (Eqs. 27a and 27b) to see how well the theory coincides with the experimental data. Since the peak of the parallel-component curve of Fig. 34 was used in the computation of Z_1 and Z_2, the theoretical curve must pass through this point. Also, since Eqs. 27a and 27b were normalized, the theoretical curves must pass through 0.5000 at normal viewing angle (i.e., $\psi = 0$). The results of these computations are shown in Fig. 39 and are tabulated in Table II.

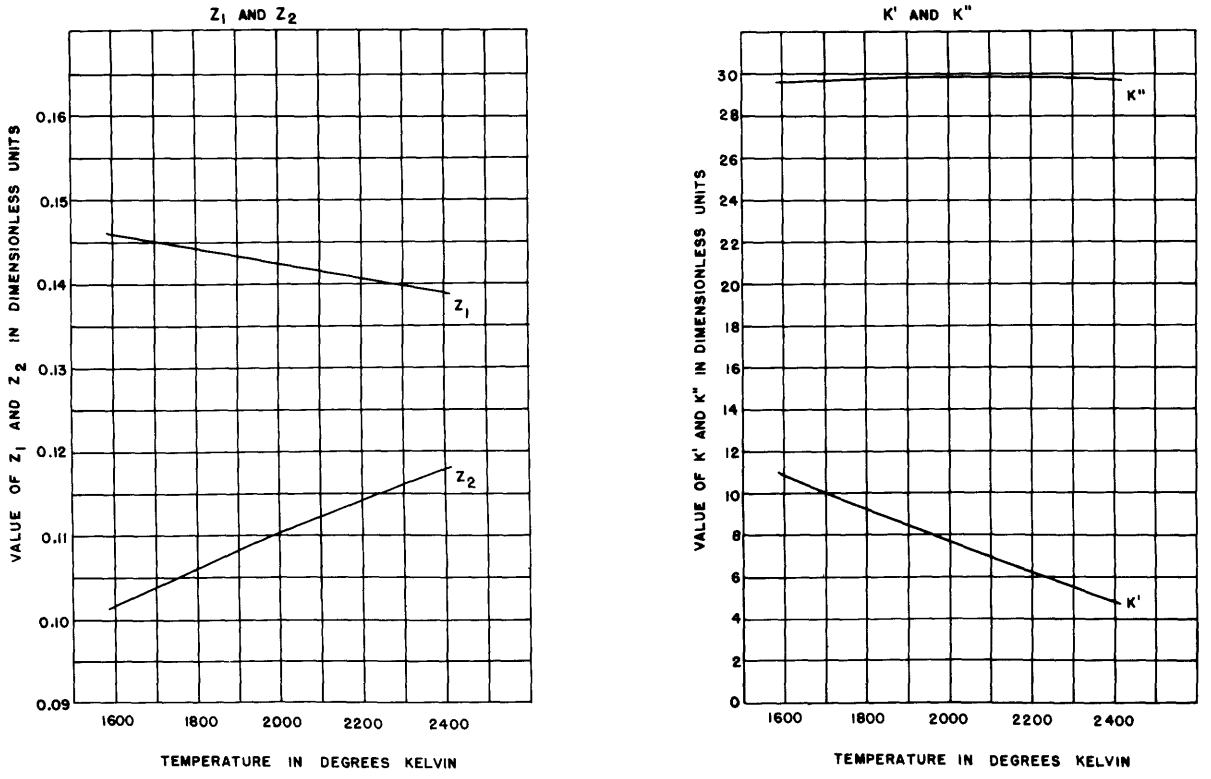

Fig. 37. Computed values of the optical constants Z_1 and Z_2, κ' and κ'' at the wavelength 665 mμ.

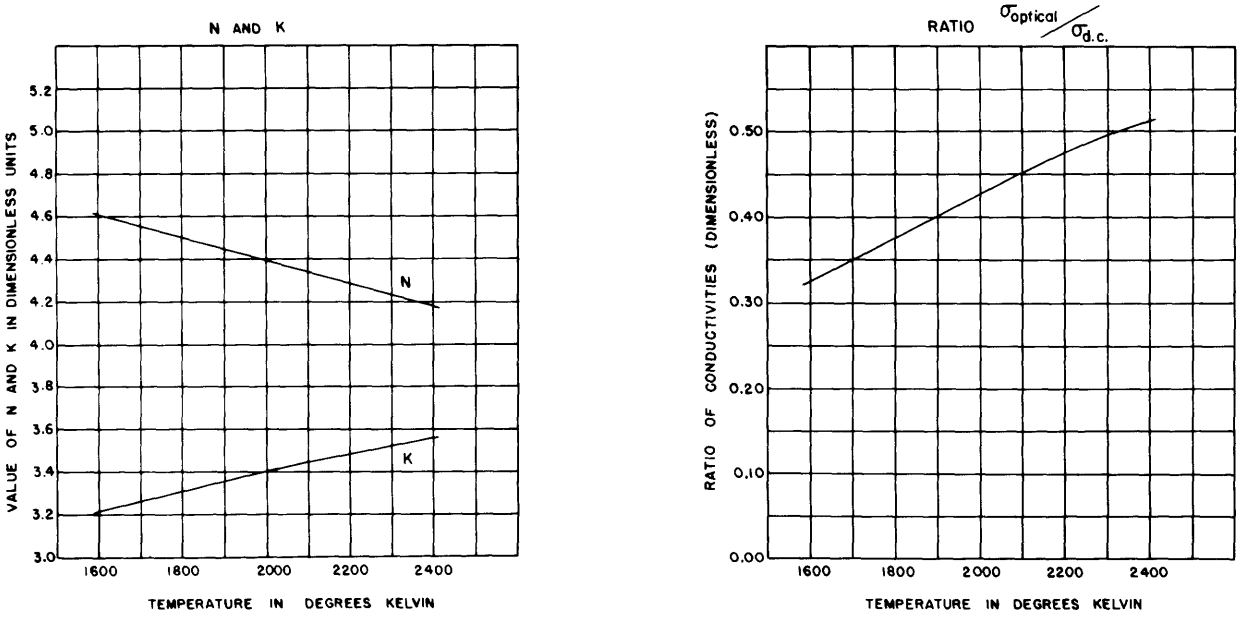

Fig. 38. Computed values of the optical constants N and K, and σ/σ_{dc} at the wavelength 665 mμ.

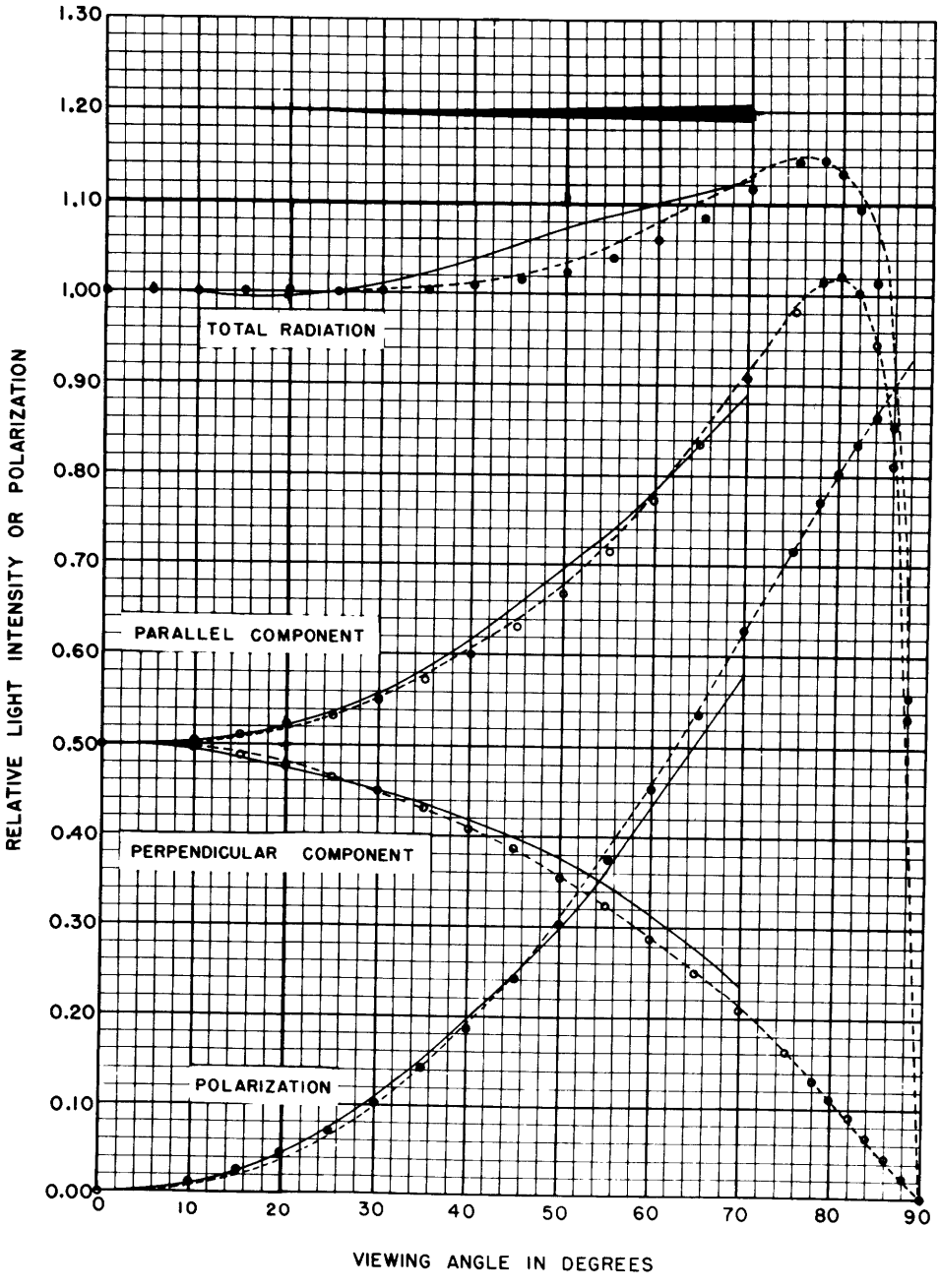

Fig. 39. Deviation from Lambert's cosine law in tungsten radiation
— present experiment
-- A. G. Worthing, J. Opt. Soc. Am. 13, 635 (1926)
● o theoretical results

Table II. Deviations from Lambert's Law in Tungsten Radiation.

Viewing Angle	Parallel Component	Perpendicular Component	Total Radiation	Polarization
0°	0.5000	0.5000	1.0000	0.0000
5	0.5013	0.4986	1.0000	0.0027
10	0.5055	0.4946	1.0000	0.0109
15	0.5124	0.4877	1.0002	0.0247
20	0.5224	0.4781	1.0005	0.0443
25	0.5357	0.4656	1.0014	0.0700
30	0.5527	0.4502	1.0029	0.1022
35	0.5739	0.4316	1.0055	0.1414
40	0.5998	0.4099	1.0098	0.1880
45	0.6314	0.3850	1.0164	0.2425
50	0.6696	0.3566	1.0262	0.3050
55	0.7155	0.3247	1.0402	0.3757
60	0.7704	0.2892	1.0596	0.4541
65	0.8351	0.2501	1.0852	0.5391
70	0.9084	0.2072	1.1156	0.6285
75	0.9819	0.1607	1.1426	0.7188
78	1.0144	0.1310	1.1454	0.7713
80	1.0216	0.1105	1.1321	0.8048
82	1.0053	0.0895	1.0948	0.8365
84	0.9466	0.0679	1.0144	0.8662
86	0.8107	0.0458	0.8565	0.8931
88	0.5326	0.0231	0.5557	0.9168
90	0.0000	0.0000	0.0000	?

Note: This table lists the values of relative light intensity of tungsten radiation corresponding to the indicated viewing angles. These data were computed for a temperature of 2000° K and a wavelength of 665 mμ (i.e., $Z_1 = 0.1423$ and $Z_2 = 0.1101$).

Notice that the theory reproduces the experimental data very well at all viewing angles. In fact, the deviation between theory and experiment is of the same order as the estimated rms error of Worthing's experiment. Consequently, we feel justified in assuming that the theory is a good approximation to what is actually occurring.

Several of the assumptions made in the development of the theory can now be justified. Notice that the numerical value of the extinction coefficient is approximately 3. This means that the electric vector of light propagating in tungsten is attenuated by the factor $e^{-2\pi K} \approx e^{-18}$ after traversing a distance of 665 mμ (one free-space wavelength) in the metal. Since this corresponds to a decrease of e^{-36} in the intensity of the light, even a layer of tungsten that is a fraction of a micron thick is sufficient to absorb all light traversing its thickness. The thermal conductivity of tungsten is large enough so that it is difficult to conceive of the development of appreciable temperature differences over a distance of one micron or less.

Notice that the value of $Z_1^2 + Z_2^2$ (at 2000° K) is approximately 0.0324. Since this value is certainly small compared with unity, the approximation for cos ϕ made in the derivation of Eqs. 27a and 27b is valid.

Consequently, all of the basic assumptions made in the development of the theory are self-consistent and the theory is in close agreement with the limited amount of experimental data that is available. Therefore, we feel justified in utilizing this theory to compute the optical properties of tungsten from the analysis of the emitted thermal radiation.

7.9 OPTICAL CONSTANTS OF TUNGSTEN

In section 7.8 the optical constants of tungsten were found at the one wavelength 665 millimicrons. The question now arises as to whether or not there are enough experimental data to find these optical constants at other wavelengths. The crude experiment discussed in section 6.2 provides just the information needed for such a computation. Since both the spectral emissivity of tungsten at normal viewing angle (Fig. 30) and the numerical values of the peak of the parallel-component curve of Fig. 35 are known as a function of wavelength and temperature, the optical properties of tungsten can be computed as a function of both the wavelength and the temperature by the method outlined in section 7.8. The results of this computation are shown in Tables III, IV, and V.

Since the rms error in the measured normal emissivity values is approximately 0.5 per cent and the rms error in the values of the peak of the parallel component curve are approximately 1 per cent in intensity and approximately 1° in location, the optical constants listed in Tables III, IV, and V should have an rms error associated with them. However, the complexity of the equations used in the computation makes it very difficult to estimate the rms error. By NO means is it to be inferred that these optical constants are correct to the number of significant figures indicated. Aside from the small fluctuations of these data (which may or may not be significant), the general trend in the variation of these optical constants with wavelength and temperature is

Table III. Computed Values of Z_1 and Z_2.

A. Values of Z_1

Wavelength	Temperature				
(mμ)	1600° K	1800° K	2000° K	2200° K	2400° K
350	0.1649	0.1641	0.1632	0.1622	0.1610
400	0.1610	0.1603	0.1595	0.1587	0.1579
450	0.1564	0.1558	0.1552	0.1547	0.1541
500	0.1534	0.1525	0.1517	0.1510	0.1502
550	0.1514	0.1502	0.1492	0.1480	0.1469
600	0.1489	0.1474	0.1461	0.1447	0.1433
665	0.1459	0.1442	0.1423	0.1405	0.1387
700	0.1444	0.1426	0.1408	0.1389	0.1373

B. Values of Z_2

Wavelength	Temperature				
(mμ)	1600° K	1800° K	2000° K	2200° K	2400° K
350	0.1126	0.1151	0.1173	0.1196	0.1218
400	0.1101	0.1120	0.1138	0.1156	0.1173
450	0.1095	0.1111	0.1125	0.1138	0.1150
500	0.1076	0.1095	0.1114	0.1131	0.1149
550	0.1056	0.1079	0.1102	0.1126	0.1150
600	0.1032	0.1067	0.1102	0.1132	0.1162
665	0.1017	0.1058	0.1101	0.1142	0.1179
700	0.1025	0.1071	0.1116	0.1157	0.1195

Table IV. Computed Values of κ' and κ''.

A. Values of κ'

Wavelength	Temperature				
(mμ)	1600° K	1800° K	2000° K	2200° K	2400° K
350	9.130	8.475	7.891	7.278	6.674
400	9.534	8.994	8.474	7.956	7.463
450	9.386	8.898	8.467	8.073	7.697
500	9.698	9.069	8.450	7.901	7.317
550	10.139	9.333	8.547	7.714	6.897
600	10.695	9.433	8.204	7.131	6.070
665	10.939	9.383	7.756	6.233	4.860
700	10.521	8.763	7.074	5.531	4.164

B. Values of κ''

Wavelength	Temperature				
(mμ)	1600° K	1800° K	2000° K	2200° K	2400° K
350	23.36	23.40	23.46	23.52	23.61
400	24.50	24.55	24.63	24.69	24.74
450	25.78	25.82	25.87	25.88	25.93
500	26.78	26.88	26.94	26.96	26.99
550	27.54	27.71	27.78	27.87	27.89
600	28.53	28.69	28.71	28.76	28.75
665	29.66	29.82	29.90	29.86	29.78
700	30.10	30.20	30.16	30.10	29.89

Table V. Computed Values of N and K.

A. Values of N

Wavelength	Temperature				
(mμ)	1600° K	1800° K	2000° K	2200° K	2400° K
350	4.136	4.084	4.040	3.994	3.950
400	4.232	4.192	4.155	4.117	4.081
450	4.291	4.255	4.224	4.194	4.168
500	4.369	4.327	4.282	4.242	4.200
550	4.443	4.392	4.337	4.280	4.221
600	4.537	4.452	4.363	4.287	4.210
665	4.613	4.508	4.396	4.286	4.186
700	4.605	4.484	4.362	4.250	4.144

B. Values of K

Wavelength	Temperature				
(mμ)	1600° K	1800° K	2000° K	2200° K	2400° K
350	2.824	2.865	2.904	2.945	2.988
400	2.894	2.929	2.964	2.999	3.032
450	3.004	3.034	3.062	3.085	3.110
500	3.065	3.017	3.145	3.178	3.213
550	3.099	3.155	3.203	3.256	3.304
600	3.144	3.222	3.291	3.354	3.414
665	3.215	3.308	3.401	3.484	3.558
700	3.269	3.367	3.457	3.540	3.607

quite apparent. In Section VIII we shall attempt to explain the main features of these variations.

Since the optical properties of tungsten are now known in the wavelength interval 350 to 700 mμ and the temperature interval 1600° K to 2400° K, the variation in spectral emissivity with polarization and viewing angle can be computed at any combination of wavelength and temperature within these ranges by substitution of the appropriate values of Z_1 and Z_2 from Table III in Eqs. 27a and 27b. In this way, curves similar to Worthing's data (Fig. 34) can be computed for any combination of wavelength and temperature within the ranges mentioned above. Consequently, by appealing to the theory presented in this section, not only could we compute the optical properties of tungsten, but also the spectral emissivity of tungsten as a function of the four variables: wavelength, temperature, polarization, and viewing angle.

VIII. FURTHER INTERPRETATION OF RESULTS

In Section VII we pointed out that the spectral emissivity of a metal is a function of the four variables: wavelength, temperature, polarization, and angle of viewing the surface. Furthermore, we demonstrated that the variation with polarization and viewing angle is a surface effect describable in terms of classical electromagnetic theory, while the variation with wavelength and temperature is attributable to changes in the basic optical properties of the metal. By utilizing the theory presented in Section VII, we found that the basic optical properties (i.e., κ' and κ'' or N and K) could be computed as a function of wavelength and temperature from an analysis of the emitted thermal radiation. In Section VIII we shall try to find a simple classical model that will explain the main features of these optical properties.

8.1 THE DRUDE-ZENER-KRONIG FREE-ELECTRON MODEL

The earliest attempts at approaching a classical model of the optical properties of metals were made by Drude (29), Zener (30), and Kronig (31). Their theory assumes that there are N_f (i.e., N_{free}) electrons per unit volume which are perfectly free to wander throughout the metallic structure, subject only to a viscous damping force proportional to the electron velocity. The equation of motion for such a free electron can be expressed as

$$m \frac{d^2y}{dt^2} + 2\pi m \gamma_f \frac{dy}{dt} = -q E_o e^{j\omega t} \tag{35}$$

where

y = a coordinate that measures the displacement of the electron in the direction of the electric field ($E_o e^{j\omega t}$) of the electromagnetic radiation,

γ_f = a parameter that measures the viscous damping force acting on the electron. γ_f has the dimension of seconds^{-1},

m = the effective electronic mass, and

$-q$ = the electronic charge.

The steady-state solution of Eq. 35 is

$$y = \frac{+q}{4\pi^2 m} \frac{E_o e^{j\omega t}}{f^2 - j\gamma_f f} \tag{36}$$

The current density corresponding to this electronic motion is given by

$$\text{Current Density} = \sigma \vec{E} = -q N_f \vec{V}$$

where

σ = the conductivity of the metal,

$\vec{E}$ = the applied electric field $\left(\text{i.e., } E_o e^{j\omega t}\right)$, and

$\vec{V}$ = the velocity of the electrons $\left(\text{i.e., } \frac{dy}{dt}\right)$.

Therefore,

$$\sigma = \frac{-q N_f}{E_o e^{j\omega t}} \frac{dy}{dt} = \frac{-q N_f}{E_o e^{j\omega t}} \left\{ \frac{+q}{4\pi^2 m} \frac{j\omega E_o e^{j\omega t}}{f^2 - j\gamma_f f} \right\}$$

A little manipulation will show that

$$\sigma = \frac{N_f q^2}{4\pi^2 m} \left\{ \frac{2\pi\gamma_f}{f^2 + \gamma_f^2} - j \frac{2\pi f}{f^2 + \gamma_f^2} \right\} \tag{37}$$

The complex permittivity of a metal can be defined in terms of this complex conductivity as

$$\text{Permittivity} = \epsilon_o - j\frac{\sigma}{\omega} = \epsilon_o (\kappa' - j\kappa'')$$

Consequently, κ' and κ'' can be expressed in terms of this theory as

$$\kappa' = 1 - \frac{N_f q^2}{4\pi^2 m \epsilon_o} \frac{1}{f^2 + \gamma_f^2} \tag{38a}$$

$$\kappa'' = \frac{N_f q^2}{4\pi^2 m \epsilon_o} \frac{\gamma_f f}{f^4 + \gamma_f^2 f^2} \tag{38b}$$

Although this theory yielded satisfactory results in the case of some metals (32), it could not begin to explain the observed optical properties of tungsten. For example, notice that, according to Eq. 38a, κ' must be less than unity and possibly even negative, whereas the observed values of κ' (see Table IV) range from +4.2 to +10.5 in the ranges of wavelength and temperature investigated. Therefore, it can be concluded that the Drude-Zener-Kronig free-electron theory is inadequate for

describing the optical properties of tungsten.

8.2 MODIFICATION OF THE FREE-ELECTRON MODEL

Since all of the electrons in the tungsten structure cannot be classified as free electrons, we should consider the possibility of modifying the Drude-Zener-Kronig model so as to also take account of the effects of the bound electrons. To a first approximation these bound electrons can be assumed to be elastically bound to their equilibrium positions. On the basis of this assumption, a general classical model would assume that each quantum state in the tungsten structure is characterized by an elastic restoring force and a viscous damping force. However, since this would involve the evaluation of an unreasonable number of parameters (two parameters per electron pair), this general classical approach leads to a very impractical theory.

However, we can assume that only a fraction of the electrons are free and that the remaining electrons are all elastically bound with the same restoring force and oscillate under the influence of the same viscous damping force. Admittedly, this is an oversimplification of the general classical model, but the results of this theory which is easier to handle will show whether the general classical model is a good approximation to what is actually taking place in the metal.

8.3 DEVELOPMENT OF THE MODIFIED FREE-ELECTRON MODEL

The electrons in the tungsten structure that are considered to be free will obey Eq. 35, and the conductivity arising from these free electrons will be given by Eq. 37.

The elastic restoring force that acts on the bound electrons can be represented by

$$\text{Restoring force} = -K_b\, y$$

where y is the displacement from the equilibrium position. Consequently, the equation of motion for the bound electrons will assume the form

$$m\frac{d^2y}{dt^2} + 2\pi m\, \gamma_B \frac{dy}{dt} + K_b\, y = -q\, E_o\, e^{j\omega t}$$

where

γ_B = a parameter that measures the viscous damping force acting on the bound electrons, and

K_b = a parameter that measures the elastic restoring force acting on the bound electrons.

We shall assume that the effective masses of the free electrons and of the bound electrons are both equal to the actual inertial mass of an isolated electron (i.e., $m = 9.1 \times 10^{-31}$ Kg).

By following the same procedure as in the derivation of Eq. 37, it can be shown that the conductivity arising from these bound electrons is given by

$$\sigma_b = \frac{N_b q^2}{4\pi^2 m} \left\{ \frac{2\pi f^2 \gamma_B}{\left(f_o^2 - f^2\right)^2 + f^2 \gamma_B^2} + j \frac{2\pi f\left(f_o^2 - f^2\right)}{\left(f_o^2 - f^2\right)^2 + f^2 \gamma_B^2} \right\} \tag{39}$$

where

N_b = the number of bound electrons per unit volume, and

$f_o = \frac{1}{2\pi}\left(\frac{K_B}{m}\right)^{1/2}$ = the resonant frequency of the bound electrons if there were no damping force present.

Since the total conductivity will be the sum of the contributions from the free electrons (Eq. 37) and the bound electrons (Eq. 39), κ' and κ'' can be computed by a method similar to that used in the derivation of Eqs. 38a and 38b to give

$$\kappa' = 1 + \frac{q^2}{4\pi^2 m \epsilon_o} \left\{ - \frac{N_f f^2}{f^4 + \gamma_f^2 f^2} + \frac{N_b\left(f_o^2 - f^2\right)}{\left(f_o^2 - f^2\right)^2 + \gamma_B^2 f^2} \right\} \tag{40a}$$

$$\kappa'' = \frac{+q^2}{4\pi^2 m \epsilon_o} \left\{ \frac{N_f \gamma_f f}{f^4 + \gamma_f^2 f^2} + \frac{N_b \gamma_B f}{\left(f_o^2 - f^2\right)^2 + \gamma_B^2 f^2} \right\} \tag{40b}$$

where the first term in Eqs. 40a and 40b represents the contribution of the free electrons and the second term represents the contribution of the bound electrons. Notice that if f_o is greater than the frequency of the electromagnetic radiation, f, the second term of Eq. 40a, will be positive and can conceivably override the negative contribution of the first term. Consequently, it is apparent that this oversimplified model can account for the observed positive values of κ'. It remains to be seen, however, how well it can account for the other experimental results.

8.4 FIRST APPROXIMATION TO THE EVALUATION OF THE PARAMETERS

Inspection of Eqs. 40a and 40b reveals that there are five parameters to be evaluated (i.e., N_f, N_b, γ_f, γ_B, and f_o). Therefore, five connections between theory and experiment must be found. Since Eqs. 40a and 40b are so complex, the five following connections were chosen for the sake of simplicity in the resulting equations rather than for obtaining the most accurate values of these parameters.

1. The measured values of the dc conductivity of tungsten coupled with the sum of Eqs. 37 and 39, with f = 0.
2. The measured values of κ' at 665 mμ coupled with Eq. 40a.
3. The measured values of κ'' at 665 mμ coupled with Eq. 40b.
4. The measured spectral emissivity of tungsten at 400 mμ coupled with Eqs. 40a and 40b, and the emissivity equations of Section VII.
5. $N_f + N_b$ taken to represent the total number of electrons in the tungsten structure (i.e., 74 electrons/atom).

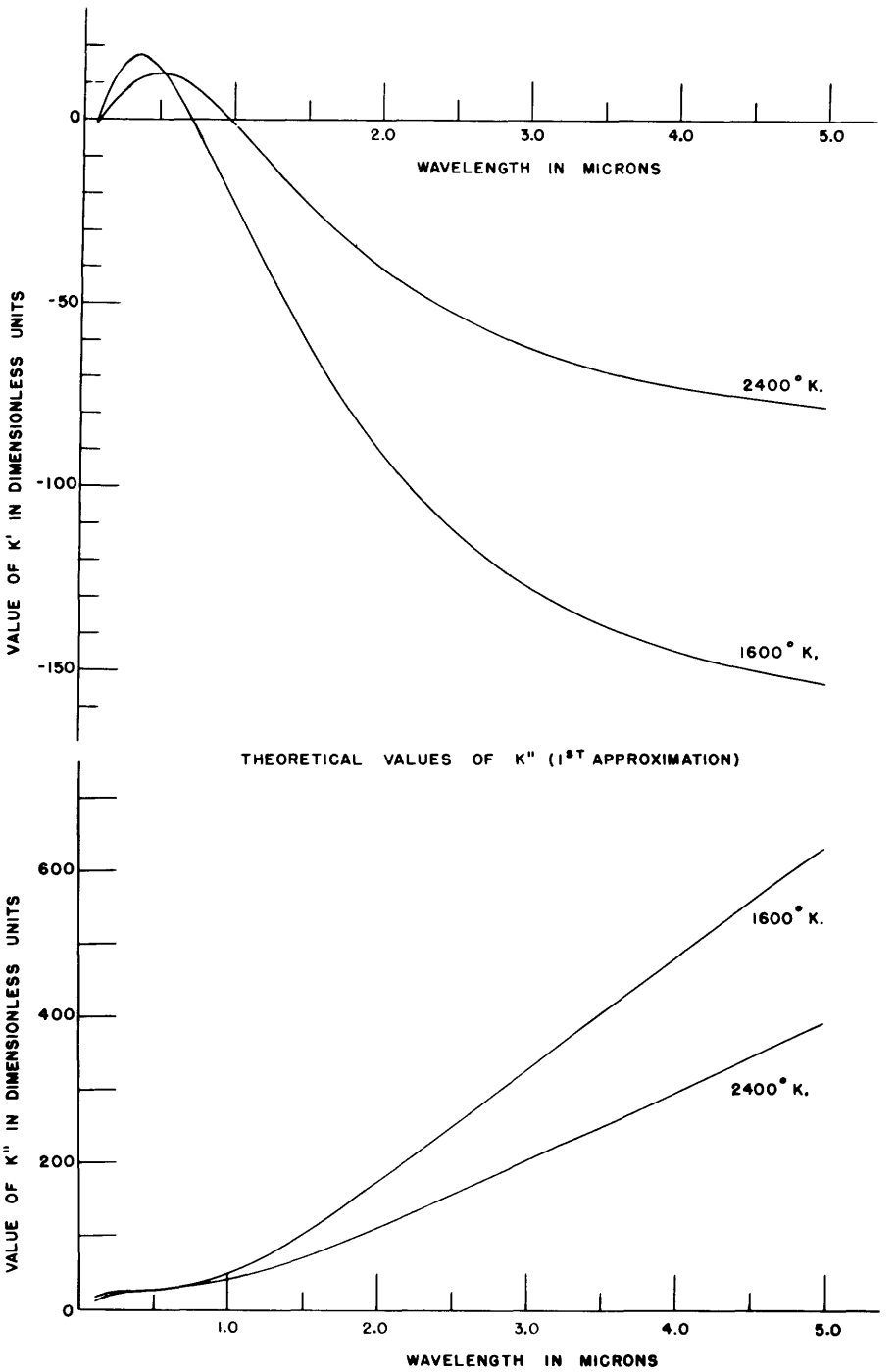

Fig. 40. Theoretical values of κ' and κ'' (first approximation).

Since all five of these measured quantities are known as a function of temperature over the interval 1600 to 2400° K, each of the parameters can be evaluated as a function of the temperature. The results of a trial-and-error solution of these five equations which fitted the five sets of experimental data best are tabulated below.

Temperature	Number of Electrons/Meter^3		Elastic Damping Parameter (sec^{-1})		Resonant Frequency (cps)
	N_f	N_b	γ_f	γ_B	f_o
1600° K	$9.806 \times 10^{+28}$	$4.501 \times 10^{+30}$	$1.915 \times 10^{+14}$	$0.790 \times 10^{+16}$	$2.92 \times 10^{+15}$
1800	8.154 "	4.501 "	1.830 "	1.040 "	2.93 "
2000	6.454 "	4.500 "	1.640 "	1.300 "	2.87 "
2200	6.113 "	4.486 "	1.740 "	1.280 "	2.86 "
2400	6.020 "	4.467 "	1.900 "	1.240 "	2.87 "

The results of substituting these parameters in Eqs. 40a and 40b are shown by the curves of Fig. 40. Notice that at long wavelengths κ' is negative, indicating that the free electrons predominate over the bound electrons. This might have been expected, since the bound electrons will not oscillate strongly at low frequencies (that are far removed from their resonant frequency). Notice that as the wavelength decreases, the effect of the bound electrons increases to the point at which κ' becomes positive in the near infrared portion of the spectrum.

Notice that the effect of increasing the temperature is to increase the value of κ' and to decrease the value of κ'' at the long wavelengths. However, as the visible region is approached, this effect decreases and even reverses itself in the optical region.

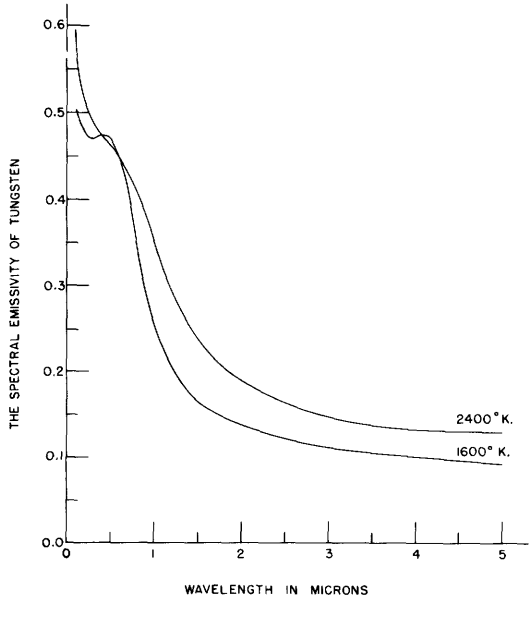

Fig. 41. Theoretical spectral emissivity of tungsten (first approximation).

It would appear as though the optical region is a transition region, as far as tungsten is concerned, in which the effects of the free electrons and the effects of the bound electrons are of almost equal importance. We would guess that, at frequencies below the optical range, the free electrons would dominate, while, at frequencies above the optical range, the bound electrons would dominate.

When the values of κ' and κ'' illustrated in Fig. 40 are inserted in the equations of Section VII (Eqs. 29 and

26) to find the corresponding values of normal spectral emissivity, the curves of Fig. 41 result. Notice that these curves are in fair qualitative agreement with the experimental data (1). Notice also that these theoretical curves predict two points at which the temperature derivative of the emissivity changes sign. One of these so-called X-points has actually been observed at a wavelength of approximately 1.27 microns (1). The observed tendency of the emissivity to reach a maximum and decline in the ultraviolet (see Fig. 32) is not evident in the curves of Fig. 41.

Therefore, it can be concluded that this model together with the present parameters does not qualitatively agree with experiment in the near ultraviolet region of the spectrum but is in good qualitative agreement in and below the optical range of frequencies.

8.5 COMMENTS ON THE EVALUATION OF THE PARAMETERS

The method used to evaluate the five parameters of this classical model was chosen for the sake of mathematical simplicity rather than for obtaining the most accurate values of the parameters. The first four criteria of this computation listed in section 8.4 represent the direct results of observation and, consequently, are not open to serious objection. The fifth criterion, that $N_f + N_d$ represent the total number of electrons in the tungsten structure, is subject to criticism, since many of the electrons are so tightly bound to the lattice atoms that they cannot oscillate very strongly under the influence of the electric field of the electromagnetic radiation. Therefore, we would guess that only a fraction of the total number of electrons would be effective in determining the optical properties of the metal.

As a first guess, it would appear that only the electrons in the conduction band of the tungsten structure would be effective, since the electrons in and below the valence band are separated from the conduction-band electrons by the interband energy gap, and, consequently, are much more tightly bound than the conduction-band electrons. As far as the author knows, the band structure of tungsten is not sufficiently well known to enable the computation of the number of electrons in the tungsten conduction band. However, by consideration of the chemical properties of tungsten (valence, oxidation number, and so forth) we would estimate that there are at least two electrons per atom in the conduction band. Therefore, we would estimate that a better set of parameters might result if the calculation outlined in section 8.4 were repeated with $N_f + N_d$ taken to represent two electrons per atom instead of 74 electrons per atom, as used in section 8.4. However, we found that such a calculation yields ridiculous results (imaginary values of f_o, for example). Therefore, we conclude that the effective number of electrons lies somewhere between two and 74 electrons per atom.

We now feel that in order to find reliable values of the parameters, the fifth criterion must be replaced by some directly measurable observable. It is suggested that both the fourth and fifth criteria be replaced by the measured values of κ' and κ'' at some wavelength conveniently removed from the wavelength 665 mμ that was used in criteria two and three. Figure 40, representing the extrapolated values of κ' and κ'' based

on the present model, suggests that some wavelength in the near infrared would be quite suitable for this purpose. However, as far as the author knows, no data on the infrared optical properties of incandescent tungsten are available at the present time. Therefore, we recommend that future observers concentrate their efforts on measuring the spectral emissivity and optical properties of tungsten in the infrared part of the spectrum rather than extend the emissivity data to higher temperatures or farther into the ultraviolet part of the spectrum. In this way, it will be possible to make a better computation of the parameters of the present model, and, also, the measured emissivity values themselves ought to be of considerable value for experimental purposes.

8.6 CONCLUSIONS

It is apparent that even the oversimplified classical model which has been presented represents a considerable amount of mathematical complexity, as far as determining the parameters is concerned. We feel that, at the present time, there are insufficient experimental data to justify a rigorous solution of this problem. However, on the basis of the approximate solution outlined in section 8.4, we believe that this model shows sufficient promise to justify future work along these lines.

Once reliable values for the parameters have been found, we think that the theory will show greater quantitive agreement with the experimental data and will be useful not only for extrapolation and calculation purposes, but also for giving an insight into what is happening in the metallic structure to give rise to the observed optical properties.

APPENDIX I

VACUUM CONSIDERATIONS

Since the emissive properties of metals may be quite sensitive to surface contaminations, very good vacuum conditions are desirable so that the attack of the surface by residual gases can be reduced to a minimum. Dushman (21) has considered this problem in great detail and De Vos (1) has summarized the part of Dushman's work that applies to this experiment. De Vos estimated that, at pressures lower than 10^{-5} mm Hg, we need not fear the chemical effects of residual gases, except possibly for the hydrocarbons which combine with the tungsten to form tungsten carbides (and hydrogen) at temperatures above 1500° K. This process can result in a considerable change in the optical and thermal properties of the specimen (33). The author feels that the presence of water vapor would tend to remove tungsten from the source and deposit it on the glass walls of the tube by means of the "water cycle" (21). De Vos found that there are no systematic changes in emissivity when the high vacuum is replaced by a 50-cm pressure of pure argon. Consequently, it would appear that the presence of inert gases does not seem to hinder the emissive properties of tungsten, but the presence of other gases (particularly hydrocarbons and water vapor) are undesirable.

Thus, we tried, initially, to obtain as good a vacuum as possible for a tube of this size. To remove the water vapor, an auxiliary side tube containing five barium getters (of the type used in industrially produced radio receiving tubes) was attached to the main tube at the tip of the exponential horn appendage (see Fig. 1). We felt that the chemical gettering action of the barium would remove many of the undesirable residual gases. The special ionization gauge used to measure the total pressure of the residual gases (see Appendix II) was equipped with four hairpin filaments composed of various refractory metals to serve as physical getters (34). When metal from any or all of these filaments is evaporated on the glass walls of the ionization gauge, any residual gas that is absorbable on these metal surfaces will be "caught" and subsequently buried by further evaporation. Since there is a possibility that metals differ in their ability to "hold on" to such absorbable gases, tungsten, tantalum, and molybdenum getter filaments were incorporated in this special ionization gauge. Since the vacuum system used to evacuate the tube was equipped with mercury diffusion pumps rather than oil pumps, we felt that the hydrocarbon content of the residual gas at the seal-off was quite small and would be further reduced by the gettering action discussed above.

The total pressure at seal-off was approximately 3×10^{-9} mm Hg, N_2 equivalent. The ionization gauge was able to reduce this seal-off pressure to 1×10^{-9} mm Hg. The partial pressure of the gases that are absorbable on tungsten, tantalum, and molybdenum was estimated (by flash-filament techniques) to be several orders of magnitude below this value. The remaining gas was, in all probability, predominantly helium, and to a lesser extent the other inert gases. However, upon heating the tungsten source, the total gas pressure was noticeably increased. Flash-filament measurements indicated

that this additional gas was not absorbable on tungsten. Consequently, this increased gas presumably arose from increased helium permeation through the heated glass walls of the emissivity tube and did not result from the metal portions of the tube-structure outgassing. The highest pressure recorded in the emissivity tube was 9.5×10^{-8} mm Hg and occurred near the termination of the experiment after an unusually long period of operation.

Consequently, the vacuum conditions within the emissivity tube are considered satisfactory for the present experiment, and we feel that very little contamination of the tungsten surface resulted from the effects of the residual gases.

APPENDIX II

DESCRIPTION OF SPECIAL IONIZATION GAUGE

There are several advantages in combining the functions of measuring the total gas pressure and of gettering absorbable gases into one glass envelope. This not only eliminates the necessity for providing a separate getter tube assembly but also has the following advantages because of the presence of the getter filaments within the ionization gauge structure:

1. An outer shield grid for the ionization gauge (35) is unnecessary, since the metal film deposited on the inside glass surface by the getter filaments can be made to serve this purpose by providing an internal connection to this glass surface. It is possible to outgas the electron-collector grid assembly by rf induction methods before this metallic layer is evaporated on the glass surface. Since more power can usually be supplied to the electron-collector grid by this method than can usually be obtained by electron bombardment, the electron-collector grid can be constructed from heavier wire for strength, rigidity, and ease of construction and still be properly outgassed.

2. The ionization gauge provides a means of measuring the partial pressure of the "metallic gas" produced by evaporation of the getter filaments. In this way, we can easily estimate the time required to provide any degree of coverage of the getter material on the glass surface.

3. The getter filaments can be used for flash-filament measurements to estimate the partial pressure of absorbable gases. With a separate getter-tube assembly, the getter filaments cannot be used for this purpose, since the gas will be trapped in the getter tube before it can get to the ionization gauge to be measured.

The ionization gauge used in this experiment was essentially a modification of a Bayard-Alpert design with the outer shield grid replaced by the getter filaments (35). Some of the constructional features of the tube are the following:

1. A 3-mil diameter tungsten wire ion collector mounted in the center of the glass envelope on a press lead that has a glass evaporation shield to prevent the metallic-getter coating from allowing excessive leakage currents to flow.

2. A cylindrical electron collector grid assembly 1 1/2 inches long and 1 inch in diameter wound spirally with 10-mil diameter tantalum wire spaced 10 turns to the inch.

3. Two 10-mil diameter tungsten hairpin filaments to serve as the ionization gauge electron emitter (and spare). These filaments were mounted diametrically opposite to each other on either side of the electron collector and spaced about 1/8 inch from it.

4. Four hairpin getter filaments mounted in the position normally occupied by the shield grid and spaced around the periphery of the "shield grid position." All of the getter filaments were constructed from 10-mil diameter wire that had been previously outgassed in a separate tube and were mounted on 40-mil diameter platinum support wires. Two of the getter filaments were of molybdenum, one was of tantalum, and one was of tungsten.

5. An internal connection to the inside glass wall (and hence to the evaporated metallic coating).

The gauge was evacuated and processed before being attached to the main emissivity tube in order to measure its characteristics. The gauge constant was measured in the range 1 to 10×10^{-4} mm Hg (of nitrogen) by comparison with a standard McLeod gauge and was found to have the value 11 $(\text{mm Hg})^{-1}$ with the getter filaments connected to the electron collector. (The gauge constant is defined as the ion current per unit electron current per unit pressure.) The gauge was then evacuated of this nitrogen and sealed off the pumps. It was found that steady operation of the molybdenum getter filaments at evaporation temperatures (5 amps through the 10-mil filament) caused the pressure to increase rather than to decrease. This was undoubtedly caused by the outgassing of the platinum support wires. However, if the filaments were pulse heated (1/2 second on, followed by 3 seconds off) so that the central portion of the getter filament reached evaporation temperatures while the support wires did not have time to get very hot, the pressure did not noticeably increase. Consequently, the getter filaments could be continuously operated in this pulsed fashion to continuously provide new getter surface (34). Since the actual evaporation time was so small (a fraction of the duty cycle), the life of the getter filaments was very much longer than with steady operation.

The gauge was considered satisfactory and was sealed to the main emissivity tube without further change (36).

Acknowledgment

The author is greatly indebted to Professor Wayne B. Nottingham for many valuable suggestions, comments, and criticisms; to Mr. Lawrence E. Sprague for his very helpful advice and assistance in the construction of the emissivity tube; to Mr. Lawrence W. Ryan and to Mr. Anthony J. Velluto for their excellent glass work; to Mr. John B. Keefe and to Mr. John B. Sanromá for their accurate machining of intricate parts; to Mrs. Zelda R. Wasserman for her accurate numerical calculations; not to mention all the students working under Professor Nottingham for their endless train of ideas and suggestions. The author is particularly indebted to Mr. Haywood Shelton who designed the electrometer used in this experiment and to Mr. Dana H. Dickey for his advice on ionization gauges.

References

1. J. C. De Vos, Physica 20, 669; 690 (1954).
2. W. B. Nottingham and W. E. Mutter, Phys. Rev. 74, 1261 (1948).
3. A. G. Worthing and W. E. Forsythe, Astrophys. J. 61, 146 (1925).
4. A. G. Worthing, Phys. Rev. 25, 846 (1925).
5. I. Langmuir, Phys. Rev. 6, 138 (1915).
6. F. J. Bradshaw, Proc. Phys. Soc. (London) 63B, 573 (1950).
7. L. V. Whitney, Phys. Rev. 48, 458 (1935).
8. D. J. Price, Proc. Phys. Soc. (London) 59B, 118 (1947).
9. H. Lund and L. Ward, Proc. Phys. Soc. (London) 65B, 535 (1950).
10. C. E. Mendenhall and W. E. Forsythe, Astrophys. J. 37, 380 (1913).
11. C. Hurst, Proc. Roy. Soc. (London) 142, 466 (1933).
12. G. V. McCauley, Astrophys. J. 37, 164 (1913).
13. W. W. Coblentz, Bull. Bur. Standards 7, 197 (1910).
14. W. W. Coblentz and W. B. Emerson, Bull. Bur. Standards 14, 307 (1918).
15. L. D. McGlauchlin, Emissivity of tantalum as a function of wavelength and temperature, S.M. Thesis, Department of Physics, M.I.T., 1950.
16. J. R. Stevenson and H. R. Philip, Spectral emissivity of tantalum and a construction of a tungsten source, S.B. Thesis, Department of Physics, M.I.T., 1950.
17. R. D. Larrabee, Design and construction of the equipment for the measurement of the spectral emissivity of tungsten, S.M. Thesis, Department of Physics, M.I.T., May 1955.
18. M. F. Angell, Phys. Rev. 33, 421 (1911).
19. H. F. Kurtz, J. Opt. Soc. Am. 13, 495 (1926).
20. W. E. Forsythe, Measurement of Radiant Energy (McGraw-Hill Book Company, Inc., New York, 1st ed., 1937), p. 119.
21. S. Dushman, Scientific Foundations of Vacuum Technique (John Wiley and Sons, Inc., New York, 1949).
22. J. C. De Vos, The emissivity of tungsten ribbon – the tungsten strip lamp as a standard source of radiation, doctoral thesis (Vrue Universiteit Te Amsterdam, 1953).
23. H. Shelton, Thermionic emission from a planar tantalum crystal, Ph.D. Thesis, Department of Physics, M.I.T., May 1956.
24. W. E. Forsythe and E. Q. Adams, J. Opt. Soc. Am. 35, 108 (1945).
25. H. C. Hamaker, Physica 3, 561 (1936).
26. A. G. Worthing, J. Opt. Soc. Am. 13, 635 (1926).
27. C. Zwikker, Verslag Gewone Vergader. Afdeel. Natuurk. 36, 856 (1927).
28. A. R. von Hippel, Dielectrics and Waves (John Wiley and Sons, Inc., New York, 1st ed., 1954).
29. P. Drude, The Theory of Optics (Longmans, Green and Company, New York, 1902).
30. C. Zener, Nature 132, 968 (1933).
31. R. de L. Kronig, Nature 133, 211 (1934).
32. F. S. Seitz, Modern Theory of Solids (McGraw-Hill Book Company, Inc., New York, 1940).

33. M. R. Andrews, J. Phys. Chem. 27, 270 (1923).

34. H. Shelton, Quarterly Progress Report, Research Laboratory of Electronics, M.I.T., Oct. 15, 1955, p. 9; R. D. Larrabee, Quarterly Progress Report, Research Laboratory of Electronics, M.I.T., July 15, 1956, p. 4.

35. W. B. Nottingham, Design and properties of the modified Bayard-Alpert gauge, Vacuum Symposium Transactions, 1954, p. 76.

36. For further information regarding the ionic pumping of this gauge see Quarterly Progress Report, Research Laboratory of Electronics, M.I.T., April 15, 1956, p. 6.